BIOCHEMICAL INVESTIGATION OF PROGEROID DISEASE-ASSOCIATED MUTATIONS IN HUMAN ZMPSTE24

by

Erh-Ting Hsu

A Dissertation

Submitted to the Faculty of Purdue University

In Partial Fulfillment of the Requirements for the degree of

Doctor of Philosophy

Department of Chemistry

West Lafayette, Indiana

December 2018

THE PURDUE UNIVERSITY GRADUATE SCHOOL
STATEMENT OF COMMITTEE APPROVAL

Dr. Christine A. Hrycyna, Chair
Department of Chemistry
Dr. Angeline M. Lyon
Department of Chemistry
Dr. Andrew D. Mesecar
Department of Biochemistry
Dr. Cynthia V. Stauffacher
Department of Biological Sciences

Approved by:

Dr. Christine A. Hrycyna
Head of the Graduate Program

For my family

謹獻給我的家人

ACKNOWLEDGMENTS

I would first like to thank my loving husband, Han-Ting Tseng. I am very lucky to marry him and have his constant love, support, and understanding in every aspect of my life. I attribute my success and accomplishment in graduate school to him. To my parents and sister, I am extremely grateful for their unconditional love and care. They always believe in me even though they hardly understand my works. I know I always have my family to count on when times are rough. Without their help, I would not have made this far in my career.

I would like to thank my advisor, Dr. Christine Hrycyna, for giving me the opportunity to work in her research lab as well as her continuous encouragement, inspiration, patience, understanding and support during my entire dissertation work. Importantly, she sets a great example of a strong independent woman that will benefit me for the rest of my life. I would also like to give thanks to Dr. Angeline Lyon, Dr. Andrew Mesecar, and Dr. Cynthia Stauffacher for serving on my thesis committee and providing helpful suggestions for my research.

I would also like to acknowledge my collaborators, Dr. Susan Michaelis and Dr. Eric Spear at Johns Hopkins, also Dr. Mark Distefano, Dr. Jeffrey Vervacke, and Dr. Veronica Diaz-Rodriguez at the University of Minnesota, for their contribution of providing essential experimental materials and critical ideas to my research. In addition, I would like to thank Dr. Mathew Tantama for providing the fluorescence microplate reader. I am also thankful for the Jonathan Amy Facility for providing Chemical Instrumentation and Dr. Patricia Bishop at Purdue University for assistance with LC/MS usage and data analysis.

I also want to acknowledge all the members that I have been working with in the Hrycyna lab. For previous lab members, Dr. Kelsey Bohn was my mentor when I first began in the lab. It was because of you that I decided to join the group. I would like to thank Dr. Patty Wiley for training and teaching me about the project basics and techniques. Dr. Karen Olsen, thank you for giving me writing advice during the last few years. For Dr. Amy Funk, I am so happy to have you as my lab mate and also a great friend. Thank you for sharing your valuable wisdom with me, both in research and life. I also want to give special thanks to Sahej Bains for being my “quiet-side” buddy. I will remember our Indian lunch outing (and Cactus night). I believe you will become an excellent doctor.

For current lab members, Chelsea Theisen, thank you for working with me together on ZMPSTE24 and Ste24 projects. I feel privileged to have taught you and have gained a lot from you as well. To my undergraduate student, Nisreen Islah, thank you for being such a good helper and of course for filling tips. I also want to give thanks to Anna Ratliff, Jason Goebel, Ari Cardillo, Elias Beretta, and Alex Piroozi, who also provided a lot of help and feedback for my research. I also want to acknowledge Liz Garland-Kuntz for managing all the lab stuff so I do not have to struggle with broken ultracentrifuges anymore. I wish all of you the best of luck in your careers and in life and I hope we can keep in touch.

I would like to thank the professors, faculty, alumni, and friends that had an impact on me throughout my time in school. Dr. Po-Huang Liang and Kuo-Hsun Teng at Academia Sinica, Dr. Bi-Fong Lin at National Taiwan University, and Dr. Chin-Su Liu at Taipei Veterans General Hospital helped me in my decision to join Purdue University for graduate school and helped me realize that I could succeed in my future as a biochemist. I also want to thank all my new and old friends, and everyone who has helped me in any way.

TABLE OF CONTENTS

LIST OF TABLES

LIST OF FIGURES

LIST OF ABBREVIATIONS

Å	angstroms
Abz	2-aminobenzoic acid
AEBSF	4-(2-Aminoethyl)benzenesulfonyl fluoride hydrochloride
APS	atypical progeria syndrome
ATP	adenosine-5'-triphosphate
BSA	bovine serum albumin
BMH	bis(maleimido)hexane
BMOE	bis(maleimido)ethane
CS	Cockayne syndrome
DDM	n-dodecyl-β-D-maltoside
DMEM	Dulbecco's modified Eagle medium
DMF	dimethyl formamide
DMSO	dimethyl sulfoxide
Dnp	dinitophenol
DRV	darunavir
DTT	dithiothreitol
E.coli	*Escherichia coli*
ESI	electrospray ionization
ER	endoplasmic reticulum
FBS	fetal bovine serum
FRET	Förster resonance energy transfer
FPLD2	Dunnigan type familial partial lypodystrophy
FPP	farnesyl pyrophosphate
FTase	farnesyltransferase
FTI	farnesyltransferase inhibitor
HAART	highly active antiretroviral therapy
HEPES	4-(2-hydroxyethyl)-1-piperazineethanesulfonic acid
HGPS	Hutchinson-Gilford progeria syndrome
HIV-PIs	HIV protease inhibitors

HMG-CoA	β-hydroxy β-methylglutaryl-CoA
HRP	horseradish peroxidase
GFP	green fluorescent protein
IAPP	islet amyloid polypeptide
IC_{50}	half maximal inhibitory concentration
ICMT	isoprenylcysteine carboxyl methyltransferase
IFITM	interferon-induced transmembrane
Ig	immunoglobulin
INM	inner nuclear membrane
K_D	dissociation constant
kDa	kilo-dalton
$K_{m(app)}$	pseudo-first-order rate constant *K* apparent
LAP2α	lamina-associated polypeptide 2α
LB	Luria-Bertani
LPV	lopinavir
MAD	mandibuloacral dysplasia
MEF	mouse embryonic fibroblasts
MES	2-(N-morpholino)ethanesulfonic acid
MOPS	3-morpholinopropane-1-sulfonic acid
MS	metabolic syndrome
min	minute
miR	mature microRNA
mTOR	mammalian target of rapamycin
MWCO	molecular-weight cutoff
NAFLD	non-alcoholic fatty liver disease
NE	nuclear envelope
NF-κB	nuclear factor kappa B
NLS	nuclear localization signal
NPCs	nuclear pore complexes
NRF2	nuclear factor, erythroid 2 like 2
ONM	outer nuclear membrane

OP	1,10-orthophenanthroline
PBS	phosphate buffered saline
PCR	polymerase chain reaction
PDB	Protein Data Bank
PGK	phosphoglycerate kinase promotor
QA	quadruple alanine
RCE1	Ras converting CAAX endopeptidase 1
RD	restrictive dermopathy
RIPA	radioimmunoprecipitation assay
RFU	relative fluorescence unit
ROS	reactive oxygen species
RTV	ritonavir
SAM	*S*-adenosyl-L-methionine
SC-URA	synthetic complete medium without uracil
SDS	sodium dodecyl sulfate
SREBP-1	sterol response element binding protein 1
SPPS	solid-phase peptide synthesis
TA	triple alanine
TCA	trichloracetic acid
T2D	type 2 diabetes
TD	triple detergent
TFA	trifluoroacetic acid
TMH	transmembrane helix
TPV	tipranavir
Tris	tris(hydroxymethyl)aminomethane
UC	uncleavable
Vmax	maximum rate achieved by the enzyme
WS	Werner syndrome
WT	wild-type
ZMPSTE24	zinc metalloprotease STE24

ABSTRACT

Author: Hsu, Erh-Ting. Ph.D.
Institution: Purdue University
Degree Received: December 2018
Title: Biochemical Investigation of Progeroid Disease-Associated Mutations in Human ZMPSTE24
Major Professor: Christine A. Hrycyna

ZMPSTE24 is a unique intramembrane zinc metalloprotease that plays critical roles in the lamin A maturation pathway. Lamin A comprises a dense network underlying the inner nuclear membrane that maintains the structural integrity and proper function of the nucleus. The precursor of lamin A, prelamin A, terminates with a CAAX motif, where "C" is cysteine, "A" is typically an aliphatic amino acid, and "X" is one of several different amino acids. Like all CAAX proteins, prelamin A undergoes a series of post-translational modifications, including farnesylation of the cysteine by farnesyltransferase, endoproteolysis of the AAX residues by ZMPSTE24 or possibly a related protease RCE1, and carboxyl methylation by isoprenylcysteine carboxyl methyltransferase (ICMT). After CAAX processing, an additional cleavage event by ZMPSTE24 occurs to remove 15 residues from the C-terminus, including the farnasylated and carboxyl methylated cysteine, releasing mature lamin A into the nucleoplasm.

Mutations in the gene encoding ZMPSTE24 that impair proteolytic activity cause a set of progeroid diseases, including B-type mandibuloacral dysplasia (MAD-B) and restrictive dermopathy (RD). Recently, ZMPSTE24 mutations were also detected in patients with metabolic syndrome (MS) and nonalcoholic fatty liver disease (NAFLD). Patients with these diseases have shown defective prelamin A processing, leading to the accumulation of persistently farnesylated prelamin A in the nucleus. However, how this accumulation causes disease remains unclear.

We demonstrated that both ZMPSTE24 and another known CAAX protease, RCE1 are both capable of mediating the C-terminal cleavage of prelamin A. RCE1 retains the capacity to cleave the AAX residues of prelamin A in progeroid diseases induced by inactive ZMPSTE24 mutants, therefore the disease molecule will be most likely farnesylated and methylated prelamin A. These factors suggest that the ability of ZMPSTE24 to perform the upstream cleavage determines the accumulation level of uncleaved prelamin A in progeroid diseases.

However, there was no available assay that could quantitatively demonstrate the *in vitro* upstream cleavage activity of ZMPSTE24. Therefore, we first developed a FRET-based assay that was able to precisely quantify the upstream cleavage activity of Ste24, the yeast homolog of ZMPSTE24. The 33-mer analog of **a**-factor, Ste24 natural substrate, has a 2-aminobenzoic acid (Abz) fluorophore at the N-terminus and a dinitophenol (Dnp) quencher located on the either side of the proposed cleavage site. After cleavage, quantification of the fluorescence from the dequenced peptide enabled us to continuously monitor the upstream cleavage activity of Ste24.

We then utilized this FRET-based assay to examine the upstream cleavage activity of wild-type ZMPSTE24 and its disease mutants. We demonstrated that the **a**-factor analog FRET substrate could be recognized and cleaved at the predicted position by ZMPSTE24. Disease variants were examined using this assay and the results revealed reduced upstream cleavage activity. Moreover, blocking ubiquitylation restored catalytic activity of some ZMPSTE24 disease variants, suggesting that diminished activity of these mutants is due to protein instability. Limited trypsin digestion results also indicated that some variants may not be properly folded, as compared to wild-type.

The crystal structure of ZMPSTE24 revealed that seven transmembrane helices of ZMPSTE24 surround a large intramembrane chamber. The HEXXH zinc metalloprotease motif faces inward to cap the top of the chamber inside which proteolysis is proposed to occur. The four side portals apparent in the structure may provide substrate entry and exit routes. Based on structural considerations, besides interfering with structural integrity, these disease mutations may decrease ZMPSTE24 activity by preventing substrate binding in the active site or occluding substrate entry into or exit from the enzyme chamber.

Using a yeast **a**-factor sequence-based photoactive analog containing benzophenone in the farnesyl portion, which can be well processed by ZMPSTE24, we have shown that certain disease mutants may affect farnesyl binding of the C-terminal cleavage substrate. We also designed several double cysteine mutants near portal 1 in Cys-less background of Ste24. We then utilized bismaleimide sulfhydryl-to-sulfhydryl crosslinkers to block the portal opening. Some of the crosslinked double mutants showed reduced AAX cleavage activity, suggesting the portal 1 may be important for the C-terminal cleavage. Together, these data will clarify how the enzyme functions and also provide further insights into progeroid diseases.

CHAPTER 1. INTRODUCTION

1.1 Maturation of Nuclear Scaffold Protein Lamin A

1.1.1 Structure and Functions of Nuclear Lamins

In eukaryotes, genetic material is stored in the nucleus, which is surrounded by the nuclear envelope (NE). The nuclear envelope, also known as the nuclear membrane, is comprised of the outer nuclear membrane (ONM), the inner nuclear membrane (INM), nuclear pore complexes (NPCs) and the nuclear lamina. The outer and inner nuclear membranes are contiguous and connected at the nuclear pore complex insertions, where the outer nuclear membrane is also continuous with the rough endoplasmic reticulum (ER) membrane and stubbed with ribosomes. The perinuclear space created by this system provides a selective barrier for transportation of macromolecules. The nuclear lamina is a meshwork of lamins and its associated membrane proteins, located at the interface between the inner nuclear membrane and chromatin[1,2] (Figure 1.1).

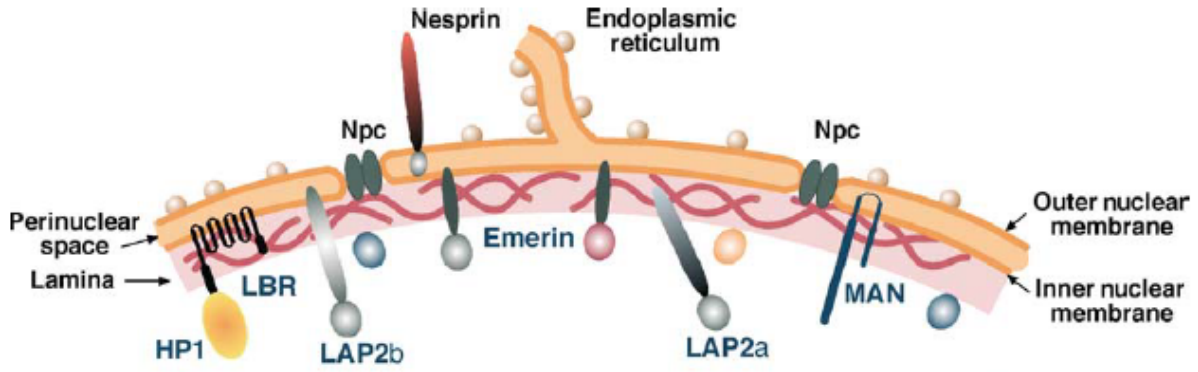

Figure 1.1. Structure of the nuclear envelope (NE).

The NE is composed of the contiguous inner and outer nuclear membranes (INM and ONM, respectively), nuclear pore complexes (NPCs), and the nuclear lamina. Associated with the NE are a variety of transcription factors and anchoring proteins[1]. Reprinted with permission from "Structural Organization and Functions of the Nucleus in Development, Aging, and Disease" by Mounkes, L. and Stewart, C.L., 2004. Current Topics in Developmental Biology, Vol. 61, pg. 191–228. Copyright (2004), Elsevier Inc.

The lamins provide mechanical stability and maintain nuclear morphology. Furthermore, lamins have been identified to have more than 30 direct and 100 indirect interactions with other

proteins, which are involved in chromatin interaction, regulation of gene expression, cytoskeleton connection and signaling pathways[1,3]. Lamins are only present in metazoans and have not been discovered in lower level eukaryotes, such as *Saccharomyces cerevisiae*. As one of the intermediate filaments (type V), lamins can be divided into three parts. The N-terminus has a short globular "head" domain, which is about 33 amino acids long and much shorter than other intermediate filaments. The central portion has a longer α-helical "rod" domain, which has four coiled-coiled regions that are connected by flexible linker regions. The C-terminus has a globular "tail" domain, which contains an immunoglobulin (Ig) fold and a nuclear localization signal (NLS)[3–5] (Figure 1.2). Lamin monomers form higher order structures. For dimerization, two lamins first coil each other using their α-helical "rod" domains to assemble as a parallel dimer, which then interact using a head-to-tail manner to form polymers. Next, protofilaments are formed through the anti-parallel association of two polymers. Lamin filaments, about 10-nm in diameter, are finally produced between three and four protofilaments[3,5].

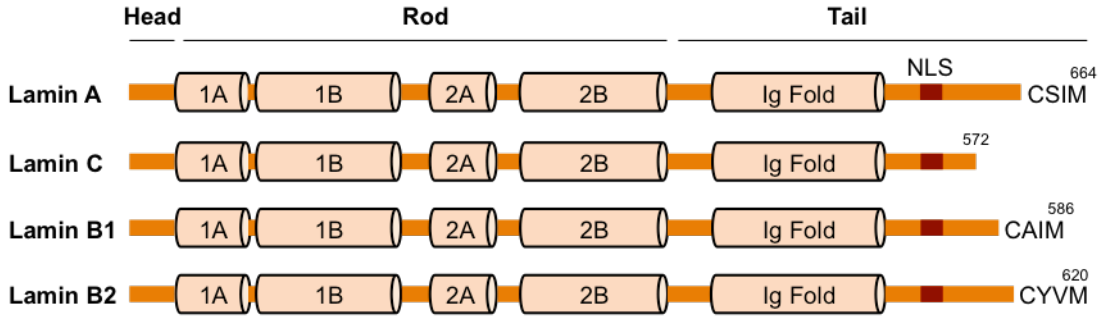

Figure 1.2. Structure of nuclear lamins.

Lamins are structurally similar, containing a small "head" domain, a central "rod" domain with four coiled-coil regions (1A, 1B, 2A, and 2B), and a globular "tail" domain with an immunoglobulin (Ig) fold and a nuclear localization signal (NLS). Apart from lamin C, other lamins terminate with a CAAX motif that direct sequential post-translational modifications called CAAX processing[3].

Based on different structures, expression, and localization patterns, lamins are classified into A- or B-types, which are encoded by three different genes in mammals (Figure 1.2). A-type lamins, including two major isoforms lamin A and C, and the two minor isoforms lamin C2 and AΔ10, are generated by alternative splicing of the *LMNA* gene and only expressed upon differentiation. Lamin A and C share the first 566 amino acids, but lamin A has an extra 98

amino acids at the end of the C-terminus, which terminates in a CAAX motif, where "C" is cysteine, "A" is generally an aliphatic amino acid, and "X" is one of several different amino acids. For B-type lamins, they are usually expressed constitutively in both undifferentiated and differentiated cells. Lamin B1 is encoded by the *LMNB1* gene, while lamin B2 and another minor isoform B3 are encoded by the *LMNB2* gene. Moreover, all B-type lamins are also CAAX proteins and need a series of post-translational modifications, including farnesylation, proteolysis and methylation, to obtain correct localization and functions[3–5]. In addition, lamins can be regulated by other post-translational modifications, including phosphorylation, acetylation, SUMOylation, and glycosylation[6].

1.1.2 The Maturation Pathway of Lamin A

There are hundreds of known CAAX protein in eukaryotes, including the yeast mating pheromone **a**-factor and small GTPases, such as Ras and Rho[7,8]. The precursor of lamin A, prelamin A, has 664 amino acids (74-kDa) and also terminates with a CAAX motif. Like all CAAX proteins, prelamin A undergoes a series of post-translational modifications to form mature lamin A with proper functions, localization, and structure. First, a 15-carbon farnesyl group is transferred from farnesyl pyrophosphate (FPP) and attached via a thioether linkage to the cysteine residue by farnesyltransferase (FTase). Next, the C-terminal SIM residues are removed by Zinc Metalloprotease STE24 (ZMPSTE24) or Ras converting CAAX endopeptidase 1 (RCE1). Finally, isoprenylcysteine carboxyl methyltransferase (ICMT) transfers a methyl group from the *S*-adenosyl-L-methionine (SAM) donor to the newly exposed cysteine carboxyl group. Unlike other CAAX proteins, including B-type lamins, prelamin A undergoes an additional upstream cleavage event, where the 15 C-terminal residues, including the newly farnesylated and carboxyl methylated cysteine of prelamin A, are removed by ZMPSTE24[9,10] (Figure 1.3).

1.1.3 Requirements for Efficient Biogenesis of Lamin A

To generate mature lamin A with correct the function and localization, each step in the processing pathway is important. The cellular location where lamin A is processed has been a controversial issue. Most of the CAAX proteins are farnesylated in the cytosol and undergo other modifications at the cytosolic side of the ER. However, several studies have suggested that lamin

A maturation pathway occurs within the nucleus[11,12]. In 2008, Barrowman *et al.* suggested that prelamin A is imported directly into the nucleus and does not shuttle continuously back and forth between the nucleus and cytoplasm. Moreover, they also demonstrated that ZMPSTE24 and ICMT involved in the maturation pathway are localized to both the ER membrane, as well as the inner nuclear membrane, supporting the idea of the nucleus being a physiological prelamin A processing compartment[13].

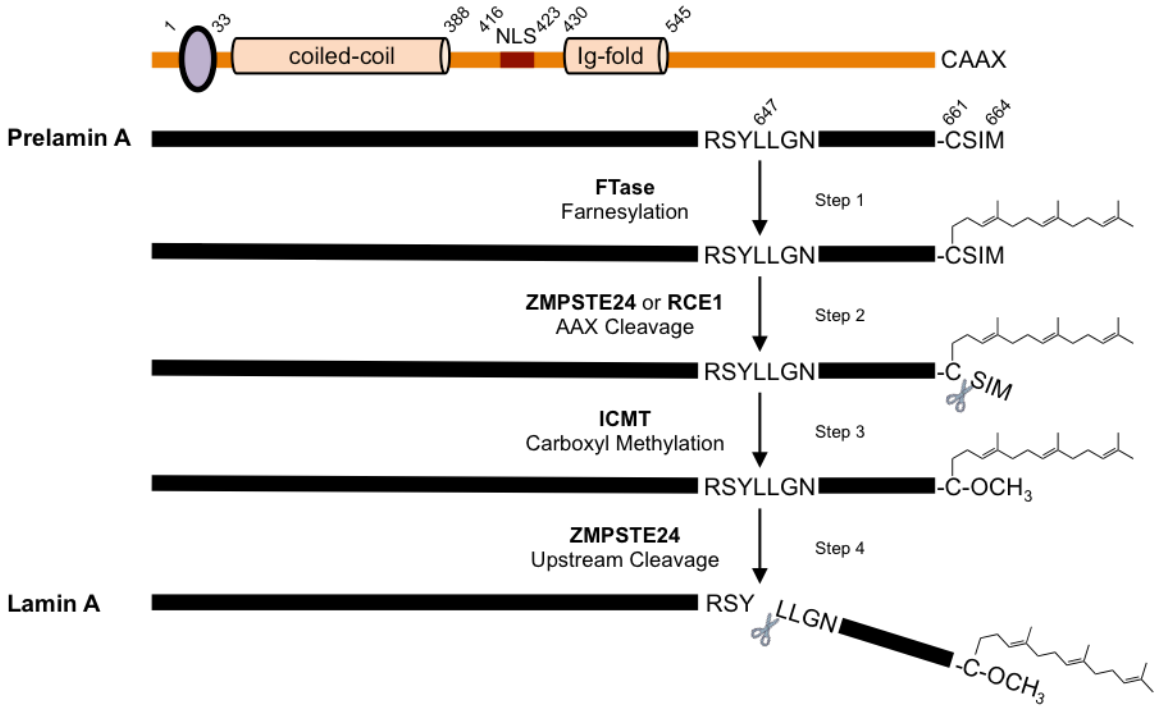

Figure 1.3. Schematic of lamin A maturation pathway.

The precursor of lamin A, prelamin A, has 664 amino acids and terminates with a CAAX motif. First, prelamin A undergoes a series of post-translational modifications, including farnesylation, endoproteolysis, and carboxyl methylation. Different to other CAAX proteins, prelamin A needs an additional cleavage by ZMPSTE24 to remove the last 15 residues, including the farnesylated and carboxyl methylated cysteine, to form mature lamin A[9,10].

So, are all steps in the prelamin A processing required to form mature lamin A? And how do these enzymes recognize their substrates? Studies have revealed that farnesylation is required for the following AAX cleavage. The fibroblasts expressing C661S, which is a non-farnesylated version of prelamin A, were not able to generate mature lamin A. Treatment with farnesyltransferase inhibitors (FTIs) or lovastatin also showed inhibition of prelamin A

processing as well[14,15]. In CAAX processing, isoprene addition usually depends on the "X" residue sequence. For example, methionine, alanine, and glutamine residues prefer farnesylation, while leucine and phenylalanine residues are more likely to undergo geranylgeranylation[8]. No geranylgeranylated prelamin A was detected from *Zmpste24*$^{-/-}$ cells using MALDI-TOF mass spectrometry[16]. However, alternative prenylation of prelamin A while inhibiting farnesylation is still controversial. Although mass spectrometry results supported alternative geranylgeranylation of prelamin A[16], other studies did not observe geranylgeranylated prelamin A accumulation upon loss of farnesylation[17–19].

After farnesylation, prelamin A undergoes an endoproteolytic event to remove the SIM tail from the C-terminus. ZMPSTE24 was thought to be the only enzyme to perform this cleavage event. However, from mass spectrometry data, the detected farnesylated peptide did not contain the C-terminal SIM residues from *Zmpste24*$^{-/-}$ cells, demonstrating that ZMPSTE24 is not necessarily required for the AAX proteolysis[16]. This is consistent with our data described in Chapter 2 demonstrating that RCE1 is able to cleave the AAX tail of prelamin A.

To date, ICMT is the only known enzyme for prelamin A methylation. Surprisingly, methylation is not essential for the prelamin A processing. Mouse embryonic fibroblasts (MEFs) with *Icmt*$^{-/-}$ reduced the efficiency of prelamin A cleavage but was still able to produce some mature lamin A[15]. This conclusion was further confirmed by mass spectrometry analysis showing that purified ZMPSTE24 was able to cleave the truncated prelamin A peptide without the carboxyl methyl group attached[20]. The function of methylation on prelamin A is still unclear.

It still remains a mystery of how ZMPSTE24 recognizes the same substrate to perform two distinct cleavages since the SIM tail and the upstream fragment have totally different sequences, lengths, and chemical compositions. From mutational analysis, ZMPSTE24 was not able to perform the upstream cleavage with a mutation of either amino acid on both sides of the upstream cleavage site, such as L647R and L648A. Cleavage efficiency was reduced with R644C and N650A, but the sequence on the C-terminus only slightly reduced the cleavage[15]. Length is also an important factor. Prelamin A is a protein with 664 amino acids but previous work has shown that the N-terminus (coiled-coil region, residue 1 to 388) is not required for ZMPSTE24 cleavage[21]. Using constructs with different lengths, the last 41 amino acids of prelamin A have been shown to be sufficient for efficient prelamin A cleavage by ZMPSTE24.

The distance between the upstream cleavage site and the CSIM motif is also important since inserting extra amino acids reduced the formation of mature lamin A[15].

1.1.4 Defective Prelamin A Processing in Progeroid Diseases

1.1.4.1 Mutations in *LMNA* or *ZMPSTE24* genes

As previously mentioned, proper post-translational modifications are important for the localization and functions of the lamins. Therefore, defects in prelamin A processing that result in failure to removing the modified tail from prelamin A are major causes of progeroid diseases. Progeroid diseases are a group of extremely rare genetic disorders that mimic physiological aging. Although sharing similar clinical features, these diseases can be categorized into two classes based on their underlying mechanisms. The first group is characterized by alterations in the lamin A maturation pathway with mutations in either *LMNA* or *ZMPSTE24* genes, including Hutchinson-Gilford progeria syndrome (HGPS), atypical progeria syndrome (APS), mandibuloacral dysplasia (MAD), and restrictive dermopathy (RD). The second group is induced by mutations in genes involved in DNA repair pathways, such as Werner syndrome (WS) and Cockayne syndrome (CS)[22]. Moreover, no evidence shows that these diseases are affected by gender and ethnicity. We will focus on introducing the first group in the following paragraph.

HGPS is one of the best-studied premature aging disorders and was first identified by Hutchinson and Gilford independently in the late nineteenth century[23]. The disease occurs in approximately 1 in 20 million people and affects an estimated 350 to 400 children worldwide at any one time based on the data provided by the Progeria Research Foundation[24]. Patients show normal features at birth and are characterized by accelerated aging symptoms by the age of two, including hair loss, joint contractures, lipodystrophy, cardiovascular disease, and death due to stroke or heart attack in their teenage years (Figure 1.4.A)[23]. Interestingly, brain development and intelligence of patients usually are not affected. A possible reason may be that lamin A is absent, while its alternative splicing isoform lamin C is normally expressed in the brain due to selective down-regulation of the prelamin A transcript by miR-9[25]. Most of the HGPS patients have a spontaneous dominant mutation (c.1824C>T; p.Gly608Gly) on one copy of the *LMNA* gene. The *de novo* mutation activates a cryptic splicing site, generating a mutant prelamin A protein called “progerin” with a deletion of 50 amino acids, which includes the sequence for the upstream cleavage by ZMPSTE24 (Figure 1.4.B)[26]. The persistently farnesylated and methylated

progerin accumulates in the nucleus and causes aberrant nuclear morphology, such as misshapen and blebbed nuclei (Figure 1.4.C), disrupted heterochromatin, shortened telomeres, and leads to premature senescence as a consequence of genome instability[22].

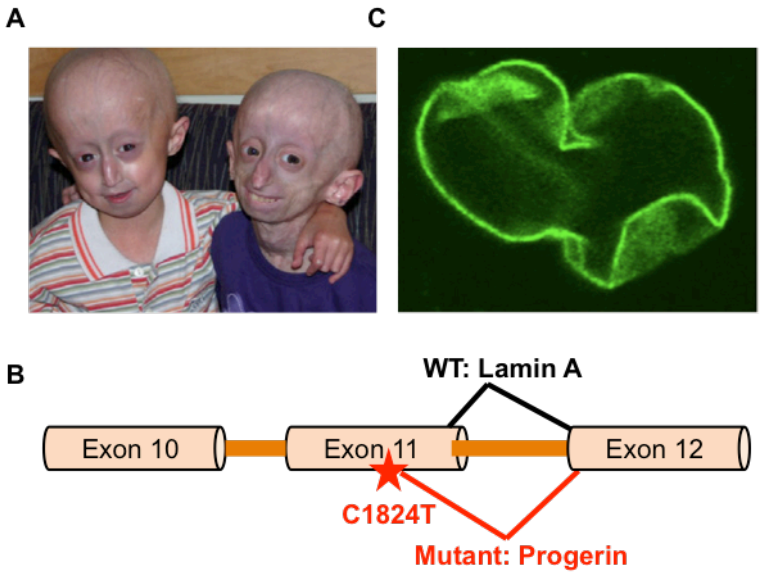

Figure 1.4. HGPS patients and disease features.

(A) Two HGPS patients showed (B) The *de novo* C1824T mutation introduces a cryptic splice site within exon 11 of the *LMNA* gene that leads to the removal of 150 nucleotides and creates an internal deletion of 50 amino acids in the translated lamin A protein "progerin". (C) GFP-tagged progerin accumulated at the periphery of nuclei and altered nuclear morphology[23]. Reprinted with permission from "Progeria: A Paradigm for Translational Medicine" by Gordon, L.B. *et al.*, 2014. Cell, Vol. 156, pg. 400–407. Copyright (2014), Elsevier Inc.

Homozygous or compound heterozygous mutations in the *ZMPSTE24* gene have been reported from MAD-B and RD patients and are listed in Table 1.1. MAD is an autosomal recessive disorder and only has approximately 40 cases reported. Mutations are found in both *LMNA* (MAD-A) and *ZMPSTE24* genes (MAD-B), where MAD-B is characterized with more generalized fat loss throughout the entire body. MAD is a much milder form among these progeroid diseases. Compared to HGPS, MAD patients (Figure 1.5.A) have a longer lifespan with an age of 20 years or above and present less severe clinical features, such as less retarded growth and slower lipodystrophy progress. However, more severe osteolysis has been observed and thus increase the risk of fractures[27]. RD is an autosomal recessive disorder caused by either dominant *LMNA* mutations or by recessive *ZMPSTE24* null mutations. As a rare neonatal lethal

disorder, patients (Figure 1.5.B) can be easily recognized at birth with features of thin, tight, and rigid skin with erosions at flexure sites, superficial vessels, typical facial dysmorphism with a small pinched nose and sparse or absent eyelashes and eyebrows, generalized joint ankylosis and normally die within the first week after birth[28].

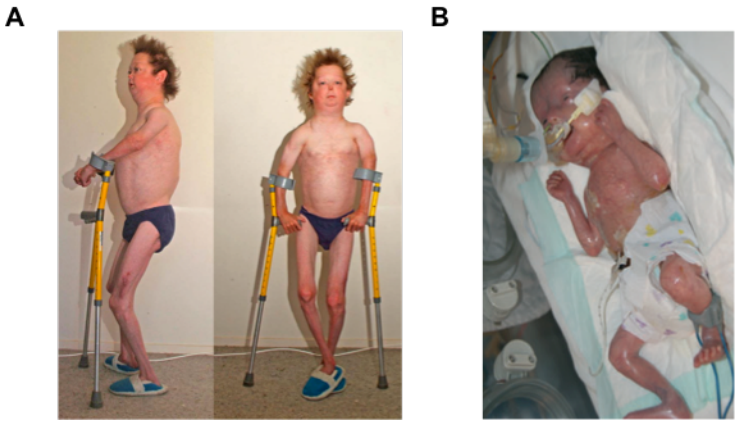

Figure 1.5. Photographs of the (A) MAD-B and (B) RD pateints.

(A) The MAD-B patient (aged 13 years) showed sparse hair, a small beaked nose, a protuberant abdomen, and fixed flexion contractures at the knees with a bowed, shortened left humerus[29]. (B) The RD patient (31 weeks of gestation) showed shiny, taut translucent skin with prominent superficial veins, and generalized joint ankylosis[30]. (A) Reprinted with permission from "Skeletal phenotype of mandibuloacral dysplasia associated with mutations in *ZMPSTE24*" by Cunningham, V. *et al.*, 2010. Bone, Vol. 47, pg. 591–597. Copyright (2010), Elsevier Inc. (B) Reprinted with permission from "A newly identified splice site mutation in *ZMPSTE24* causes restrictive dermopathy in the Middle East" by Sander, C. *et al.*, 2008. British Journal of Dermatology, Vol. 159, pg. 961–967. Copyright (2008), British Association of Dermatologists

Recently, patients of metabolic syndrome (MS) and non-alcoholic fatty liver disease (NAFLD) were also found to have *LMNA* or *ZMPSTE24* mutations, which are listed in Table 1.1. MS is a cluster of metabolic risk factors, including hypertension, insulin resistance and abnormal cholesterol level, affecting about 34% of Americans based on the data from the American Heart Association. NAFLD is a condition in which excess fat is stored in the liver of people who drink little to no alcohol, affecting about 31% of Americans based on the data from the American Liver Foundation. Both MS and NAFLD are associated with lipodystrophy and have shown abnormal nuclear morphology and prelamin A accumulation in the nucleus[31–34].

Table 1.1. ZMPSTE24 mutations identified in patients with progeroid diseases

Type	Disease	Allele 1 Mutation	Allele 2 Mutation	Reference
1	RD	p.Lys17Serfs*21	p.Leu362Phefs*19	28,35
2	RD	p.Tyr70Serfs*4	p.Tyr70Serfs*4	28
3	RD	p.Ile19Tyrfs*28	p.Arg276*	28,36
4	RD	p.Arg369*	p.Arg369*	28
5	RD	p.Thr159_Leu209del	p.Val210Aspfs*21	28
6	RD	p.Gly256Glufs*2	p.Leu362Phefs*19	28
7	RD	p.Leu362Phefs*19	p.Leu362Phefs*19	36–43
8	RD	p.Leu362Phefs*19	pLeu91_Leu209del	37
9	RD	p.Leu362Phefs*19	p.Gln417*	37
10	RD	p.Leu362Phefs*19	p.Pro99Leufs*38	37
11	RD	p.Ile198fs*19	pIle198fs*19	36
12	RD	p.Ile19Tyrfs*28	p.Ile19Tyrfs*28	36
13	RD	p.Leu362Phefs*19	p.Ile198fs*19	36
14	RD	p.Thr159_Leu209del	p.Thr159_Leudel	30
15	RD	p.Leu462Arg	ND	44
16	RD	p.Glu239*	p.Glu239*	45,46
17	RD	p.Glu231*	p.Glu231*	47
18	RD	p.Trp340*	p.Trp340*	39,40
19	RD	p.Lys17Serfs*21	p.Tyr195Phefs*22	35
20[a]	MAD-B	p.Leu362Phefs*19	p.Asn265Ser	48,49
21	MAD-B	p.Val402Phefs*6	p.Asn265Ser	28
22	MAD-B	p.Leu362Phefs*19	p.Trp340Arg	50
23	MAD-B	p.Val402Serfs*1	p.Val402Serfs*1	51
24	MAD-B	p.Gln41*	p.Pro248Leu	52
25	MAD-B	p.Pro248Leu	p.Trp450*	39,40
26	MAD-B	p.Asn256Ser	p.Tyr70Serfs*4	29
27	MAD-B	p.Leu94Pro	p.Leu94Pro	53
28	MAD-B	p.Tyr399Cys	p.Tyr399Cys	54
29	MAD-B	p.Leu425Pro	p.Leu425Pro	55
30	MS/NAFLD	p.Leu438Phe	ND	32–34

[a] Some patients with these mutations showed mixed symptoms of HGPS, MAD-B and RD.

Lipodystrophy, a medical problem with an abnormal fat distribution in the body, is a typical symptom of patients with progeroid diseases. Interestingly, this is also a common side effect for HIV patients receiving highly active antiretroviral therapy (HAART) with HIV protease inhibitors (HIV-PIs)[56]. Neither *LMNA* or *ZMPSTE24* mutations have been identified in patients with HIV-related lipodystrophy. Caron *et al.* reported that prelamin A accumulation and sterol response element binding protein 1 (SREBP-1) mislocalization were observed in adipocytes treated with certain types of HIV-PIs, such as indinavir and nelfinavir[57]. SREBP-1 is

a transcription factor that regulates genes involved in lipid biosynthesis and has been reported as a prelamin A interactor[58,59] with binding to the C-terminus of prelamin A[60]. SREBP-1 was still able to bind to with the disease mutants of prelamin A, such as R482W from Dunnigan type familial partial lipodystrophy (FPLD2), Δ607-656 from HGPS, and the uncleavable form of prelamin A, L647R. The complexes were highly distributed at the nuclear periphery and not in the nucleoplasm, as seen in the complex with wild-type prelamin A, and thus deregulated SREBP1 function[60,61].

The effect of HIV-PIs on lamin A processing was still unclear until Coffinier *et al.* showed that a subset of HIV-PIs, including lopinavir, ritonavir, and tipranavir, inhibited ZMPSTE24 and led to the accumulation of uncleaved, farnesylated prelamin A in fibroblast cells[62,63]. Several studies support ZMPSTE24 inhibition by HIV-PIs. For example, Clark *et al.* used a FRET-based assay to demonstrate that the AAX cleavage by ZMPSTE24 was inhibited by HIV-PIs using a competitive mechanism[64]. Mehmood *et al.* observed binding between HIV-PIs and ZMPSTE24 with a K_D around 30 μM, utilizing a competitive drug-binding assay and QToF mass spectrometry[65]. In Chapter 4, we also examined whether the upstream cleavage of ZMPSTE24 is inhibited by HIV-PIs using a newly established FRET-based assay and showed that the IC_{50} of lopinavir was about 30 μM.

1.1.4.2 Mouse Models of Progeroid Diseases

Mouse models have been widely used to study the molecular mechanisms of progeroid diseases. The mouse and human amino acid sequences of ZMPSTE24 share 93% identity[66]. In 2002, Pendas *et al.* and Bergo *et al.* generated *Zmpste24*$^{-/-}$ mice independently, which was the first mouse model of progeroid disease (Figure 1.6)[67,68]. *Zmpste24*$^{-/-}$ mice have shown many features that are similar to the progeroid phenotypes, including growth retardation, less weight gain, loss of adipose tissue, muscle weakness, multiple spontaneous bone fractures, and premature death with an average lifespan of 20 weeks. Moreover, biochemical activities of membrane extraction from the cells and tissues of *Zmpste24*$^{-/-}$ mice were examined, demonstrating that prelamin A is the substrate of ZMPSTE24. Defective prelamin A processing in *Zmpste24*$^{-/-}$ mice led to farnesylated prelamin A accumulation at the nuclear envelope, which might cause abnormality in nuclear architecture and premature senescence at the cellular level[66–68].

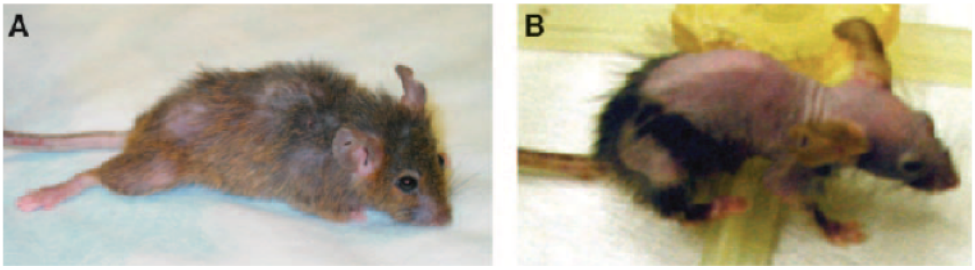

Figure 1.6. Photographs of *Zmpste24*$^{-/-}$ mice.

(A) Zmpste24-/- mouse showed a hobbling gait with dragging of the hind limbs. (B) Zmpste24-/- mouse at the age of 6 months showed loss of fur and subcutaneous fat[68]. Reprinted with permission from "*ZMPSTE24* deficiency in mice causes spontaneous bone fractures, muscle weakness, and a prelamin A processing defect" by Bergo, M. *et al.*, 2002. PNAS, Vol. 99, pg. 13049–13054. Copyright (2002), National Academy of Sciences, U.S.A.

Other mouse models were generated as well by modifying the *LMNA* gene. In 2005, Yang *et al.* created *Lmna*$^{HG/+}$ mice by the deletion of intron 10, the last 150 nucleotides of exon 11, and intron 11, and thus produced large amounts of progerin to induce nuclear blebbing. The *Lmna*$^{HG/+}$ mice showed slow growth, weight loss, bone abnormalities, loss of fat, and 50% died or were sick by the age of 27 weeks. However, compared to *Zmpste24*$^{-/-}$ mice, *Lmna*$^{HG/+}$ mice had normal grip strength and did not show cardiovascular defects[69,70]. In 2011, Osorio *et al.* described a new mouse model by introducing a nucleotide mutation (c.1827C>T; p.Gly609Gly) into one allele to mimic the human LMNA cryptic splicing site. The *Lmna*$^{G609G/G609G}$ mice also displayed a slower growth rate, reduced weight gain, increased vascular smooth muscle calcification, cardiovascular alternation, and died at age of 14 weeks. They also developed abnormal nuclear morphology with progerin accumulation in the nucleus[71,72]. These progeroid mouse models have provided valuable insights into the mechanism of disease development.

1.1.4.3 Premature and Normal Aging

It remains a mystery as to why losing the cleavage of the last 15 residues from prelamin A by ZMPSTE24 leads to cell dysfunction[a]. Under normal circumstances, lamin A and other lamin proteins form a meshwork that underlies the nuclear envelope to support the nucleus structure and interact with different binding partners. If the maturation pathway is blocked, this may disrupt the structural and functional integrity of the nuclear lamina and alter regulation of

[a] All affected mechanisms and pathways are reviewed in Reference 73 and 74.

gene expression and signaling pathways[73,74]. For example, disturbed Wnt signaling[75,76], up-regulated Notch signaling[77], and hyperactivated NF-κB[78] were found in progeroid mice.

One of the best-characterized interaction partners of lamin A is lamina-associated polypeptide 2α (LAP2α). Unlike other LAP isoforms, LAP2α lacks a transmembrane domain and localizes in the nuclear interior, where it tightly binds to nucleoplasmic lamin A and regulates cell proliferation[79]. Lower LAP2α levels have been observed in normal aging, as well as in HGPS patient cell lines. Vidak *et al.* proposed that progerin expression dramatically reduces the cellular levels of LAP2α and prevents cell proliferation[80]. Moreover, Chojnowski *et al.* reported a weaker interaction between progerin and LAP2α and observed reduced LAP2α association with telomeres, which may interfere with cell division[81].

Prelamin A accumulation also elevates genomic instability by negatively affecting DNA damage repair pathways. Recruitment of DNA repair factors, such as 53BP1 and Rad51, to the damage sites were impaired in *Zmpste24*$^{-/-}$ cells, resulting in defective DNA repair[82]. Accumulation of reactive oxygen species (ROS) also results in genomic instability. Recently, Kubben *et al.* reported that progerin tightly bound to nuclear factor, erythroid 2 like 2 (NRF2), a transcription factor that regulates the expression of antioxidant proteins, resulted in NRF2 mislocalization and thus increased oxidative stress[83].

Notably, growing evidence suggests that the cleavage of prelamin A by ZMPSTE24 is important for normal aging. Besides similar symptoms of premature aging diseases and normal aging, Scaffidi *et al.* first discovered that the cryptic splicing site (p.Gly608Gly in the *LMNA* gene) was also used in skin fibroblasts from healthy individuals, with 50-fold lower use compared to HGPS patients. The use was not affected by the age of the donors and the progerin amount showed no significant increase. However, cells from older donors showed lamin A mislocalization to the nuclear rim, which is similar to the distribution pattern in HGPS[84]. Rodriguez *et al.* also confirmed that the cryptic splicing products were more than 160-fold lower in healthy donors compared to HGPS patients[85]. McClintock *et al.* reported similar observation that the mRNA levels of progerin were low in all skin fibroblast samples from all ages. However, increased protein levels of progerin were detected from the biopsies of older individuals. These cultures from older individuals also showed abnormal nuclear morphology, such as blebs and larger nuclei[86]. Besides affecting the *LMNA* gene, Ragnauth et al. reported that ZMPSTE24

expression was diminished in vascular smooth muscle cells from older individuals, resulting in uncleaved prelamin A accumulation, which induced DNA damage[87].

1.1.4.4 Current Treatments

To date, there is no cure for these diseases. Several potential therapeutic targets have been evaluated using cell-based assays or animal experiments, including targeting the prelamin A processing pathway, modifying progerin turnover, blocking alternative *LMNA* splicing, or targeting affected proteins in the nucleus or cytoplasm[23,88].

Among these candidates, lonafarnib, a farnesyltransferase inhibitor (FTI), was first used in clinical trials. FTIs were originally developed for cancer treatment, functioning by inhibiting protein farnesylation. Preclinical studies administrating FTIs showed positive effects in both *in vitro* and *in vivo* progeria disease models, including improvements in nuclear morphology in cell lines from patients and progeroid mice[17,69,89,90], as well as lifespan extension, improved body weight curves, and other disease symptoms[70,91–93]. The first clinical trial with lonafarnib began in 2007 with 26 patients enrolled and results were published in 2012. Although with certain variations, patients have experienced improvement in one or more areas, including weight gain, hearing, bone structure, and cardiovascular functions[94], and had reduced frequency of headaches and strokes[95]. Moreover, the clinical trial with lonafarnib increased the estimated lifespan by 1.6 years[96]. The mortality rate was significantly lower in the treated group at 3.7%, compared to the control group at 33.3%[24]. Recently, a survey of plasma proteins in patients before and on-therapy with lonafarnib reported that the level of alpha-2-macroglobilin, a novel stroke-associated factor, normalized with lonafarnib therapy. This study may help identify biomarkers for further disease status evaluation[97].

The clinical trial with lonafarnib was successful; however, Varela *et al.* indicated that prelamin A may have the potential for alternative prenylation[16]. Moreover, the same study indicated that using combined treatment with statin and aminobisphosphonate, which disrupt the HMG-CoA reductase pathway and prevent the formation of isoprenoids, provided phenotype improvements in progeroid mice, such as reduced growth retardation, weight gain, and extended longevity[16]. Therefore, another clinical trial with lonafarnib, pravastatin, and zoledronate began in 2009 with 37 patients enrolled and results were published in 2016. Patients have shown improvements in weight gain and cardiovascular and skeletal systems. However, compared to the

lonafarnib monotherapy treatment, only bone mineral density received more benefit and there was no cardiovascular benefit added[98].

A new clinical trial with lonafarnib and everolimus just initiated in 2016 and is still ongoing. Everolimus, an analog of rapamycin, works similarly to the inhibitor of the mammalian target of rapamycin (mTOR) but is easier for drug administration. Rapamycin has been reported to increase lifespan in a wide range of species, including yeast, drosophila and mouse[99]. Previous studies have proven that rapamycin rescued abnormal nuclear structure and delayed senescence in fibroblast cells from patients by enhancing progerin clearance through autophagy[100,101]. Other treatments, such as sulforaphane, all-trans retinoic acid and temsirolimus, also utilized autophagy mechanism and demonstrated similar beneficial effects to rapamycin[102–104]. Rapamycin and temsirolimus treatments also showed positive effects on progeroid mice, including improved heart and skeletal muscle function, increased body weight, and enhanced survival time[105–107].

Others potential treatment strategies have also been proposed[b]. Ibrahim *et al.* showed that targeting the *Icmt* gene by generating a hypomorphic allele ameliorated disease phenotypes, including extended lifespan, increased body weight, improved skeletal properties, and reduced premature senescence in fibroblasts by activating the AKT signaling pathway. The only unexpected result was that the ratio of misshapen nuclei was not affected[108]. Besides targeting post-translational modification enzymes, sequence-specific antisense oligonucleotides were utilized to block the cryptic splicing sites of progerin. Several studies indicated that treatments with antisense oligonucleotides rescued abnormal nuclear morphology and alleviated disease phenotypes in both progeroid cell lines and animal models[71,109,110]. Proteins or functions affected by abnormal prelamin A are also promising targets. For example, elevated levels of reactive oxygen species (ROS) were shown to cause accumulated DNA damage in progeria cells. Thus, several antioxidants, such as resveratrol[111] and methyl blue[112], were tested and showed ability to ameliorate progeroid features.

Dietary intervention may also be helpful for disease treatment. Kreienkamp *et al.* reported that the expression of the nuclear vitamin D receptor was reduced in fibroblasts derived from progeria patients. Supplementation of vitamin D significantly reduced progerin production and rescued the disease phenotypes[113]. A recent study by Bárcena *et al.* revealed that methionine

[b] All candidate treatment strategies are reviewed in Reference 88.

restriction extended lifespan and restored gene expression and lipid metabolism in progeroid mouse models[114]. Together, these approaches through different biological processes provide potential benefits for developing new combination therapies for future treatments.

1.2 Maturation of Yeast Mating Pheromone **a**-factor

All enzymes responsible for prelamin A processing were initially identified, well-characterized and highly conserved in *Saccharomyces cerevisiae*, which does not express prelamin A. These yeast homolog enzymes are responsible for the biogenesis of mating pheromone **a**-factor. Studies of yeast **a**-factor maturation have provided the groundwork for investigation of lamin A maturation pathway in human.

1.2.1 Yeast Mating

In *Saccharomyces cerevisiae*, when haploid cells with opposite mating types come in contact with one another, a series of physiological responses occurs. First, the mating pheromones, **a**-factor and α-factor, are expressed and exported to the G-protein coupled receptor on the surface of the haploid cells of opposite mating type, MATα or MAT**a**. Next, the G1 cell cycle arrest is induced. The mating projection, shmoo, is formed by polarization of the cell in the direction with the highest mating pheromone concentration. Once both haploid cells have polarized toward each other, they fuse to form a diploid cell, which is capable of replicating asexually via mitosis to generate identical daughters or sexually via meiosis when under nitrogen starvation to generate four haploid cells (Figure 1.7)[115].

Both mating pheromones **a**-factor and α-factor share equivalent functions in the mating process, however, they undergo significantly different post-translational modifications for maturation. The pheromone α-factor, secreted from MATα cells, is a hydrophilic 13-mer peptide without any add-on moieties and is transported from the ER through the Golgi apparatus and then to the cell surface for secretion. In contrast, the pheromone **a**-factor, which uses a non-classical secretory pathway for export from MAT**a** cells, is a farnesylated and carboxyl methylated 12-mer peptide and thus has high hydrophobicity[116].

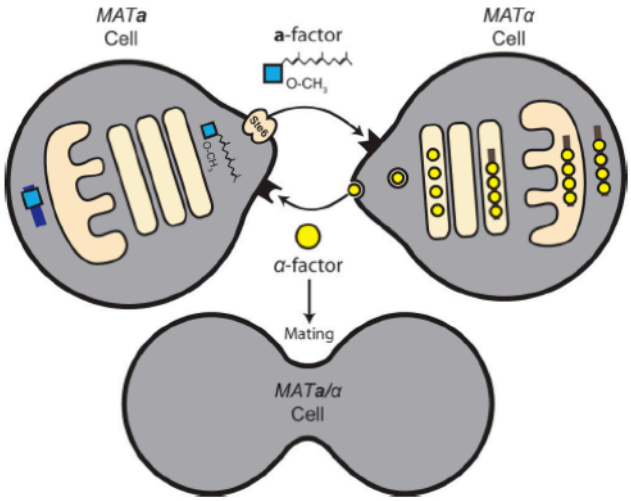

Figure 1.7. Overview of the biogenesis and secretion of **a**-factor and α-factor.

Haploid yeast cells can be one of two mating types: MAT**a** (left) and MATα (right). The two cell types release pheromones, **a**-factor and α-factor, respectively, to initiate the formation of shmoos. Cells fuse at these shmoo tips to form MAT**a**/MATα diploid cells[116]. Reprinted with permission from "Biogenesis of the Scaaharomyces cerevisiae Pheromone a-factor, from Yeast Mating to Human Disease" by Michaelis, S. *et al.*, 2012. Microbiology and Molecular Biology Reviews, Vol. 976, pg. 626–651. Copyright (2012), American Society for Microbiology

1.2.2 The Maturation Pathway of **a**-factor

The precursor of **a**-factor, redundantly encoded by the *MFA1* and *MFA2* genes, is initially synthesized as a peptide with 36 amino acids containing a CAAX motif at the end of the C-terminus. The CAAX motif triggers a set of modifications, including farnesylation by Ram 1/2, endoproteolysis of the AAX residues by either Ste24 or Rce1, and carboxyl methylation by Ste14. The second phase of the maturation pathway involves upstream cleavage of the N-terminus in two sequential steps catalyzed by Ste24 and Axl1. Lastly, the resulting mature **a**-factor is then exported from the MAT**a** cell by Ste6, an ATP-binding cassette transporter (Figure 1.8)[116,117].

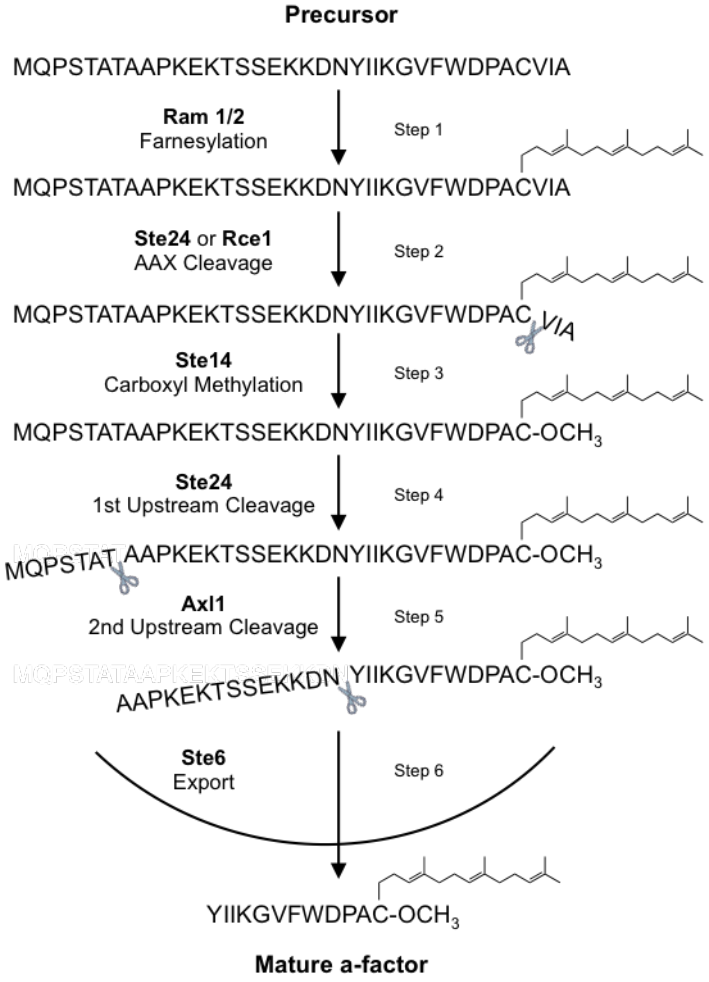

Figure 1.8. Schematic of yeast **a**-factor biogenesis pathway.

First, like all CaaX proteins, the precursor of yeast **a**-factor undergoes a series of post-translational modifications including farnesylation, endoproteolysis, and carboxylmethylation. Next, the N-terminal extension is removed by two additional cleavage events. Finally, the resulting mature **a**-factor is then exported from the cell by the ATP-binding cassette transporter[116,117].

1.2.3 Requirements for Efficient Biogenesis of **a**-factor

Like most of the CAAX proteins, **a**-factor may be farnesylated in the cytosol, transferred by an escort protein, and further modified at the cytosolic side of the ER[116]. Metabolic labeling and mating assays with the Δ*ram1* yeast strain demonstrated that farnesylation is essential for **a**-factor biogenesis[118]. No evidence indicates that **a**-factor will undergo geranylgeranylation under normal circumstances or during inhibition of farnesylation. However, Caldwell *et al.* suggested that geranylgeranylated precursor may still be able to process to mature **a**-factor, though with lower efficiency[119]. Ste24 and Rce1 are functionally redundant in that both of them can cleave the VIA tail from the precursor[118,120,121] but they have been shown to have distinct substrate specificities based on the AAX sequence[122]. Ste14, the yeast homolog of ICMT, is also the only known methyltransferase of **a**-factor. Similar to human prelamin A, methylation is not required for the following upstream cleavages of Ste24 and Axl1, but is essential for export by the Ste6 transporter[118].

The precursor of **a**-factor is required to have two additional cleavages to remove 7 and 14 residues from the N-terminus. However, the metabolic labeling experiment showed that CAAX processing was not required for these cleavages. Mutational analysis demonstrated the importance of the residues nearby the cleavage site for efficient cleavage by Ste24. For example, A8G, A8T and A9P showed completely defective **a**-factor processing[118]. Sequence of **a**-factor residues is also an important factor for Axl1 cleavage and Ste6 exportation. Surprisingly, while Δ*ste24* strain was expected to be sterile, it still showed residual mating. A possible reason may be that Axl1 was still able to perform N-terminal cleavage in the Δ*ste24* strain, though with reduced efficiency[118].

1.3 Human ZMPSTE24 and its Yeast Homolog Ste24

1.3.1 Cellular Location and Structure

ZMPSTE24 and its yeast homolog Ste24 share 36% identity and 51% similarity of sequence (Figure 1.9)[121]. Both ZMPSTE24 and Ste24 contain an ER targeting sequence, either KKXX or KXXKXX, at the C-terminus and are localized to the endoplasmic reticulum (ER) membrane. They are also dual localized to the inner nuclear membrane (INM), where the N- and C-terminus are on opposite sides of the membranes[13].

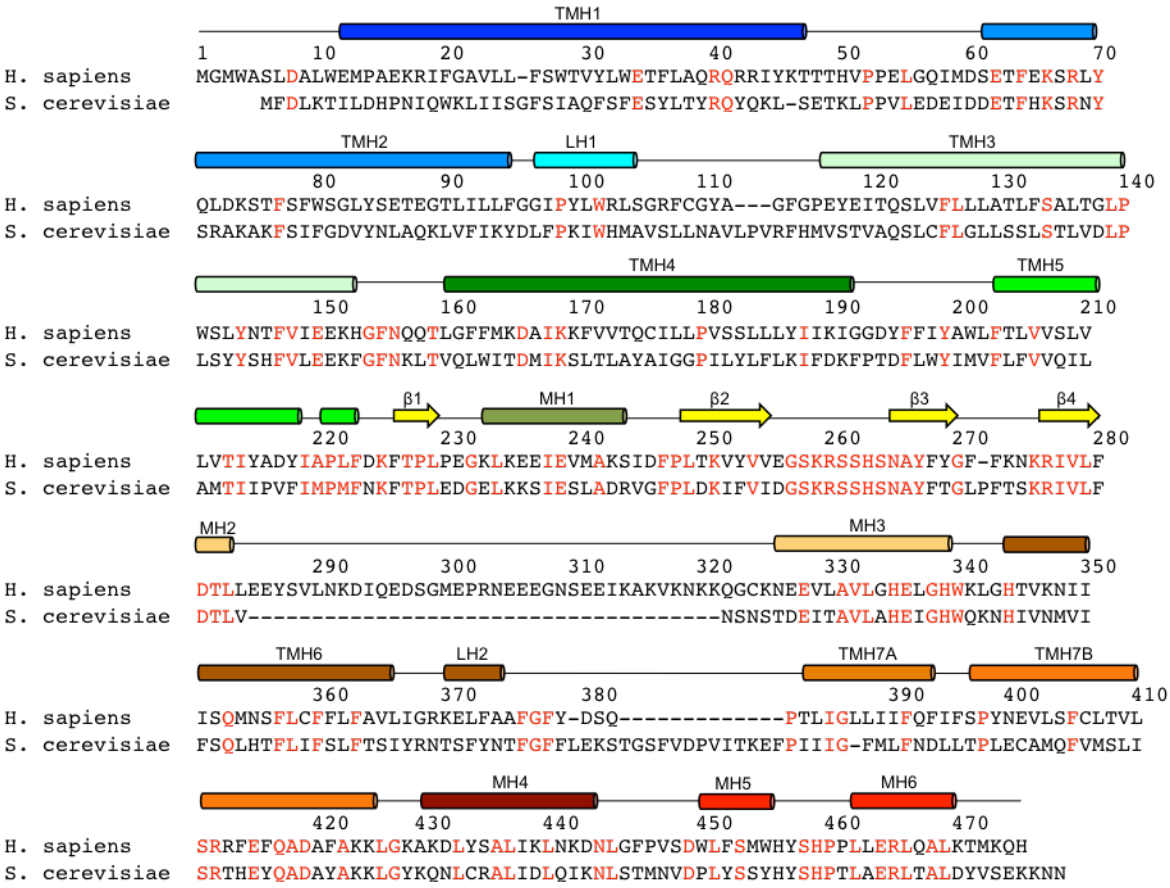

Figure 1.9. Alignment of human ZMPSTE24 and yeast Ste24 sequences.

Residues that exhibit a high degree of conservation are colored red. Secondary structure elements from the human ZMPSTE24 crystal structure are shown and labeled[20]. Reprinted with permission from "The structural basis of ZMPSTE24-dependent laminopathies" by Quigley, A. *et al.*, 2013. Science, Vol. 339, pg. 1604–1607. Copyright (2013), American Association for the Advancement of Science

These two enzymes are fundamentally different from other proteases because of their unique structures. In 2013, Quigley *et al.* utilized purified ZMPSTE24 from insect cells to solve the first crystal structure of ZMPSTE24 (PDB: 4AW6, 3.4 Å)[20]. Around the same time, Pryor *et al.* also reported the crystal structure of Ste24 (PDB: 4IL3, 3.1 Å)[123]. In 2016, Clark *et al.* published a ZMPSTE24 crystal structure (PDB: 5SYT, 2.0 Å)[64] using purified proteins from yeast. The seven transmembrane helices of the proteases surround an intramembrane hollow chamber that is capped at both ends and large enough to contain a 10-kDa protein or about 450 water molecules. The N-terminus is located in the lumen while the C-terminus, including the HEXXH zinc-binding motif, is found in the cytosol and forms the top portion of the chamber.

There are also four side portals apparent in the structure, allowing access to the chamber (Figure 1.10)[20,64].

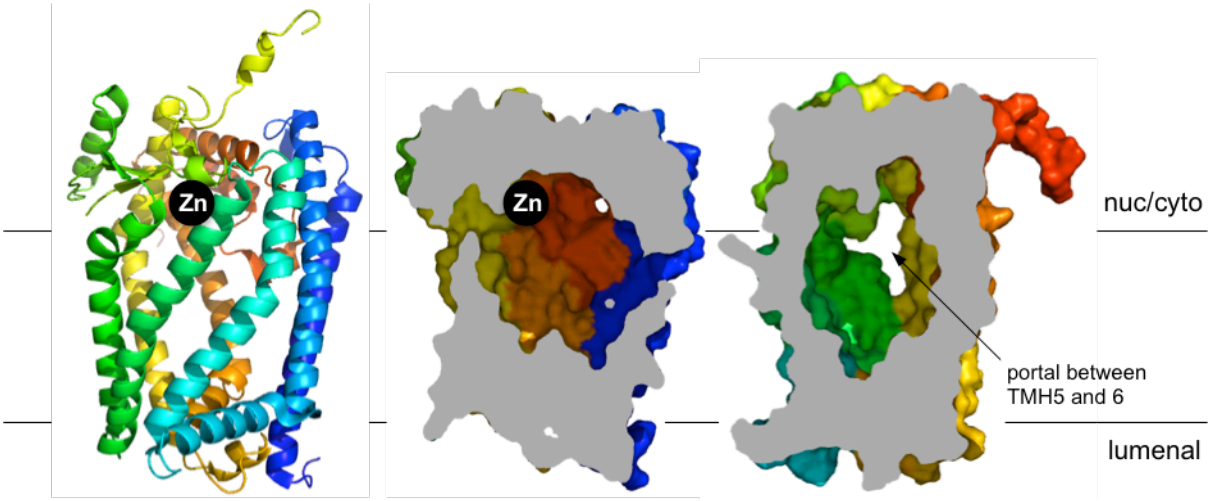

Figure 1.10. Crystal structure of ZMPSTE24.

Cartoon representation (left) of the structure, viewed in the plane of the membrane. The structure is colored from blue to red from N- to C-terminus. The zinc ion is indicated. ZMPSTE24 enclosed a hollow intramembrane chamber (middle & right), shown in the cutaway. Horizontal lines indicate the approximate extent of the lipid bilayer as observed in MD simulation[20]. PDB: 4AW6

In the co-crystal structure (PDB: 2YPT, 3.8 Å), the unmodified CSIM tetrapeptide is bound inside the chamber near the zinc ion[20]. This suggests that ZMPSTE24 mediates catalysis within the voluminous intramembrane chamber. The hypothetical reaction is that the C-terminal farnesylated tail of prelamin A inserts into the chamber to the active site through a side portal. After AAX cleavage, the substrate may completely or partially leave the chamber using one of the side portals for methylation by ICMT and then position in the chamber again for the upstream cleavage. The cleaved, farnesylated, and methylated tail may be sequestered in the chamber or be released through a side portal (Figure 1.11)[20,124]. However, the precise mechanism is still unclear.

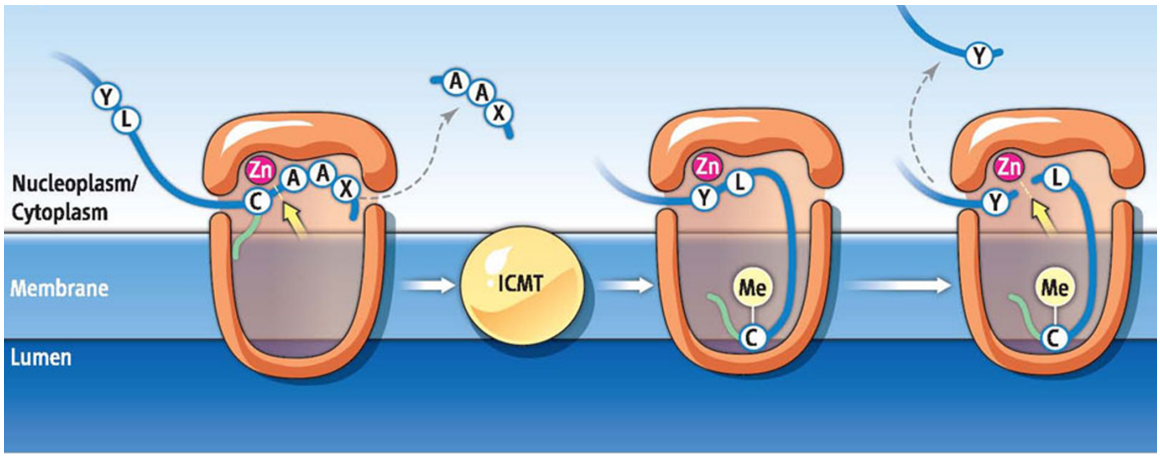

Figure 1.11. Proposed model of prelamin A processing.

ZMPSTE24 is a membrane protein with a large hollow barrel-shaped chamber enclosing the active site. Model shows farnesylated prelamin A, enters the cavity through a gap in the chamber wall between two transmembrane spans, and aligns in the active site for the first cleavage to remove the AAX tail from the C-terminus. The substrate then exits ZMPSTE24 and is methylated by ICMT. Prelamin A then re-enters and re-positions itself in ZMPSTE24, followed by the second cleavage to remove 15 residues including the farnesylated and methylated cysteine and the release of lamin A. Farnesyl group is labeled as a green line and methyl group is labeled as "Me"[124]. Reprinted with permission from "A protease for the ages" by Michaelis, S. and Hrycyna, C.A., 2013. Science, Vol. 339, pg. 1529–1530. Copyright (2013), American Association for the Advancement of Science

1.3.2 Zinc Dependency

Both ZMPSTE24 and Ste24 are zinc metalloproteases, containing a consensus zinc-binding motif HEXXH, where "H" is histidine, "E" is glutamate, and "X" can be any amino acid. The importance of zinc for ZMPSTE24 and Ste24 activities has been demonstrated. When ZMPSTE24 or Ste24 were treated with the zinc chelator 1,10-orthophenanthroline (OP), the production of **a**-factor decreased significantly. The reduced activities could be rescued by adding zinc back to the reaction mixtures[21,66,125,126].

The proposed catalytic mechanism of ZMPSTE24 by Quigley *et al.* was predicted based on the peptide hydrolysis of thermolysin, which is a classical zinc metalloprotease[127]. His-335, His-339 and Glu-415 coordinate the zinc ion. Glu-336 is predicted to be the catalytic residue by aligning and activating the catalytic water molecule, which attacks the substrate. His-459 and Asp-265 are proposed to stabilize the transition state during catalysis (Figure 1.12)[20].

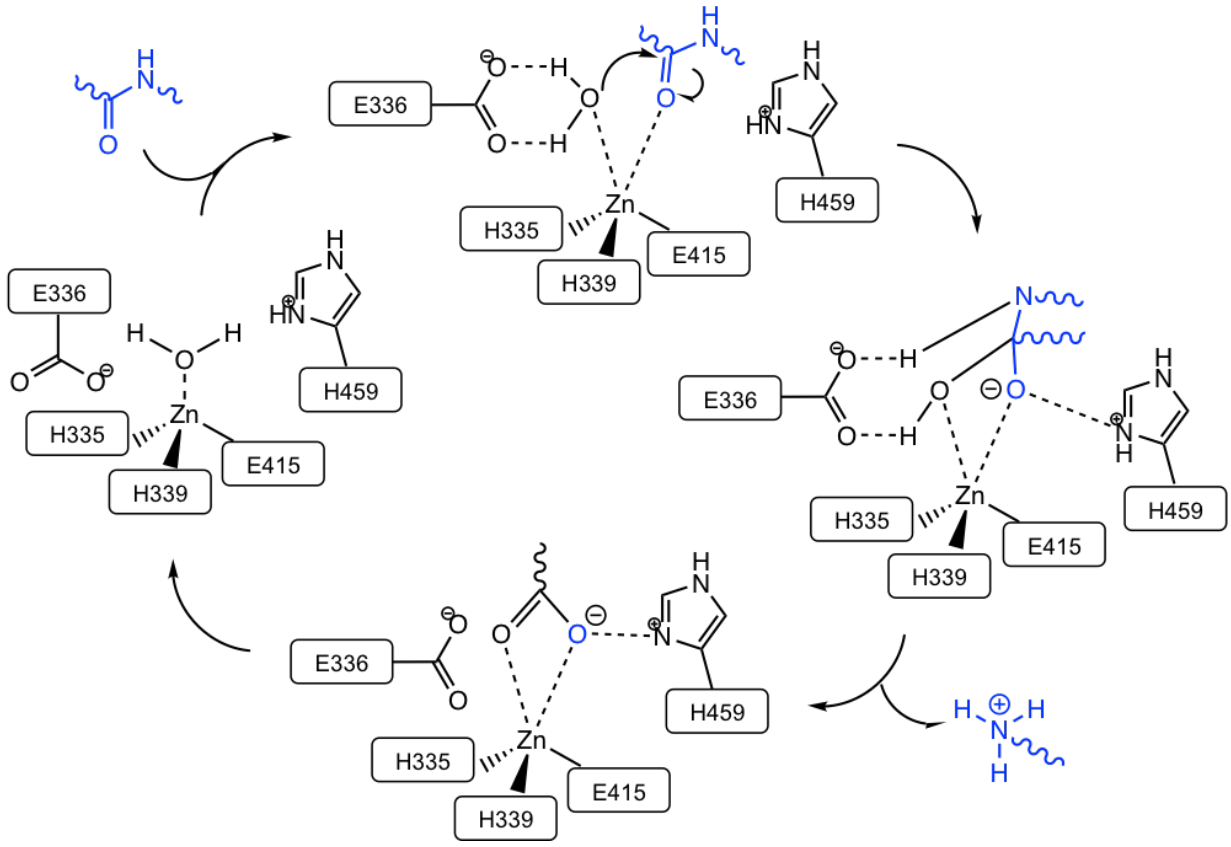

Figure 1.12. Proposed catalytic mechanism for ZMPSTE24

Reaction mechanism is predicted based on peptide hydrolysis steps of thermolysin, a classical zinc metalloprotease. The scissile peptide bonds of the substrate are represented in blue[20]. Reprinted with permission from "The structural basis of ZMPSTE24-dependent laminopathies" by Quigley, A. *et al.*, 2013. Science, Vol. 339, pg. 1604–1607. Copyright (2013), American Association for the Advancement of Science

It was unclear whether the zinc-binding motif was responsible for both cleavages due to the distinct recognition sequences at the two different cleavage sites. From mutational studies, the alanine mutation of the proposed zinc-coordinating and catalytic residues in Ste24, H297A and E298A, were not able to complement the defective mating of the Δ*ste24* strain[128]. Schmidt *et al.* demonstrated that the Ste24 mutant E298D lost the upstream cleavage activity[125]. Moreover, using the radioactive endoprotease-coupled methylation assay and the FRET-based assay, we have shown that E298A had no activity to perform both AAX and upstream cleavages *in vitro*, described in Dr. Wiley's dissertation[129] and in Chapter 3, respectively.

The alanine mutation of the ZMPSTE24 proposed catalytic residue, E336A, showed no AAX cleavage activity and no interaction with the truncated prelamin A peptide[20,65]. Barrowman

et al. demonstrated that the proposed zinc-coordinating mutation, H335A, was not able to perform the AAX cleavage using the radioactive endoprotease-coupled methylation assay[130]. The H335A also showed no upstream cleavage activity using the yeast-based platform from Spear *et al.*[131] and this result was further confirmed by the FRET-based assay, described in Chapter 4.

1.3.3 Other Functions and Associated Diseases

Besides progeroid diseases, defective prelamin A processing has been linked to cancer treatment. Moiseeva *et al.* indicated that the expression of progerin in tumor cells inhibited cell proliferation and induced p53-independent tumor cell senescence[132]. Therefore, ZMPSTE24 might be able to serve as a target for the design of p53-independent cancer inhibitors[133]. But this therapeutic idea was only examined in cell cultures and the effect in animal models is still unknown. Moreover, Lee *et al.* identified that colorectal and gastric cancer patients with a high microsatellite instability phenotype carried ZMPSTE24 frameshift mutations[134].

Prelamin A and **a**-factor were the only substrates known for ZMPSTE24 and Ste24, respectively. Interestingly, although **a**-factor is not expressed in mammalian cells, ZMPSTE24 is able to catalyze both cleavages of yeast **a**-factor and complements the mating defect of *ste24* deletion yeast strain[121,125,126,130]. ZMPSTE24 is also able to process the **a**-factor peptide with a CAMQ sequence that can only be processed by Ste24 but not Rce1[66]. Moreover, Ste24 is able to process both prelamin A cleavages, which is reported by Spear *et al.*[131] and is described in Chapter 2. However, recently there are more possible substrates and functions that have been reported for these enzymes. From Hildebrandt *et al.*, Ste24 showed substrate specificity to cleave both isoprenylated and non-prenylated peptides *in vitro*. These peptides, such as Aβ and insulin chains, may not be primary substrates of Ste24 or ZMPSTE24 since they are not localized in the ER or INM[135]. Blanden *et al.* also demonstrated that proteins other than those containing a CAAX motif undergo post-translational modifications, as **a**-factor variants with "CAAAX" could be farnesylated as well[136]. Nevertheless, this study provides a new idea that Ste24 or ZMPSTE24 may have more possible substrates and broader physiological roles.

In 2016, Ast *et al.* first linked the function of ZMPSTE24 and Ste24 to protein quality control by cleaving clogged proteins to maintain the translocation machinery across the ER membrane. Moreover, the proposed catalytic mutants, E298G of Ste24 and H335A of ZMPSTE24, were not able to cleave the clogged proteins, which indicated that the protease

activity is required for clearance of the translocon[137]. Furthermore, recently Kayatekin *et al.* demonstrated that both Ste24 and ZMPSTE24 rescued the toxicity of islet amyloid polypeptide (IAPP), which form aggregates within cells and may contribute to β cell failure in diabetes. The study also examined the rescue ability of ZMPSTE24 progeroid disease mutants and confirmed that their abilities were directly correlated to the reported declogging activity[137] and thus suggested that ZMPSTE24 may utilize the declogging activity to inhibit the toxicity of IAPP by digesting oligomeric forms of IAPP. Moreover, examination through a genetic database of patients with type 2 diabetes (T2D), 14 mutations were identified as loss-of-function variants, including previously identified progeroid mutations, such as L94P and P248L, as well as 12 mutations, which have not been previously reported[138].

Another interesting finding reported by Fu *et al.* showed ZMPSTE24 may play a role in defending cells against several enveloped viruses, which is independent of the protease activity. Co-immunoprecipitation results indicated that ZMPSTE24 interacted with interferon-induced transmembrane (IFITM) proteins, a family of antiviral effectors that prevent viral entry into the cytoplasm. Additionally, the animal study results suggesting that *Zmpste24*$^{-/-}$ mice are unable to control influenza infection, which further confirmed the antiviral function of ZMPSTE24[139].

1.4 Statement of Intent

As discussed above, several ZMPSTE24 mutations have been discovered from patients with progeroid diseases and lead to defective prelamin A processing. However, how these disease-associated mutations affect ZMPSTE24 function is still unclear. Based on structural considerations, we hypothesize that the disease mutations decrease ZMPSTE24 activity by affecting catalysis directly, preventing substrate binding in the active site, partially occluding substrate entry into or exit from the enzyme chamber, or interfering with protein folding. In this work, we have developed and utilized several different biochemical assays to examine each factor that is defective ZMPSTE24 disease mutations. Together, these data will clarify how the enzyme can malfunction, and also provide further insights into progeroid diseases.

CHAPTER 2. ZMPSTE24 AND RCE1 BOTH EFFICIENTLY CLEAVE THE CAAX MOTIF OF PRELAMIN A

The dissertation author examined the activity of MEF membranes using radioactive endoprotease-coupled methylation assays. Dr. Patricia Wiley examined the activity of yeast crude membranes using radioactive endoprotease-coupled methylation assays and performed radiolabeling and immunoprecipitation with base release assay. Dr. Sarah Hudon cloned the Ste24 and Rce1 plasmids. Dr. Susan Michaelis at Johns Hopkins University provided the ZMPSTE24 plasmid and MEF cell lines.

2.1 Introduction

Lamin A, along with lamin B and C proteins, are intermediate filament proteins that comprise the laminar network underlying the inner nuclear membrane. These nuclear lamins maintain structure and proper functioning of the nucleus, such as regulation of transcription factors and interaction with heterochromatin[2,3].

The precursor of lamin A, prelamin A, ends with a CAAX motif, in which "C" is cysteine, "A" is typically an aliphatic amino acid, and "X" is one of several amino acids. The maturation of prelamin A to lamin A occurs through a series of post-translational modifications. These include farnesylation, endoproteolysis of the AAX residues, and carboxyl methylation. After CAAX processing, an additional cleavage event occurs to remove 15 residues from the C-terminus, including the farnesylated cysteine, resulting in mature lamin A[9,10] (Figure 2.1.A).

Improper prelamin A processing caused by mutations in the genes encoding ZMPSTE24 leads to several progeroid diseases, including B-type mandibuloacral dysplasia (MAD-B) and restrictive dermopathy (RD). Recently, ZMPSTE24 mutations were also detected in patients with metabolic syndrome (MS) and nonalcoholic fatty liver disease (NAFLD)[32–34]. These mutations result in complete or partial loss of the AAX proteolytic ability of ZMPSTE24 and the accumulation of an abnormal form of prelamin A in the nucleus[28,130].

ZMPSTE24 catalyzes two distinct cleavage steps in the lamin A maturation pathway, including the endoproteolytic removal of the C-terminal AAX residues and a discrete site-specific upstream cleavage. However, many CAAX proteins have their AAX residues removed solely by another novel CAAX protease, RCE1. One exception is the yeast mating pheromone **a**-factor that can be redundantly cleaved by both CAAX proteases, yeast Rce1 and Ste24, which

are the homolog of human RCE1 and ZMPSTE24, respectively[118,120,121]. In *Saccharomyces cerevisiae*, prelamin A is not expressed, but all the proteases in prelamin A processing were first identified as homologs in yeast. The biogenesis of the yeast mating pheromone, **a**-factor, requires these same enzymes[116]. However, it remains unclear if ZMPSTE24, RCE1 or both enzymes are responsible for cleaving the CAAX box from prelamin A.

This study aims to determine if both CAAX proteases, ZMPSTE24 or RCE1 can remove the AAX tripeptide from prelamin A and if ZMPSTE24 mutations can independently affect the upstream cleavage in a ZMPSTE24-deficient expression system. If RCE1 is capable of removing the AAX tripeptide, prelamin A will be farnesylated and carboxyl methylated (Figure 2.1.B). On the other hand, if RCE1 cannot cleave the AAX amino acids from prelamin A, the disease molecule will be farnesylated but the AAX tripeptide will remain on the C-terminal tail (Figure 2.1.C).

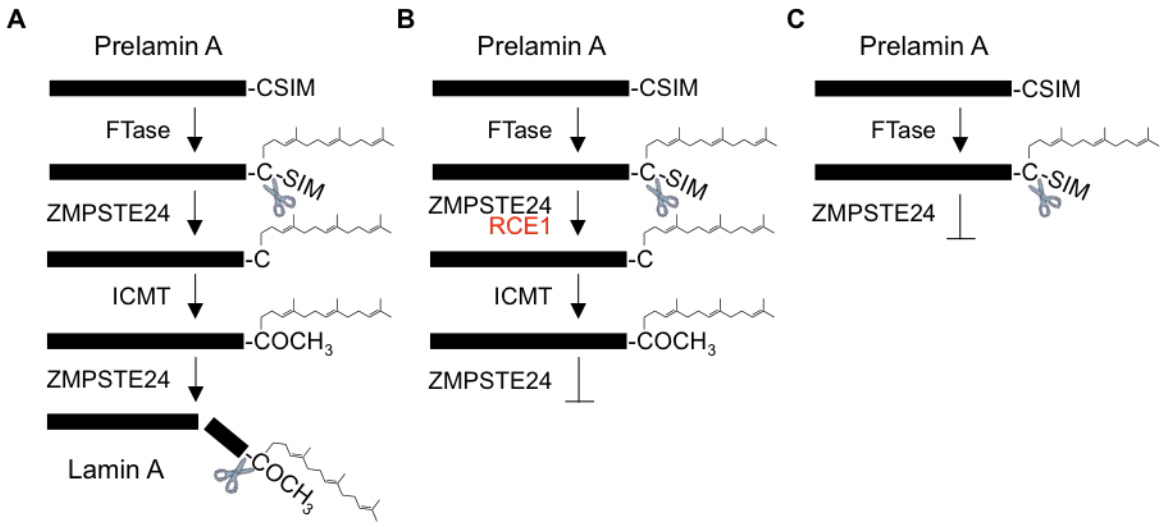

Figure 2.1. Prelamin A processing and hypothetical disease model.

(A) Normal prelamin A processing. Prelamin A terminates in the CSIM sequence, which signals CAAX processing, including farnesylation by farnesyltransferase (FTase), endoproteolysis by ZMPSTE24 and carboxyl methylation by isoprenyl carboxyl methyltransferase (ICMT). Furthermore, an additional cleavage event is required by ZMPSTE24 to remove the last 15 residues, including the newly farnesylated and carboxyl methylated cysteine from the C-terminus. (B) If RCE1 is able to cleave the AAX residues from prelamin A, the disease molecule will most likely be the farnesylated and carboxyl methylated prelamin A. (C) However, if RCE1 cannot perform the C-terminal proteolysis event, the disease molecule will be the farnesylated prelamin A with AAX residues remaining on the C-terminus.

In brief, we studied the ability of the proteases, ZMPSTE24 and RCE1 to cleave the CAAX motif of prelamin A. Using a radioactive endoprotease-coupled assay, we found that both endogenous ZMPSTE24 and RCE1 were able to cleave the AAX tail of the truncated prelamin A peptide *in vitro*. Moreover, by measuring the release of tritiated methyl group from MEFs incubated with radioactive [^{3}H-methyl]-methionine, we determined that endogenous ZMPSTE24 and RCE1 were able to mediate the C-terminal cleavage of GFP-prelamin A fusion protein *in vivo*. These findings demonstrate that ZMPSTE24 and RCE1 both cleave the CAAX motif of prelamin A. This study will help establish the nature of accumulated prelamin A that causes progeroid disorders.

2.2 Methods

2.2.1 Plasmids and Yeast Strains

The pCH1283 plasmid was generated by amplifying a fragment containing the *STE24* gene with the primers 5'-CAGGCGGCCGCTTTGATCTTAAGACGATTCTC-3' and 5'-CATGCGGCCGCTTAGTTTTTCTTCTTTTCACTAAC-3' from pCHH$_{10}$m$_3$N-Ste24 (plasmid encodes yeast *STE24* gene). The fragment was inserted into pSM1282 vector[126] by the *Not*I digestion sites. The pCHH$_{10}$m$_3$C-Rce1 plasmid was generated by amplifying a fragment containing the *RCE1* gene with the primers 5'-AGGCCCCGGGATGCTACAATTCTCAAC-3' and 5'-TGACCCCGGGCCAAGTGTTATTCTATAAC-3' from pSM1798 (plasmid encodes yeast RCE1 gene). The fragment was inserted into the pCHH$_{10}$m$_3$C[140] vector by the *Xma*I digestion sites. All constructs were sequenced bidirectionally to confirm the DNA sequence. The pCH1283 (*2μ URA3 P_{PGK}-His_{10}-HA_3-STE24*), pCHH$_{10}$m$_3$C-Rce1 (*2μ URA3 P_{PGK}-RCE1-His_{10}-myc_3*), pSM1282-ZMPSTE24 (*2μ URA3 P_{PGK}-His_{10}-HA_3-ZMPSTE24*)[130] and pCHH$_{10}$m$_3$N-Ste14 (*2μ URA3 P_{PGK}-His_{10}-myc_3-STE14*)[140] plasmids were transformed into SM3614[121], a double protease deletion yeast strain (*MAT**a** trp1 leu2 ura3 his4 can1 ste24Δ::LEU2 rce1Δ::TRP1*), using the Elble protocol[141]. After transformation, all yeast cells were grown at 30°C on synthetic complete medium without uracil (SC-URA).

2.2.2 Crude Membrane Preparation from Yeast Cells

Yeast crude membranes were prepared as described previously[130,140,142]. In brief, yeast cells were grown in SC-URA media and harvested to log phase (3-5 OD$_{600}$/ml). Cell pellets were

resuspended in lysis buffer (800 OD_{600}/ml) plus protease inhibitors (300 mM sorbitol, 100 mM NaCl, 6 mM $MgCl_2$, 10 mM Tris-HCl, pH 7.5, 1% aprotinin and 2 mM AEBSF-HCl). The cell suspension was frozen with liquid nitrogen, thawed twice and lysed by passing through a French press twice at 18,000 psi. Cellular debris was removed by centrifugation at 500 × *g* for 10 min at 4°C twice. The membrane fraction was pelleted by centrifugation at 100,000 × *g* for 1 hr at 4°C. The supernatant was removed and the membranes were resuspended on ice in 10 mM Tris-HCl, pH 7.5. The protein concentration was determined by a Coomassie protein assay using a standard curve of bovine serum albumin (BSA).

2.2.3 Crude Membrane Preparation from Mouse Embryonic Fibroblasts (MEFs)

MEFs were prepared from wild-type, *Rce1*$^{-/-}$, or *Zmpste24*$^{-/-}$ deficient mice as previously described with minor modifications[66,68,143]. All fibroblasts were cultured in 5% CO_2 and at 37°C in DMEM containing 10% FBS, 2 mM L-glutamine, 1% Penicillin-Streptomycin, 1 mM sodium pyruvate, and 1 × non-essential amino acid supplements. Cells were scraped and washed in cold phosphate buffered saline (PBS) with 1% aprotinin. Cells were then resuspended and rocked in lysis buffer with protease inhibitors (10 mM Tris-HCl, pH 7.5, 10 mM NaCl, 1 mM $MgCl_2$, 1 mM DTT, 1% aprotinin and 2 mM AEBSF). The resuspensions were then homogenized on ice with a Dounce homogenizer, and then subjected to centrifugation at 450 × *g* for 10 min at 4°C. The pellets were discarded. The supernatants with 1 mM $CaCl_2$ and 50 U/µl micrococcal nuclease were incubated on ice for 20 min and spun at 100,000 × *g* for 1 hr at 4°C. The pellets were resuspended in buffer with protease inhibitors (10 mM Tris-HCl, pH 7.5, 50 mM NaCl, 250 mM sucrose, 1 mM DTT, 1% aprotinin and 2 mM AEBSF) and 10% glycerol then frozen at -80°C.

2.2.4 Radioactive Endoprotease-Coupled Methylation Assay

The AAX proteolytic activity of yeast Ste24, Rce1, and human ZMPSTE24 crude membranes from yeast and wild-type, *Rce1*$^{-/-}$, or *Zmpste24*$^{-/-}$ membranes from MEFs were determined using a radioactive *in vitro* endoprotease-coupled methylation assay as described previously[126,130]. Briefly, 5 µg of Ste24, Rce1, and ZMPSTE24 membranes from yeast or 50 µg of wild-type, *Rce1*$^{-/-}$, or *Zmpste24*$^{-/-}$ membranes from MEFs, 10 µg of the Ste14 membranes, varying concentrations of farnesylated 15-mer **a**-factor (YIIKGVFWDPAC(Fr)-VIA, EZBioLab)

or 18-mer prelamin A (RSYLLGNSSPRTQNC(Fr)-SIM, EZBioLab) peptides, and 20 μM *S*-adenosyl-[^{14}C-methyl]-L-methionine (Perkin Elmer) were incubated in 100 mM Tris-HCl, pH 7.5. The reaction mixtures were incubated for 30 min at 30°C, quenched by 1 M NaOH and 1% SDS mixture, spotted onto pleated filter paper and then placed in the neck of a scintillation vial containing 10 ml of Biosafe II scintillation fluid (RPI) and capped. As a result of the quench reaction, the [^{14}C]-methanol was released from the cleaved and methylated substrate and diffused into the scintillation fluid for 3 hr at room temperature. After removing the filter paper, the radioactivity was quantified using a Packard TriCarb Scintillation counter. Specific activity was determined as pmol of AAX residues removed per min per mg of protease. Each value was derived from three assays performed in duplicate.

2.2.5 Radiolabeling and Immunoprecipitation with Base Release Assay

MEFs prepared from wild-type, *Rce1*$^{-/-}$, and *Zmpste24*$^{-/-}$ deficient mice overexpressing GFP-UC-PLA were utilized to analyze *in vivo* AAX cleavage of GFP-UC-PLA. Uncleavable (UC) indicates a L647R mutation of prelamin A abolishing upstream cleavage activity, there by only detecting downstream cleavage in subsequent assays. Two T-25 flasks of each cell line and NIH 3T3 fibroblasts were plated (1×10^6 cells/flask) and incubated in supplemented DMEM until cells adhered. One flask of each type of fibroblasts was incubated with 30 μM lovastatin overnight in fresh media. The three remaining flasks were incubated with only fresh media. All cell lines were labeled overnight with [^{3}H-methyl]-methionine (100 μCi/ml, specific activity 84.2 Ci/mmol, Perkin Elmer) in fresh media with or without lovastatin[144]. Radiolabeled cells were washed in cold PBS, scraped and counted by a Beckman Coulter Z1 cell counter. Cells from each cell line (approximately 1×10^6 cells) were lysed in 100 μl of Triple Detergent (TD) lysis buffer with protease inhibitors (0.1% SDS, 1% sodium deoxycholate, 1% Triton X-100, 50 mM NaCl, 100 mM Tris-Helm pH 7.5, 1% aprotinin, 670 μM AEBSF, 5 μg/μl pepstatin A, 5 μg/μl E-64, 2.5 U/ml micrococcal nuclease and 1 mM DTT) and subjected to three freeze and thaw cycles. Freeze cycles lasted for 3 min on dry ice followed by thawing in a 37°C water bath for 2 min. Following lysis, the resulting protein samples were solubilized in 400 μl of radioimmunoprecipitation assay (RIPA) buffer (25 mM Tris-HCl, pH 7.5, 150 mM NaCl, 1% Triton X-100, 1% sodium deoxycholate, 0.1% sodium dodecylsulfate) with 1% SDS and incubated with 65 μl of 50% slurry protein A sepharose beads (GE Healthcare) and 0.2 μg/ml α-

GFP antibody (ThermoFisher) for 2 hr at 4°C. Following incubation, the beads were centrifuged at 13,000 × *g* for 1 min and washed three times with RIPA buffer with 1% SDS. Following washing, proteins were eluted from protein A sepharose beads using 80 µl of 5× SDS loading buffer. Samples were incubated for 30 min at 65°C and resolved on 6% SDS-PAGE gels. Pre-stained Bio-Rad low molecular weight markers were used as standards and applied to wells between each of the MEF samples. Radiolabeled methyl esters were assayed as previously reported[145,146]. Each radioactive lane on the gel was excised into 3 mm slices and inserted into a microcentrifuge tube. Gel slices were incubated with 200 µl of 1 M NaOH, and placed into a scintillation vial containing 5 ml of scintillation fluid and capped. After 24 hr incubation at 37°C, the radioactivity diffused into the scintillation fluid and was quantified using a liquid scintillation counter. The remaining gel was transferred to a 0.2 µm nitrocellulose membrane and blocked overnight in 20% milk. Blots were probed with α-lamin A (H-102) antibody (1:400, Santa Cruz Biotechnology). Binding of the primary antibody was detected with a goat α-rabbit IgG-HRP antibody (1:10,000, ThermoFisher) and detected using the SuperSignal® West Pico Chemiluminescent Substrate (ThermoFisher) and autoradiography.

2.2.6 Immunoblot Analysis

To determine the expression levels of GFP-UC-PLA, one T-25 flask of each of the following MEF cell lines, the wild-type, *Rce1*$^{-/-}$, and *Zmpste24*$^{-/-}$, were plated and grown to 80% confluency. Cells were collected, resuspended in TD buffer, and then incubated with 5× SDS loading buffer as the last paragraph described. The samples were resolved on 6% SDS-PAGE gels then transferred to 0.2 µm nitrocellulose membranes and blocked overnight in 20% milk at 4°C. Blots were probed with α-GFP antibody (1:1,000) to detect GFP-UC-PLA. Binding of the primary antibody was detected with a goat α-rabbit IgG-HRP antibody (1:10,000, ThermoFisher) and detected using the SuperSignal® West Pico Chemiluminescent Substrate (ThermoFisher) and autoradiography.

2.3 Results and Discussion

2.3.1 C-terminal cleavage of **a**-factor and prelamin A peptides by yeast Rce1 and human ZMPSTE24 from yeast crude membranes

We first examined the ability of the farnesylated 15-mer **a**-factor and the 18-mer prelamin A peptides to act as substrates for yeast Ste24, yeast Rce1, and human ZMPSTE24. The saturation curves for **a**-factor and prelamin A peptides were performed with enzymes overexpressed in yeast membranes and determined using a radioactive endoprotease-coupled methylation assay. The $K_{m(app)}$ and V_{max} values (Table 2.1) were calculated using Graph Pad Prism for each enzyme. The negative control membranes with empty vector[130] did not demonstrate measurable activity and activity levels were subtracted as background.

The $K_{m(app)}$ value of **a**-factor for Ste24 was 4.1 ± 0.7 μM, for ZMPSTE24 was 4.5 ± 2.1 μM and for Rce1 was 15.8 ± 2.3 μM. Ste24 and ZMPSTE24 exhibited similar affinities for **a**-factor while Rce1 had a three times higher $K_{m(app)}$. The V_{max} value of **a**-factor for Ste24 was 764.5 ± 27.2 pmol/mg/min, for ZMPSTE24 was 543.1 ± 56.1 pmol/mg/min, and for Rce1 was 1696.7 ± 76.3 μM. ZMPSTE24 showed 30% lower V_{max} compared to Ste24, while Rce1 turned substrate over with a much higher V_{max}. These results are consistent to previous studies suggesting yeast Ste24, Rce1 and human ZMPSTE24 serve redundant functions in posttranslational processing of **a**-factor[66,121,125,126].

The $K_{m(app)}$ value of prelamin A for Ste24 was 0.9 ± 0.4 μM, for ZMPSTE24 was 2.5 ± 0.6 μM and for Rce1 was 12.8 ± 2.0 μM. Each enzyme obtained a similar affinity for the prelamin A substrate compared to the **a**-factor peptide. Moreover, Rce1 had more than five times higher $K_{m(app)}$ than Ste24 and ZMPSTE24. The V_{max} value of prelamin A for Ste24 was 141.7 ± 6.7 pmol/mg/min, for ZMPSTE24 was 122.2 ± 5.0 pmol/mg/min and for Rce1p was 1589.7 ± 73.0 μM. Ste24 and ZMPSTE24 demonstrated lower V_{max} values than Rce1. These data indicate that yeast Ste24, Rce1, and human ZMPSTE24 all are able to cleave both **a**-factor and prelamin A peptides but Rce1 can turn over both peptides more quickly.

Table 2.1. Kinetic constants for crude Ste24, ZMPSTE24 or Rce1 with **a**-factor and prelamin A peptides as substrates

a-factor	$K_{m(app)}$[a] (μM)	V_{max} (pmol/mg/min)	prelamin A	$K_{m(app)}$ (μM)	V_{max} (pmol/mg/min)
Ste24	4.1 ± 0.7	764.5 ± 27.2	Ste24	0.9 ± 0.4	141.7 ± 6.7
ZMPSTE24	4.5 ± 2.1	543.1 ± 56.1	ZMPSTE24	2.5 ± 0.6	122.2 ± 5.0
Rce1	15.8 ± 2.3	1696.7 ± 76.3	Rce1	12.8 ± 2.0	1589.7 ± 73.0

[a] K_m values are reported as apparent values because the concentration available to the enzyme in the crude membrane cannot be accurately determined.
[b] We used all capital letters to indicate human/mouse enzymes, such as RCE1 and ZMPSTE24. For yeast enzymes, we used sentence case letters to label, such as Rce1 and Ste24.

2.3.2 C-terminal cleavage of **a**-factor and prelamin A peptides by endogenous RCE1 and ZMPSTE24 from MEFs

We then determined the ability of the **a**-factor or prelamin A peptides to act as substrate for endogenous mouse RCE1 and ZMPSTE24 by measuring the specific activities through the radioactive endoprotease-coupled methylation assay. Reactions contained mixtures of membrane extracts from MEF cells, **a**-factor or prelamin A peptide, and with or without metalloprotease inhibitor 1,10-orthophenanthroline (OP). The specific activity with either **a**-factor or prelamin A peptides of endogenous ZMPSTE24 (from *Rce1*$^{-/-}$ MEFs) was approximately half that of endogenous RCE1 (from *Zmpste24*$^{-/-}$ MEFs) or both proteases (from wild-type MEFs) (Figure 2.2, *grey* bars). These results confirm previous *in vitro* findings that either yeast Ste24 or Rce1, homologs of human ZMPSTE24 or RCE1, can mediate AAX cleavage of both **a**-factor and prelamin A peptides. Moreover, the higher specific activities obtained from endogenous RCE1 are also consistent to the higher V_{max} obtained from yeast Rce1 crude membranes (Table 2.1).

To confirm the proteolytic activity was not generated from other proteins in MEFs, the reactions were incubated with the zinc chelator, OP. As expected, we found the proteolysis of both peptides by endogenous ZMPSTE24 were inhibited by OP (Figure 2.2, *black* bars)[66,126]. This demonstrated the cleavage was performed by ZMPSTE24, and no other protease in *Rce1*$^{-/-}$ MEF membrane preps. Protease activities from wild-type and *Zmpste24*$^{-/-}$ MEFs with OP were slightly lower than reactions without OP due to partial inhibition of RCE1[147,148]. Together, these results suggest that endogenous RCE1 and ZMPSTE24 isolated from MEFs are both able to perform the C-terminal proteolysis to remove the AAX residues from **a**-factor and prelamin A peptides *in vitro*, but RCE1 most likely plays a more dominant role.

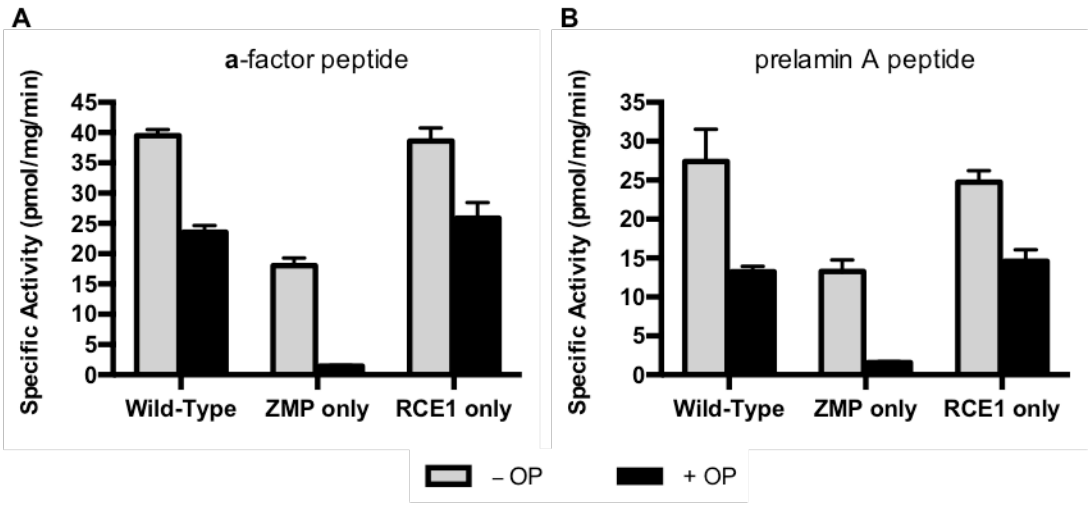

Figure 2.2. Farnesylated 15-mer **a**-factor and 18-mer prelamin A peptides are cleaved by both endoproteases, ZMPSTE24 and RCE1.

Cleavage of (A) farnesylated 15-mer a-factor and (B) farnesylated 18-mer prelamin A peptide by endogenous RCE1 or ZMPSTE24 were demonstrated by radioactive endoprotease-coupled methylation assays. Reactions contained membranes from wild-type, *Rce1*$^{-/-}$ (expressing ZMPSTE24 only), or *ZMPSTE24*$^{-/-}$ (expressing RCE1 only) MEF cells either in the absence (*grey*) or presence of 5 mM 1,10-orthophenanthroline (OP) (*black*). Specific activity was calculated as the pmol of AAX groups removed per mg of enzyme in a minute.

2.3.3 ZMPSTE24 and RCE1 are both able to mediate the C-terminal cleavage of prelamin A in MEFs

We next examined the AAX proteolysis of prelamin A by RCE1 or ZMPSTE24 *in vivo*. MEFs prepared from wild-type, *Rce1*$^{-/-}$, and *Zmpste24*$^{-/-}$ mice expressing GFP-UC-PLA and NIH 3T3 fibroblasts in the presence or absence of lovastatin, a farnesylation inhibitor. Uncleavable (UC) prelamin A, containing a L647R mutation that blocks the upstream cleavage site of prelamin A, was used here so only the AAX cleavage would be detected. Cells were labeled overnight with [^{3}H-methyl]-methionine, which was converted to ^{3}H-SAM inside the cell and used by ICMT as methyl donor. Treated cells were then lysed and size fractionated on SDS-PAGE gel. Bands were excised from the gel and incorporation of tritiated methyl group was quantified via scintillation counting.

The treatments with lovastatin, which blocks the upstream of the farnesyl pyrophosphate (FPP) production, successfully inhibited farnesylation of the prelamin A precursor and no proteolysis of the AAX tripeptide by ZMPSTE24 or RCE1 was observed.

Therefore, it is used as a negative control in the experiment (Figure 2.3.A). MEFs without lovastatin treatment displayed an increase in radioactive counts in gel slice 4 around the 100 kDa molecular weight marker where a band for GFP-UC-PLA was observed. These data indicated that the AAX tail of GFP-UC-PLA was cleaved by either ZMPSTE24 or RCE1, which allowed ICMT to transfer ^{3}H-SAM to the substrate and the release of tritiated methyl group.

Moreover, no signal was observed in samples with NIH 3T3 fibroblasts, which did not express GFP-UC-PLA (Figure 2.3.A). This indicated that the signals were not from endogenous prelamin A. All samples presented similar expression levels of endogenous prelamin A (Figure 2.3.B) and GFP-UC-PLA (Figure 2.3.C).

2.4 Conclusions

In summary, these data demonstrate that both RCE1 and ZMPSTE24 are capable of mediating the C-terminal cleavage of the truncated prelamin A peptide *in vitro* or modified prelamin A *in vivo*. Moreover, our results suggest that the disease molecule will be most likely farnesylated and methylated prelamin A, since RCE1 may retain the capacity to cleave the AAX residues of prelamin A in progeroid diseases induced by inactive ZMPSTE24 mutants. Several studies also support this suggestion. For example, a study using mass spectrometry showed that no farnesylated peptide contained the C-terminal SIM residues from prelamin A in *Zmpste24*$^{-/-}$ fibroblasts, suggesting that ZMPSTE24 is not the only enzyme can perform the AAX proteolysis of prelamin A[16]. Moreover, a animal study revealed reducing expression levels of ICMT ameliorated disease phenotypes in *Zmpste24*$^{-/-}$ mice and extended their lifespan[108], suggesting that prelamin A may be methylated in progeroid diseases. Overall, this study gives evidences that the accumulated prelamin A proteins in patients with progeroid patients are farnesylated and methylated, which provides critical insights into progeroid diseases and will benefit the development of future treatments.

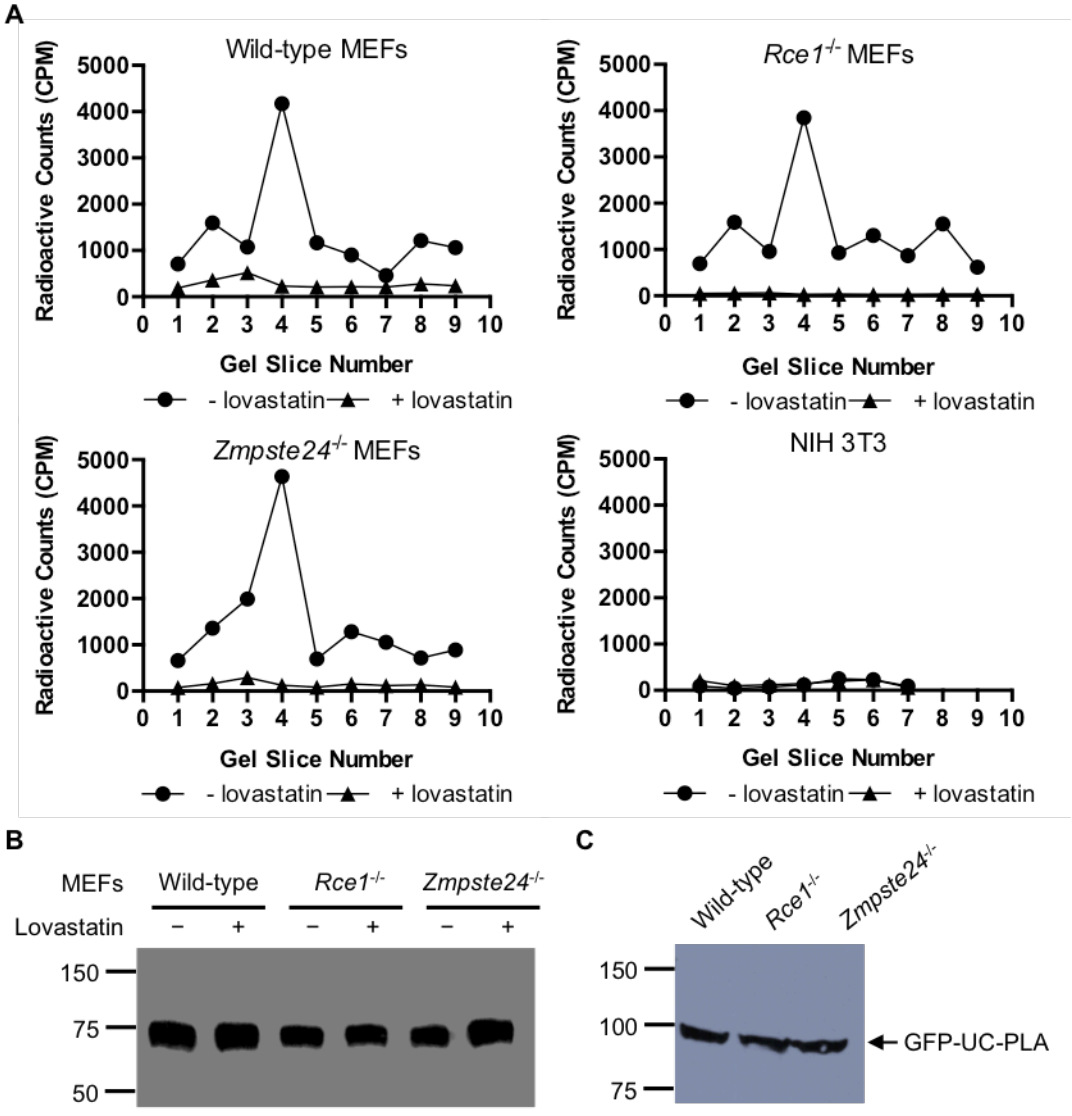

Figure 2.3. C-terminal cleavage of GFP-prelamin A is completed by both endoproteases, ZMPSTE24 and RCE1.

(A) Each MEF cell line and NIH 3T3 fibroblasts were incubated in [^{3}H-methyl]-methionine with (●) or without (▲) 30 μM lovastatin overnight. Cells were lysed and immunoprecipitated using protein A sepharose beads and α-GFP antibody. Samples were resolved on two SDS-PAGE gels, excised to nine or seven 3 mm bands, stopped upon addition of NaOH and diffused into scintillation fluid overnight. Base releasable counts were measured using liquid scintillation analysis. (B) The remaining gel was transferred to nitrocellulose membrane and probed with a α-lamin A (H-102) antibody as a loading control. (C) Each MEF cell line was lysed and subjected to SDS-PAGE and transferred to a nitrocellulose membrane. Equal expression of GFP-UC-PLA was visualized with a α-GFP-antibody in each MEF cell line.

CHAPTER 3. QUANTITATIVE FRET-BASED ASSAY FOR THE UPSTREAM CLEAVAGE ACTIVITY OF STE24

Portions of the data and text in the following chapter will be published in the book chapter "A quantitative FRET assay for the upstream cleavage activity of the integral membrane proteases human ZMPSTE24 and yeast Ste24". The dissertation author established the assay and performed all the experiments. Dr. Shengfeng Xu and Chelsea Theisen generated the Ste24 mutant plasmids. Dr. Mark Distefano at University of Minnesota synthesized the FRET peptides.

3.1 Introduction

Ste24 is a zinc metalloprotease from *Saccharomyces cerevisiae* that plays important dual roles in yeast mating pheromone **a**-factor maturation[121]. Briefly, the precursor of yeast **a**-factor undergoes a sequential of post-translational modifications including farnesylation by Ram 1/2, endoproteolysis of the AAX residues by Ste24 or Rce1 and carboxylmethylation by Ste14. Next, Ste24 removes the first seven residues from the N-terminus. Finally, Axl1 performs an additional cleavage to form mature a-factor, which is then exported from the cell by the ATP-binding cassette transporter Ste6[116,149] (Figure 3.1).

From the sequence alignment result, yeast Ste24 shares 36% identity and 51% similarity with its human homolog ZMPSTE24. ZMPSTE24 also performs two distinct cleavages to its known substrate, prelamin A. Mutations in ZMPSTE24 were found from patients with progeroid diseases or metabolic syndrome[28,131] and might lead to failure of proper prelamin A processing, causing uncleaved prelamin A accumulation in the nucleus[9,10]. Recently, our research results have suggested that the upstream cleavage ability of ZMPSTE24 may determine the accumulation level of uncleaved prelamin A in progeroid diseases (unpublished data from Dr. Wiley, shown in Chapter 2). Interestingly, ZMPSTE24 complements the mating defect of a *STE24* deletion yeast strain and is able to catalyze both cleavages in yeast **a**-factor[125,130].

Moreover, the crystal structures of Ste24 and ZMPSTE24 are highly similar and reveal a fascinating architecture distinct from other proteases[20,64,123,124]. The seven transmembrane helices of the protease surround a large intramembrane chamber that is capped at both ends. The HEXXH zinc metalloprotease consensus motif forms the top portion inside of the chamber where proteolysis is proposed to occur. Moreover, there are openings apparent in the structure, at least some of which are likely to provide sites for substrate entry and product release from the

chamber. However, the precise catalytic mechanisms of these unique enzymes are still unclear due to the lack of available assays.

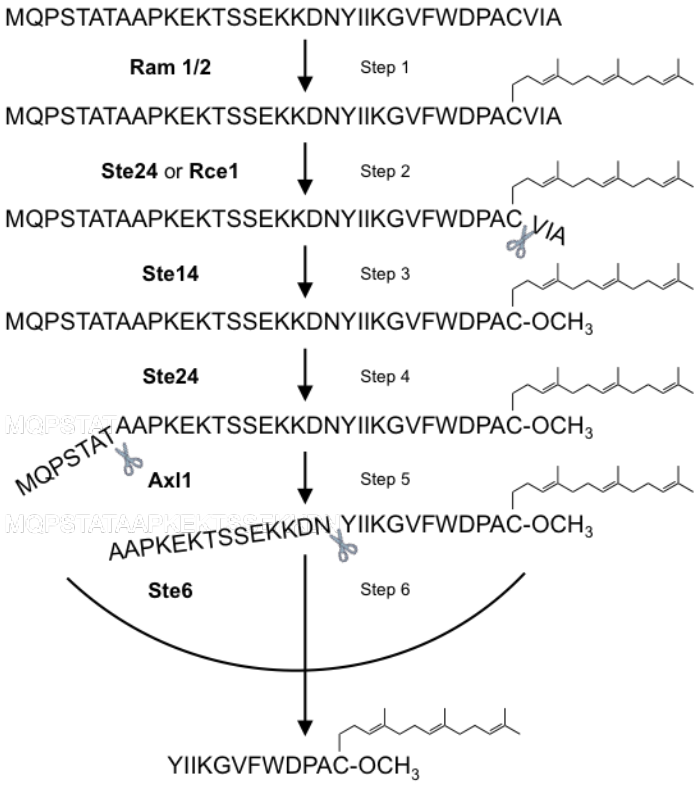

Figure 3.1. Schematic of yeast **a**-factor biogenesis pathway.

The **a**-factor precursor is a 36-mer peptide containing a CVIA motif at the C-terminus. Like other CAAX proteins, the **a**-factor maturation pathway undergoes three sequential post-translational modifications, including farnesylation by Ram1/2, endoproteolysis by Ste24 and Rce1 and carboxyl methylation by Ste14. Next, the N-terminal extension is removed by two additional cleavages by Ste24 and Axl1 to form mature **a**-factor. Finally, the resulting mature **a**-factor is then exported from the cell by Ste6[116,117].

Assays for detecting the AAX proteolysis (Figure 3.1, *step 2*), for which Ste24 function is redundant with another novel CAAX protease, Rce1, have been reported for use in examination and quantification of Ste24 activity[62–64,123,130,135,142,150–152]. For the upstream cleavage (Figure 3.1, *step 4*), cleavage of a radiolabeled substrate by Ste24 can be detected as a mobility shift by SDS-PAGE[118,121,125,126]. Mass spectrometry has also been reported to monitor proteolysis and substrate binding[65]. However, there is no available assay that can demonstrate quantitatively the *in vitro* upstream cleavage activity. Here, we developed an assay adapted from

a previously reported FRET assay for CAAX proteases that measures the fluorescence from a dequenched K-Ras 4B derived peptide[64,123,135,152].

The probe used in this assay was designed based on the sequence of yeast **a**-factor, the only known natural substrate of Ste24. This 33-mer **a**-factor analog (Peptide **1**) has a 2-aminobenzoic acid (Abz) fluorophore at the N-terminus and a dinitophenol (Dnp) quencher located on the other side of the proposed cleavage site. The peptide does not contain the AAX tail, but instead contains a carboxyl methyl group on the C-terminal cysteine, which mimics the processed substrate for the upstream cleavage. After cleavage, fluorescence from the dequenched peptides enabled us to continuously monitor and quantify Ste24 upstream proteolytic activity (Figure 3.2).

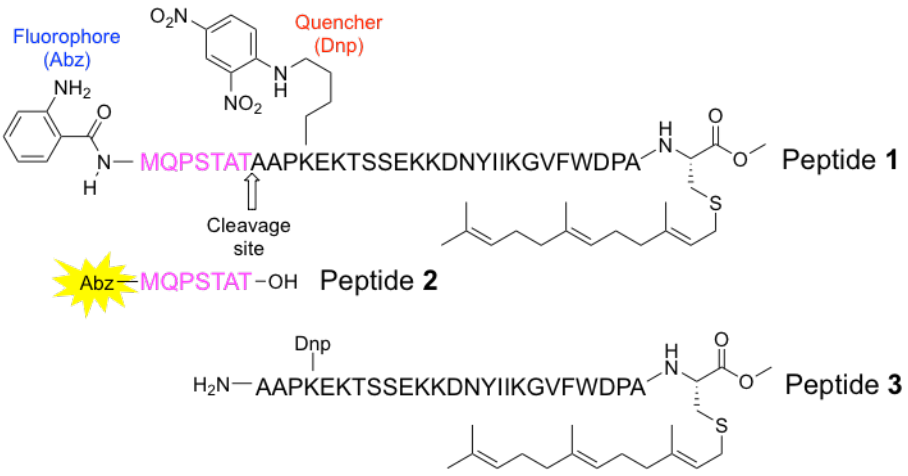

Figure 3.2. Schematic depiction of the FRET-based assay for Ste24 cleavage.

Peptide **1** mimics the natural farnesylated and carboxyl methylated Ste24 substrate. The Abz (fluorophore) and the Dnp (quencher) are attached at the N and C terminus of the peptide, respectively. Ste24 cleavage results in two cleavage products, Peptide **2** and Peptide **3**. Fluorescence released from the Abz group is measured at 420 nm.

To our knowledge, this is the first assay described that is able to precisely quantify the kinetics of the upstream cleavage activity of Ste24. In this study, we demonstrated that Ste24 could recognize and efficiently cleave the internally quenched fluorescent probe at the natural cleavage site. The kinetic parameters of the Ste24 upstream cleavage were determined. This novel assay was also capable to characterize the effect of Ste24 mutations and inhibitors.

Together, our FRET assay provides a new useful tool with which to further study the properties of Ste24.

3.2 Methods

3.2.1 Peptide Synthesis

All peptides were synthesized by the Distefano lab (University of Minnesota). All solvents and reagents used for the synthesis of the fluorescent assay peptides and cleaved products were of analytical grade and purchased from Peptides International, NovaBioChem®, or Sigma-Aldrich. Fmoc-Cys(Trityl-Resin)-OCH_3 was prepared as previously described[153,154]. HR-ESI-MS analysis was performed using a Bio-TOF-II (Bruker) mass spectrometer.

3.2.1.1 Abz-MQPSTATAAPK(Dnp)EKTSSEKKDNYIIKGVFWDPAC-OMe

Peptide synthesis was carried out using the PS3 automated solid-phase peptide synthesizer (Protein Technologies Inc) employing standard Fmoc/HCTU based chemistry. Synthesis was initiated on 0.1 mmol Fmoc-Cys(Trityl-Resin)-OCH_3 resin. The peptide chain was elongated using HCTU/*N*-methylmorpholine-catalyzed, single coupling steps with 4 eq of both protected amino acids and HTCU for 30 min. Following complete chain elongation, the N-terminal Met residue of the peptide was deprotected with 20% (v/v) piperdine in DMF, and the presence of the resulting free amine was confirmed by ninhydrin analysis followed by manual coupling of the Abz group. The peptide was cleaved from the resin along with simultaneous side chain deprotection by treatment with Reagent K containing 10 ml of TFA, 0.5 g of crystalline phenol, 250 µl of 1,2-ethanedithiol, 500 µl of thioanisole, and 500 µl of H_2O for 2 hours at room temperature. The released peptide was collected and combined with TFA washes of the resin before precipitation of the peptide in 100 ml of chilled ethanol. The crude solid peptide was collected by centrifugation, the supernatant was removed, and the resulting pellet was washed twice with 50 ml of chilled ethanol, repeating the centrifugation and supernatant removal steps each time. The crude peptide was purified using a semi-preparative C_{18} RP-HPLC column with detection at 220 and 280 nm and eluted with a gradient of Solvent A (H_2O and 0.1% (v/v) TFA) and Solvent B (CH_3CN and 0.1% (v/v) TFA). For purification, the crude peptide was dissolved in 10 ml of DMF, applied to the column equilibrated in Solvent A, and washed with 15% Solvent B until no absorbance was detected at 220 nm. The peptide was eluted using a linear gradient

(15-85% Solvent B over 1.5 hours at a flow-rate of 5 ml/min). Fractions containing the desired mass determined by MS analysis were checked for purity by analytical C_{18} RP-HPLC employing a linear gradient (0-100% Solvent B over 1 hour at a flow-rate of 1 ml/min) and detected at 214 nm. Fractions that contained the desired mass and had above 90% purity were pooled and lyophilized to yield 138 mg (35%) of desired peptide as a yellow powder. ESI-MS calculated for $C_{175}H_{262}N_{44}O_{56}S_2$ $[M+3H]^{+3}$: 1314.2894, found 1314.2854.

3.2.1.2 Abz-MQPSTATAAPK(Dnp)EKTSSEKKDNYIIKGVFWDPAC(Fr)-Ome

Peptide **1** will be used to indicate this peptide in the following section. 1 eq of Abz-MQPSTATAAPK(Dnp) EKTSSEKKDNYIIKGVFWDPAC-OMe (75 mg, 19 μmol) from Chapter 3.2.1.1 was dissolved in 15 ml of DMF/H_2O (9:1) and 0.1% (v/v) TFA after which 5 eq of farnesyl bromide (27 mg, 95 μmol) and 5 eq of $Zn(Oac)_2$•$2H_2O$ (20.8 mg, 95 μmol) were added, and the reaction was mixed for 12 hours. The reaction mixture was purified by semi-preparative C_{18} RP-HPLC chromatography using a similar procedure as described above, and identified via ESI-TOF-MS. The reaction yielded 19.7 mg (25%) of the desired alkylated peptide (Peptide **1**). Purity by HPLC: 95.2%; ESI-MS: calculated for $C_{190}H_{286}N_{44}O_{56}S_2$ $[M+3H]^{+3}$: 1382.3521, found 1382.3482.

3.2.1.3 Abz-MQPSTAT

Peptide **2** will be used to indicate this peptide in the following section. Peptide synthesis was initiated on 0.05 mmol Fmoc-Thr(tBu)-Wang resin and followed the same SPPS and purification as described in Chapter 3.2.1.1. Reagent K cleavage and HPLC purification yielded 22.3 mg (52%) of desired peptide as a white powder. Purity by HPLC: 92.8%; ESI-MS: calculated for $C_{36}H_{55}N_9O_{13}S$ $[M+1H]^+$ 854.3718, found 854.3702.

3.2.1.4 AAPK(Dnp)EKTSSEKKDNYIIKGVFWDPAC(Fr)-OMe

Peptide **3** will be used to indicate this peptide in the following section. Peptide synthesis was initiated on 0.05 mmol Fmoc-Cys(Trityl-Resin)-OCH_3 resin and followed by the same SPPS and purification as described in Chapter 3.2.1.1. After Reagent K cleavage and HPLC purification, 1 eq of free thiol-containing peptide (30 mg, 9.6 μmol) was prenylated using the same conditions as used in Chapter 3.2.1.2. This reaction yielded 6.7 mg (21%) of the desired

alkylated peptide. Purity by HPLC: 93.4%; ESI-MS: calculated for $C_{154}H_{233}N_{35}O_{44}S$ $[M+3H]^{+3}$ 1103.9008, found 1103.8942.

3.2.2 Plasmids and Yeast Strains

The plasmids and primers used in this study are listed in Table 3.1. Ste24 mutants were generated by overlap extension Polymerase Chain Reaction (PCR) site-directed mutagenesis. In brief, designed mutant oligonucleotides were used to introduce the single alanine mutations into *STE24*. SVEC primers were for aligning within the pCH1283 vector. A two-step PCR procedure was used to introduce mutation using GoTaq® Green Master Mix (Promega). Amplified products were purified using QIAquick PCR Purification Kit (Qiagen). The purified fragments and pCH1283 vector were digested with EagI restriction enzyme, excised, and purified with QIAquick Gel Extraction Kit (Qiagen). Products were ligated into vector using the Rapid DNA Ligation Kit (Invitrogen). The plasmids were transformed into *E. coli* DH5α competent cells (Invitrogen). Single colonies were selected for overnight growth in Luria-Bertani (LB) broth containing 100 μg/ml ampicillin, and plasmids were purified using QIAprep Spin Miniprep Kit (Qiagen). Sequences were confirmed using bi-directional dye-terminator sequencing (BigDye® Terminator v3.1) by Purdue University Genomics Facility. Each plasmid was transformed and expressed in the strain SM3614 (*MAT**a** trp1 leu2 ura3 his4 can1 ste24Δ::LEU2 rce1Δ::TRP1*)[121] using the Elble protocol[141]. After transformation, all yeast cells were grown at 30°C on synthetic complete medium without uracil (SC-URA).

3.2.3 Protein Purification

Ste24 wild-type and mutant proteins were purified as previously described[140,142]. In brief, crude membranes were prepared as in Chapter 2.2.2 described , and then solubilized in buffer S (300 mM sorbital, 100 mM NaCl, 6 mM $MgCl_2$, 10 mM Tris-HCl, pH 7.5, 10% glycerol, 10 μg/ml aprotinin and 2 mM AEBSF) with 20 mM imidazole and 1% (w/v) DDM for 1 hour at 4˚C. The insoluble fraction was removed by ultracentrifugation at 100,000 × *g* for 45 min at 4˚C. The soluble fraction was mixed with Talon® Metal Affinity Resin (Clontech) for 1 hour at 4˚C. The resin was then washed with 5 column volumes of buffer A (Buffer S, 40 mM imidazole and 1% (w/v) DDM) twice, buffer B (buffer S, 500 mM KCl, 40 mM imidazole and 1% (w/v) DDM) and buffer C (buffer S, 500 mM KCl, 40 mM imidazole and 0.1% (w/v) DDM). The protein was

then eluted with buffer E (buffer S, 250 mM imidazole and 0.1% (w/v) DDM) and concentrated using Amicon® Ultra Centrifugal Filter 30,000 MWCO (Millipore) at 5,000 × *g* for 30 min at 4˚C. Protein concentration was determined using the Amido Black protein assay.

Table 3.1. Plasmids and primers used in this study

Plasmid	Genotype	Reference
pCH1283	*2μ URA3* P_{PGK}*-His*$_{10}$*-HA*$_3$*-STE24*	Chapter 2.2.1
pCH1307	*2μ URA3* P_{PGK}*-His*$_{10}$*-HA*$_3$*-STE24-H297A*	This study
pCH1308	*2μ URA3* P_{PGK}*-His*$_{10}$*-HA*$_3$*-STE24-E298A*	This study
pCH1309	*2μ URA3* P_{PGK}*-His*$_{10}$*-HA*$_3$*-STE24-H301A*	This study
pCH1314	*2μ URA3* P_{PGK}*-His*$_{10}$*-HA*$_3$*-STE24-E390A*	This study
pCH1292	*2μ URA3* P_{PGK}*-His*$_{10}$*-HA*$_3$*-STE24-P246L*	This study
pCH1301	*2μ URA3* P_{PGK}*-His*$_{10}$*-HA*$_3$*-STE24-N263S*	This study
pCH1310	*2μ URA3* P_{PGK}*-His*$_{10}$*-HA*$_3$*-STE24-W302R*	This study
pCH1347	*2μ URA3* P_{PGK}*-His*$_{10}$*-HA*$_3$*-STE24-L400P*	This study
pCH1346	*2μ URA3* P_{PGK}*-His*$_{10}$*-HA*$_3$*-STE24-L413F*	This study
pCH1380	*2μ URA3* P_{PGK}*-His*$_{10}$*-HA*$_3$*-STE24-L437R*	This study

Primer	Sequence (5’ to 3’)
SVEC (+)	CAGGGGGTGGTTTAGTTTAG
SVEC (−)	CAACTGTTGGGAAAGGCGATC
Ste24-H297A (+)	GGCTGTTTTGGCCGCTGAAATCGGTC
Ste24-H297A (−)	GACCGATTTCAGCGGCCAAAACAGCC
Ste24-E298A (+)	GTTTTGGCCCATGATATCGGTCAC
Ste24-E298A (−)	GTGACCGATATCATGGGCCAAAAC
Ste24-H301A (+)	GAAATCGGTGCCTGGCAAAAAAACC
Ste24-H301A (−)	GGTTTTTTTGCCAGGCACCGATTTC
Ste24-E390A (+)	TTCCAGAACTCATGCATATCAAGCT
Ste24-E390A (−)	AGCTTGATATGCATGAGTTCTGGAA
Ste24-P246L (+)	GAGTTGGGTTCCTACTAGATAAG
Ste24-P246L (−)	CTTATCTAGTAGGAACCCAACTC
Ste24-N263S (+)	CTCATTCAAGCGCATATTTC
Ste24-N263S (−)	GAAATATGCGCTTGAATGAG
Ste24-W302R (+)	CGGTCATCGGCAAAAAAAC
Ste24-W302R (−)	GTTTTTTTGCCGATGACCG
Ste24-L400P (+)	GCTTATGCTAAAAAACCAGGCTACAAGCAA
Ste24-L400P (−)	TTGCTTGTAGCCTGGTTTTTTAGCATAAGC
Ste24-L413F (+)	GGGCTCTAATTGATTTTCAAATCAAAAACC
Ste24-L413F (−)	GGTTTTTGATTTGAAAATCAATTAGAGCCC
Ste24-L437R (+)	CATCCAACTCGAGCTGAAAGA
Ste24-L437R (−)	TCTTTCAGCTCGAGTTGGATG

3.2.4 Immunoblot and Coomassie Stain Analysis

Crude membranes (1 μg for immunoblot) or purified proteins (0.01 μg for immunoblot and 1 μg for Coomassie staining) were resolved on a 10% SDS-PAGE gel and either stained with Coomassie stain (0.25% (w/v) Coomassie Brilliant Blue R-250, 50% methanol and 10% acetic aid) or transferred to a 0.22 μm Protran® Nitrocellulose Membrane (GE Healthcare). The nitrocellulose membrane was blocked with 20% (w/v) nonfat milk in phosphate-buffered saline (137 mM NaCl, 2.7 mM KCl, 4 mM Na_2HPO_4, 1.8 mM KH_2PO_4, pH adjusted to 7.4) and 0.05% (v/v) Tween-20 (PBST), probed with α-HA antibody (1:15000) in 5% (w/v) nonfat dry milk in PBST and then detected with a horseradish peroxidase conjugated goat α-mouse antibody (1:4000). The protein bands were visualized using the SuperSignal® West Pico Chemiluminescent Substrate (Thermo Scientific).

3.2.5 LC/MS Analysis

Reactions contained 5 μg of wild-type or E298A purified Ste24 proteins, 50 μM Peptide **1** and 100 mM Tris-HCl, pH 7.5 in a total volume of 200 μl and were incubated at 30°C for 6 hours. Reactions were stopped by heating at 95°C for 2 min and then centrifuged at 13,000 × *g* to remove any precipitate. A sample with only 100 μM Peptide **1** was prepared as a control. Cleavage products were analyzed by LC/MS using Waters 600 HPLC system interfaced with Waters ZQ ESI mass spectrometer. The solvent system used acetonitrile (solvent A) and water (solvent B). The reaction mixtures were injected directly onto a C8 column (2.1 mm × 25 cm) and the peptides were separated using a linear gradient from 5% to 95% A over 20 min at a flow rate of 33 μl/min. Eluted samples were monitored at 214 nm. Peptide intact masses were determined using ESI mass spectrometry and identified manually with software.

3.2.6 FRET-Based Assay

The assay can work with either purified enzyme or enzyme in crude membrane preparations. To perform the assay, 0.75 μg of purified Ste24 was rapidly reconstituted[140,142] into 6.25 μg of *E.coli* polar lipid (Avanti Polar Lipids) in 100 mM Tris-HCl, pH 7.5, incubated on ice for 5 min. For enzyme in crude membrane, 30 μg of Ste24 crude membrane was added into 100 mM Tris-HCl, pH 7.5 with 10 μg/ml Chymostatin and 2 mM AEBSF. Protease inhibitors were added to reduce background. Samples were equilibrated at 30°C for 5 min then transferred to a

96-well plate. Peptide **1** was dissolved in DMF to 1 mM stock concentration and diluted to 150 μM with 100 mM Tris-HCl, pH 7.5. Assays were initiated by adding Peptide **1** to final concentration of 30 μM and mixed by shaking for 30 seconds.

For assay optimization, different reaction conditions were examined adapting from the standard FRET assay condition. To characterize the enzymatic activity in detergent micelles and in liposomes, 0.75 μg of purified Ste24 was incubated in 0 to 0.25% DDM (w/v) or rapidly reconstituted into 0 to 100 μg of *E.coli* polar lipid in 100 mM Tris-HCl, pH 7.5. Different buffers were tested in the liposome system based on previously reported Ste24 assay conditions, Tris-HCl, pH 7.5, HEPES, pH 7.2, MOPS, pH 7.2 or MES, pH 7.0. Optimal protein concentrations (0.25 to 1.5 μg) or DMSO concentrations (0 to 10%) were determined as well.

Fluorescence readings were measured using the Synergy™ H4 microplate reader (BioTek) at excitation and emission wavelengths of 320 ± 9 nm and 420 ± 9 nm every 30 seconds over a 30 to 240 min time course at 30˚C. To record the excitation and emission spectra, excitation wavelengths ranged from 280 to 400 nm with a 5-nm increment, and the emission was measured at 420 nm. The emission wavelengths ranged from 360 to 500 nm with a 5-nm increment and excitation at 320 nm.

3.2.7 Assay Calibration

Different concentrations of dequenched Peptide **2** (0 to 50 μM) were incubated in the same condition as the standard assay. Fluorescence readings were plotted against concentration to construct a standard curve (Abz) to obtain the extinction coefficient for converting from relative fluorescence unit (RFU) to concentration of the dequenched peptide product. To correct the inner filter effect, a calibration curve (Abz + Dnp) was generated from the fluorescence measurements of dequenched Peptide **2** incubated with an equimolar amount of another cleavage product Peptide **3** (0 to 50 μM). A correction factor (C) for the inner filter effect was calculated based on the ratio of fluorescence reading between two calibration curves at each concentration of peptide used in the assay. C was multiplied by the raw fluorescence data to yield the corrected fluorescence values. Each value was obtained from triplicate experiments.

3.2.8 Kinetic Analysis

Samples were assembled following standard assay conditions and incubated with increasing concentrations (0 to 30 μM) of Peptide **1**. The initial rates of each reaction were measured using the first linear region (usually the first 10 minutes) and converted to specific activities using the extinction coefficient. Specific activities were then corrected by multiplying C and plotted against substrate concentration. Each value was derived from three assays performed in duplicate. The kinetic parameters were established by fitting specific activity and substrate concentrations to the Michaelis-Menton equation using GraphPad Prism 6.

3.2.9 Inhibitor Studies

HIV protease inhibitors Lopinavir and Darunavir were prepared as 10 mM stock solutions in DMSO. Ste24 proteins were reconstituted in liposomes then incubated with each inhibitor at different concentrations (0 to 200 μM) on ice for 5 min. Assays were initiated by adding diluted Peptide **1** to 30 μM. Specific activities were calculated and corrected as previously described. IC_{50} values were determined from three assays performed in duplicate and calculated using GraphPad Prism 6.

3.3 Results and Discussion

3.3.1 Design of FRET-Based Peptides

The FRET substrate corresponding to the yeast **a**-factor peptide was synthesized. The sequence is Abz-MQPSTATAAPKEK(Dnp)EKTSSEKKDNYIIKGVFWDPAC(Fr)-OMe and will be referred to in the text as Peptide **1**. This 33-mer peptide contains a farnesyl cysteine methyl ester to mimic the processed substrate for the upstream cleavage. For the sake of synthetic simplicity, the 2-aminobenzoic acid (Abz) fluorophore was chosen to be appended to the N-terminus of the peptide, seven amino acids upstream of the cleavage site. Placement of the dinitophenol (Dnp) quencher on the side chain of the furthest upstream lysine residue satisfied the requirement for fluorescence evolution upon proteolysis while also taking advantage of commercially available Lys(Dnp) during peptide synthesis. The distance between the fluorophore/quencher is sufficiently close for FRET to occur. Previously published mutagenic analyses also suggest that these positions are not critical for Ste24 recognition[118]. Two predicted

cleavage products, Abz-MQPSTAT and AAPKEK(Dnp)EKTSSEKKDNYIIKGVFWDPAC(Fr)-OMe, were synthesized and labeled as Peptide **2** and Peptide **3**, respectively (Figure 3.2).

SPPS synthesis began on Fmoc-Cys(Wang)-OMe resin that was made as previously described[153,154], and utilized standard Fmoc/HCTU coupling conditions for chain elongation (Figure 3.3). Upon determination of the free amino N-terminus by ninhydrin testing, the peptide was cleaved and deprotected by treatment with Reagent K, yielding a yellow peptide with a C-terminal cysteine bearing a free thiol and a methyl ester. Interestingly, previous reports have noted that some epimerization of C-terminal cysteine residues can occur when Cys-functionalized Wang resin and Reagent K cleavage conditions are used[155], but after RP-HPLC purification, no evidence for epimerization was observed using the thiol anchoring methodology. Alkylation of the thiol was done with 3 eq of farnesyl bromide in the presence of 3 eq of $Zn(OAc)_2$ in acidic DMF and yielded the prenylated peptide, Peptide **1**. The wild type **a**-factor peptide and long C-terminal standard peptide, Peptide **3**, were synthesized in the same fashion, while the Abz containing peptide fragment, Peptide **2**, started with Fmoc-Thr(Boc)-Wang resin. All peptides were purified by preparative RP-HPLC. Their purities were confirmed by analytical RP-HPLC and the identities were determined via ESI-MS (Figure 3.4 to Figure 3.7).

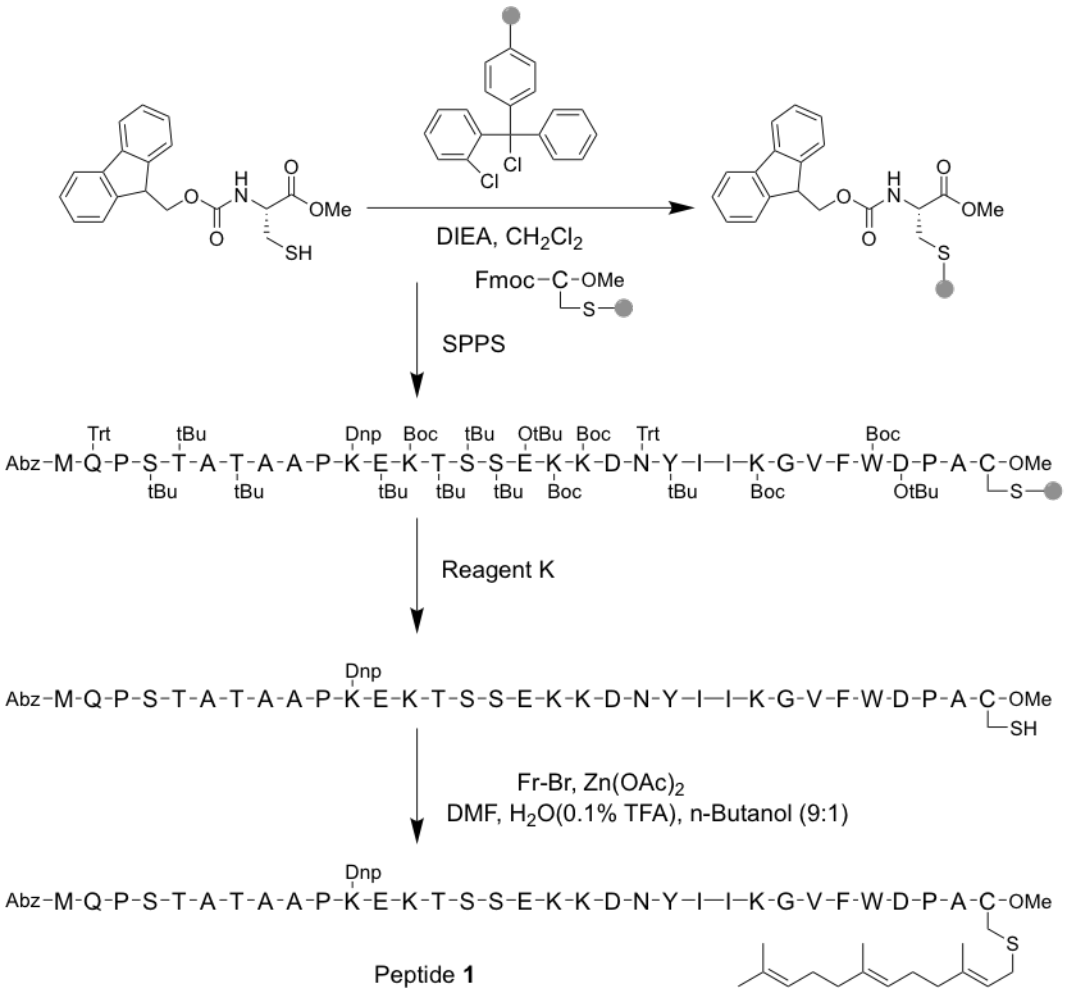

Figure 3.3. Synthesis of FRET probe (Peptide **1**).

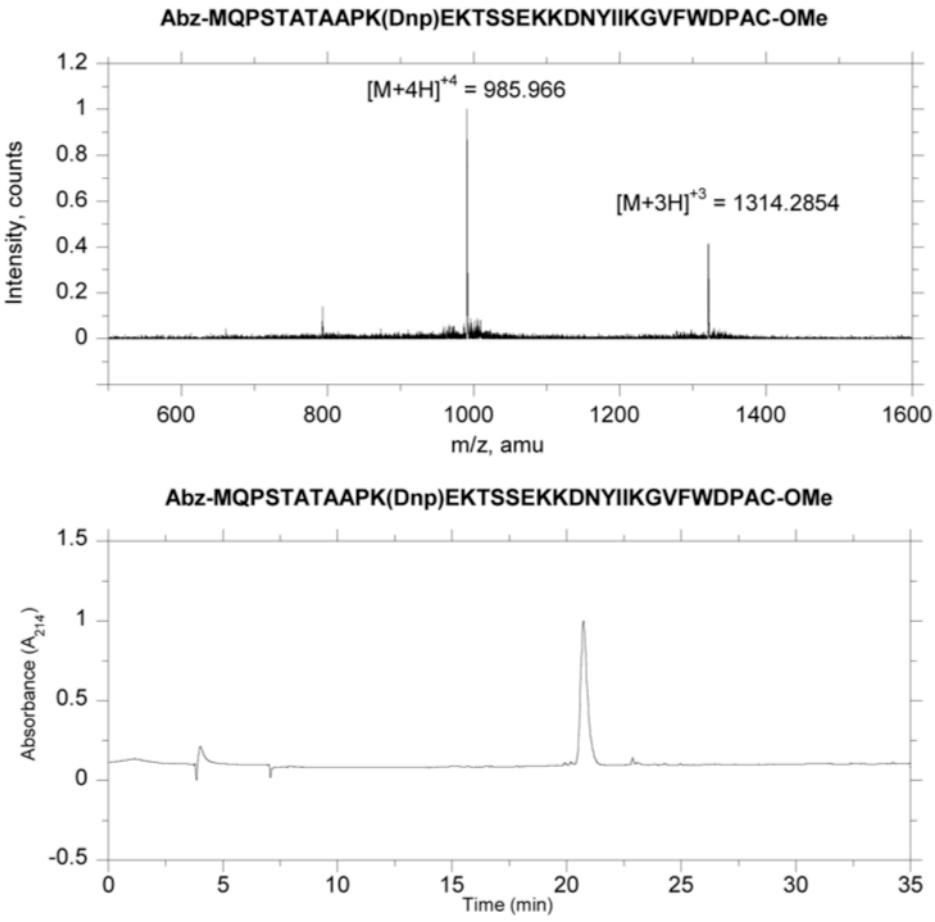

Figure 3.4. Mass spectrum and analytical RP-HPLC chromatogram for Abz-MQPSTATAAPK-(Dnp)EKTSSEKKDNYIIKGVFWDPAC-OMe.

Linear gradient 0-100% CH_3CN (0.1%TFA) in 30 min, detected at 214 nm. Purity by HPLC: 90%; ESI-MS calculated for $C_{175}H_{262}N_{44}O_{56}S_2$ $[M+3H]^{+3}$: 1314.2894, found 1314.2854.

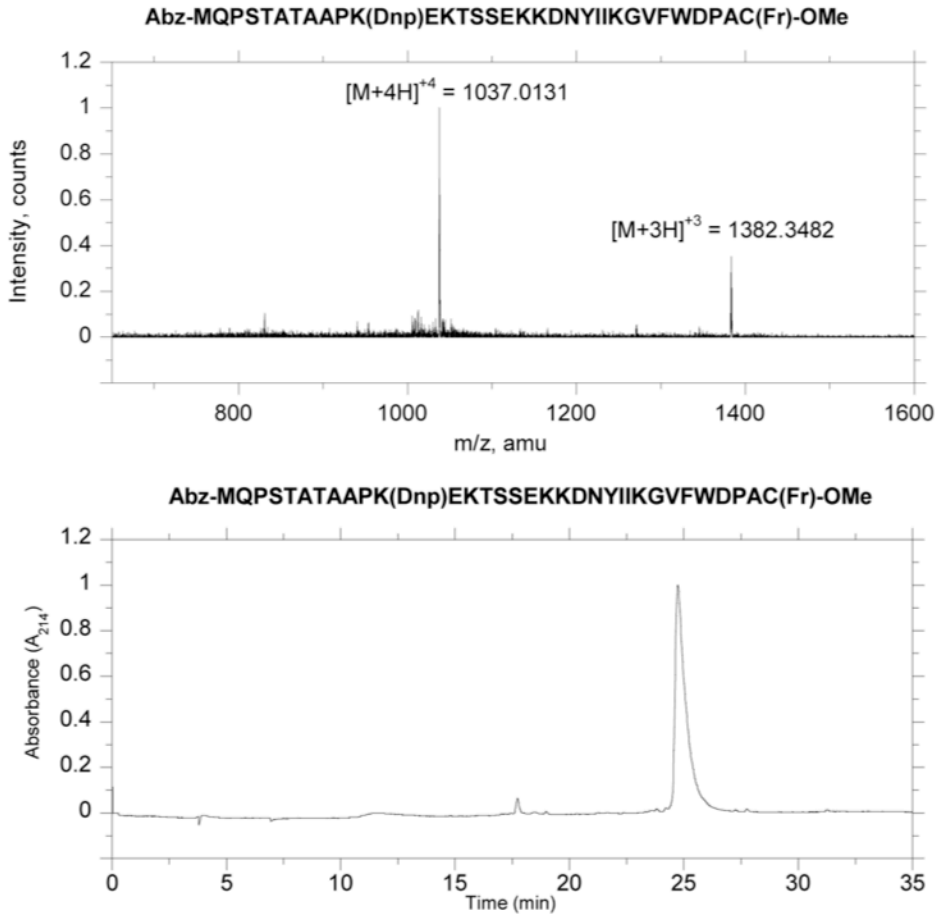

Figure 3.5. Mass spectrum and analytical RP-HPLC chromatogram for Peptide **1**.

Linear gradient 0-100% CH_3CN (0.1%TFA) in 30 min, detected at 214 nm. Purity by HPLC: 95.2%; ESI-MS calculated for $C_{190}H_{286}N_{44}O_{56}S_2$ $[M+3H]^{+3}$: 1382.3521, found 1382.3482.

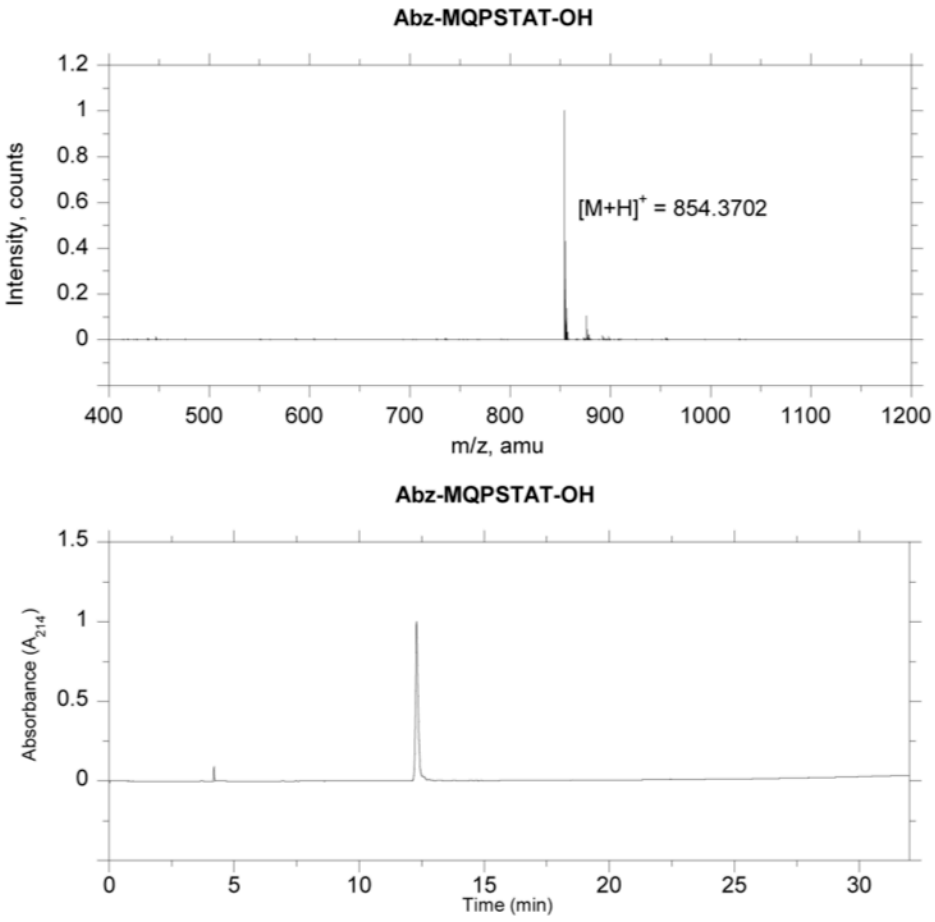

Figure 3.6. Mass spectrum and analytical RP-HPLC chromatogram for Peptide **2**.

Linear gradient 0-100% CH_3CN (0.1%TFA) in 30 min, detected at 214 nm. Purity by HPLC: 92.8%; ESI-MS calculated for $C_{36}H_{55}N_9O_{13}S$ $[M+1H]^+$ 854.3718, found 854.3702.

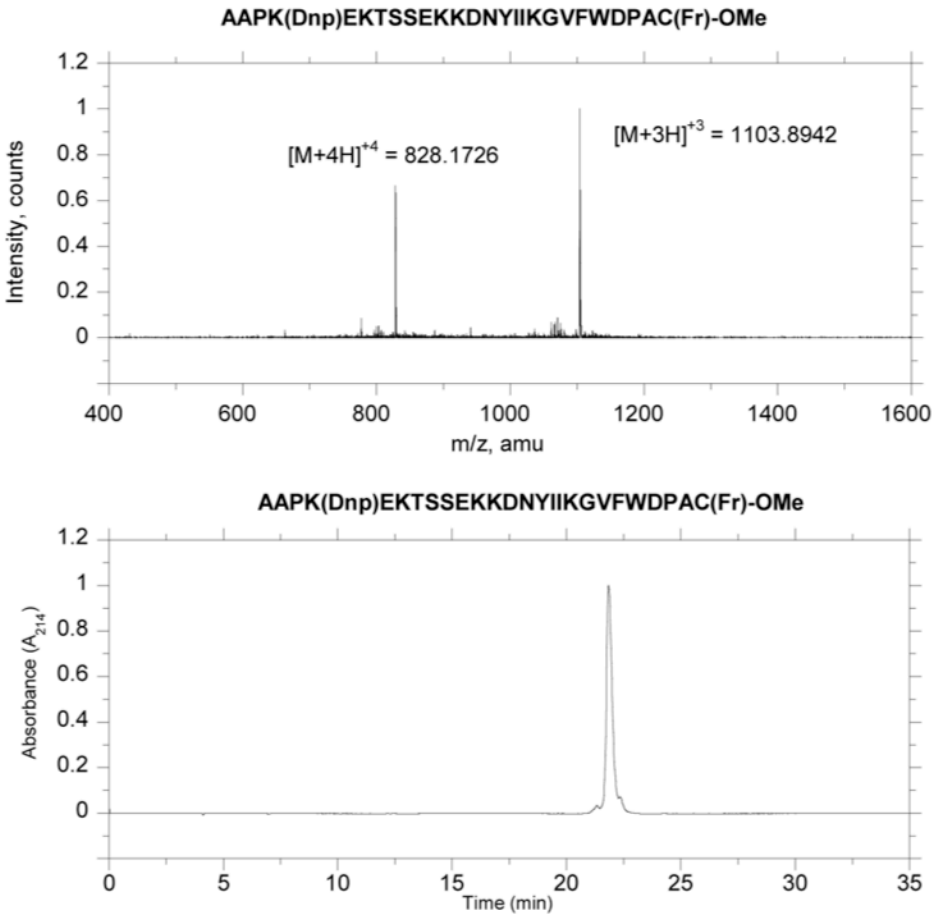

Figure 3.7. Mass spectrum and analytical RP-HPLC chromatogram for Peptide **3**.

Linear gradient 0-100% CH_3CN (0.1%TFA) in 30 min, detected at 214 nm. Purity by HPLC: 93.4%, ESI-MS calculated for $C_{154}H_{233}N_{35}O_{44}S$ $[M+3H]^{+3}$ 1103.9008, found 1103.8942.

3.3.2 Characterization of Ste24 Wild-Type and Catalytic Mutants

Wild-type and several catalytic mutants of Ste24 were constructed for this study. From the published crystal structure of Ste24[123], the enclosed chamber is capped at one end by a canonical HEXXH zinc metalloprotease motif, positioning the active site facing inward of the chamber. Based on the structure, the zinc ion is coordinated by H297, H301 and E390. By analogy with the mechanism of another known zinc metalloprotease, thermolysin, E298 is proposed to be the catalytic residue[123,124]. The three zinc-coordinating residues, H297, H301 and E390, and the proposed catalytic residue E298 (Figure 3.8) were mutated to alanine by site-directed mutagenesis. Wild-type and mutant proteins were then expressed in *Saccharomyces cerevisiae* cells. Yeast crude membranes were prepared and proteins solubilized in the detergent n-Dodecyl-β-D-maltoside (DDM) as previously reported[142]. Immunoblot analysis demonstrated that both crude membrane and purified protein of catalytic mutants were expressed at similar levels as wild-type Ste24. Coomassie stained SDS-PAGE showed the expected molecular weight of His-HA-Ste24 at 58 kDa and purity of each mutant was >90% (Figure 3.8).

3.3.3 Development of a FRET-Based Assay

To assess the ability of Peptide **1** to act as a substrate for Ste24, we adapted previously reported FRET assays for CAAX proteases[150,152,156]. After Ste24 cleavage, the Abz fluorophore is dequenched and the proteolytic activity can be measured directly in real-time using a fluorometer. We first tested the assay with the yeast crude membrane overexpressing Ste24. The fluorescence signal increased during the cleavage by wild-type Ste24. Reactions with catalytic mutants showed smaller increases in fluorescence (Figure 3.9). This might be due to non-specific cleavage activity by endogenous proteases present in the crude membranes.

We then examined this assay with purified Ste24 proteins. As a membrane protein, it is important to maintain enzymatic activity by adding detergents or reconstitution into liposomes[123,135,142]. The assay was examined in the detergent DDM or after rapid reconstitution into *E.coli* lipid. Purified Ste24 was active in both conditions but showed larger changes of fluorescence intensity in liposomes. Other assay parameters, such as buffer, lipid, detergent and enzyme concentration, and DMSO tolerance amount were optimized for fluorescence signals (Figure 3.10).

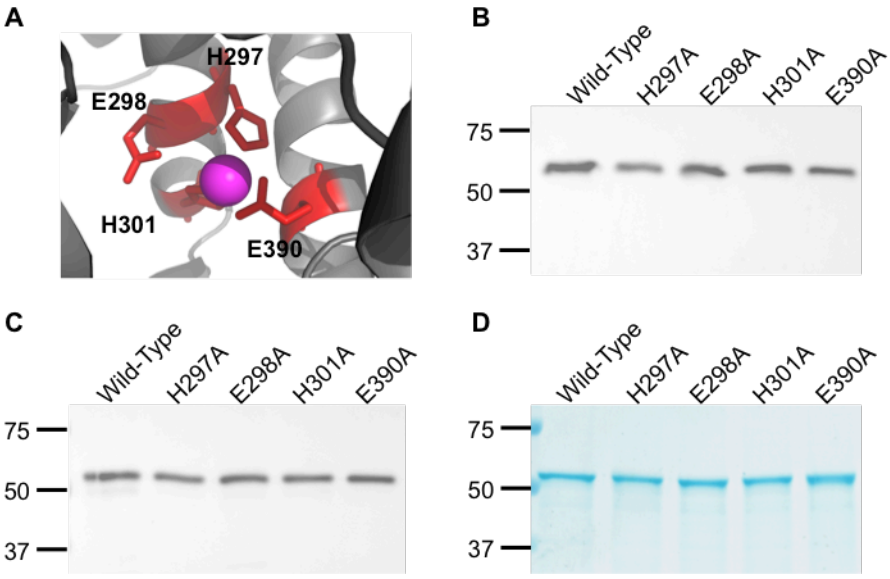

Figure 3.8. Purification of Ste24 wild-type and catalytic domain mutant proteins.

(A) Ste24 residues proposed to mediate catalysis or bind substrate. The zinc ion is shown in purple. The proposed catalytic residue, E298, and residues that coordinate Zn^{2+}, H297, H301, and E390, are labeled in red. Immunoblot analysis using the α-HA antibody indicated that expression levels of the mutant (B) crude membranes (1 μg) and (C) pure proteins (0.01 μg) were at a similar level as wild-type Ste24. (D) Coomassie stain showed all proteins (1 μg) were >90% pure.

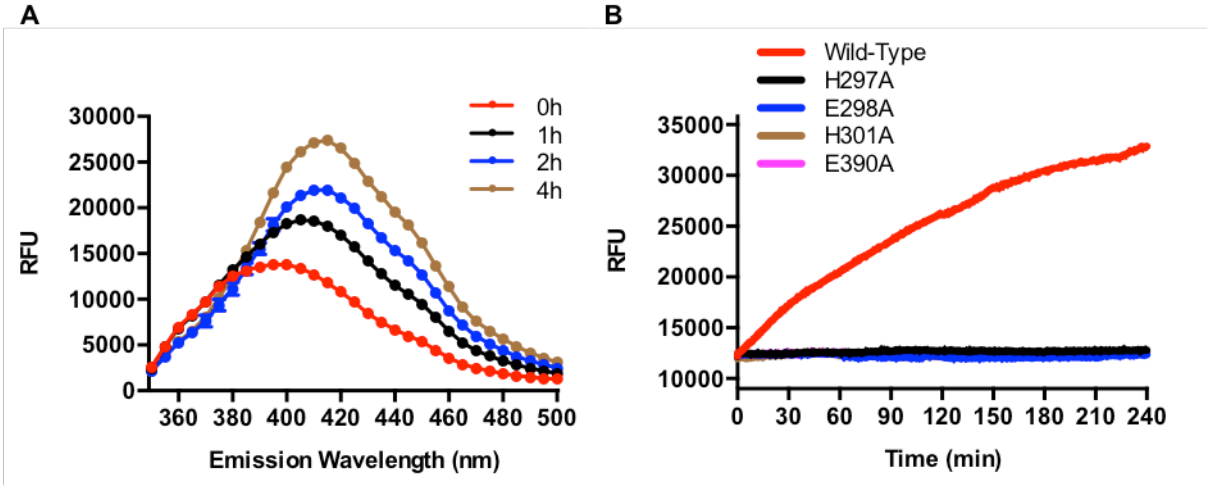

Figure 3.9. Proteolytic activity of Ste24 crude membrane using Peptide **1** as the substrate.

(A) The fluorescence released from substrate cleavage by crude Ste24 was measured at different time points. The emission spectra were recorded and scanned from 350 to 500 nm with excitation wavelength at 320 nm. (B) Fluorescence readings over a time course of 4 hours were detected with excitation wavelength at 320 nm and emission wavelength at 420 nm.

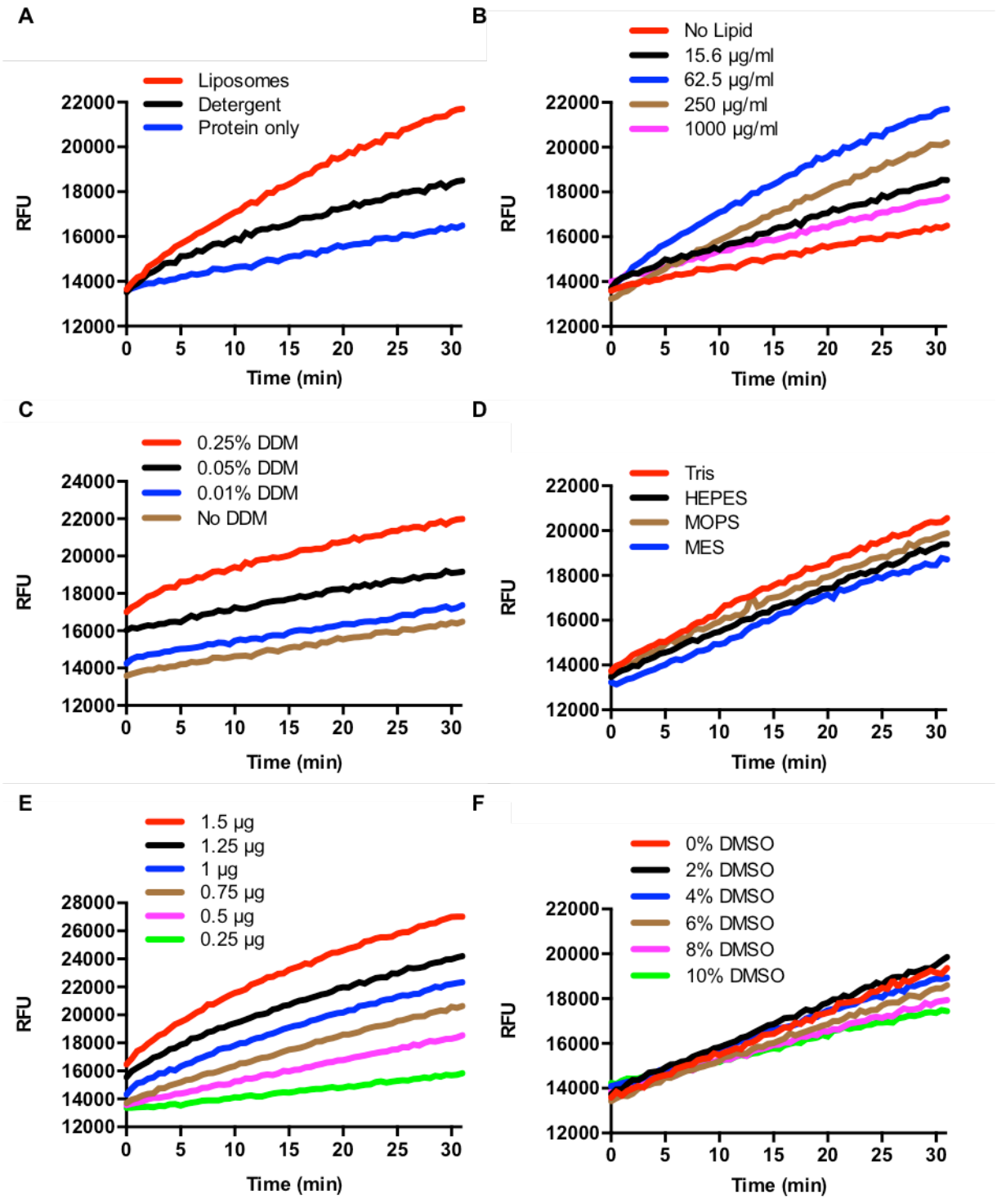

Figure 3.10. Optimization of the developed assay system.

Reactions (A) in liposomes or the detergent micelle system, or with varying (B) lipid, (C) DDM, (D) buffer, (E) protein or (F) DMSO concentrations were measured over a time course of 30 minutes.

Purified wild-type Ste24 in liposomes was incubated with Peptide **1**, and the emission spectra with excitation at 320 nm were scanned and recorded over wavelength (Figure 3.11.A). The maximum emission peaks occurred at 415 nm, which is close to the theoretical emission maximum of Abz fluorophore at 420 nm upon excitation at 320 nm. By contrast, reactions with proposed catalytic mutants showed no change in the fluorescence intensity (data not shown). In the presence of purified wild-type Ste24, the reaction mixture increased in fluorescence over time, suggesting that Peptide **1** is recognized and processed by Ste24. Furthermore, incubation with the purified catalytic mutants showed no significant increase in fluorescence, providing evidence that proteolysis of the quenched peptide is dependent upon Ste24 activity (Figure 3.11.B). This is also consistent with the gel-based analysis result[125,126,128] suggesting that Ste24 does use a classical zinc metalloprotease mechanism for the upstream cleavage.

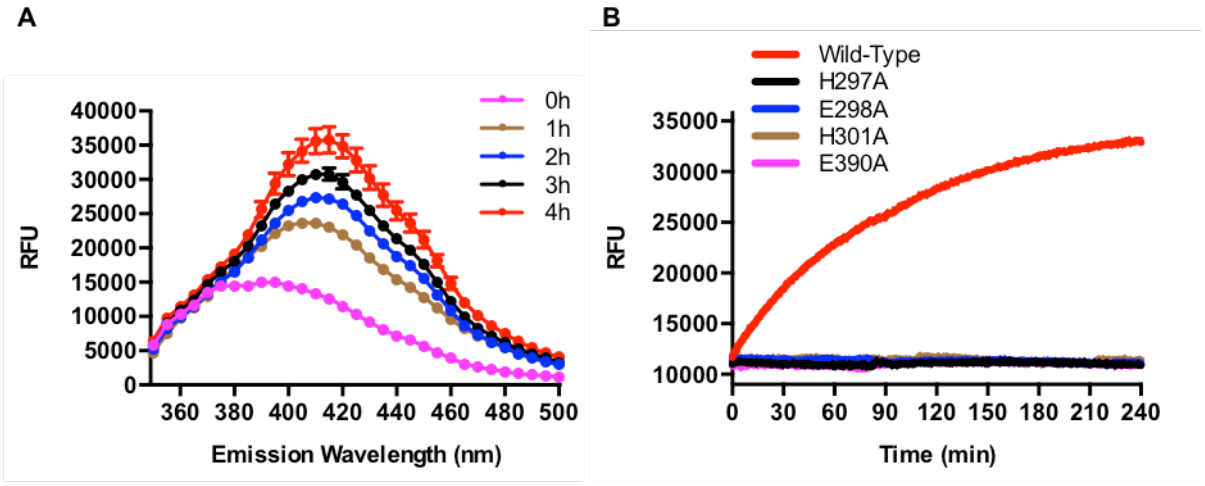

Figure 3.11. Proteolytic activity of purified Ste24 using Peptide **1** as the substrate.

(A) The fluorescence released from substrate cleavage by Ste24 was measured at different time points. The emission spectra were recorded and scanned from 350 to 500 nm with excitation wavelength at 320 nm. (B) Fluorescence readings over a time course of 4 hours for purified Ste24 in liposomes were detected using excitation wavelength at 320 nm and emission wavelength at 420 nm. Initial rates were found to be within the first 10 minutes of reaction. Catalytic domain mutants showed no increase in fluorescence.

3.3.4 Verification of Ste24 Cleavage Site

The real-time monitoring results indicate that Ste24 proteolytic activity could be investigated with this new FRET-based assay. However, cleavage could occur anywhere

between the fluorophore and quencher and lead to the release of fluorescence from the substrate. Therefore, it was important to confirm whether the cleavage site is consistent with the known substrate specificity of Ste24.

To determine the precise cleavage site of the FRET substrate by Ste24, Peptide **1** was incubated with purified wild-type Ste24 or catalytic mutant E298A proteins for 6 hours and the reaction mixtures were subjected to LC-MS for separation and identification of cleavage products. The LC-MS analysis showed that Peptide **1** was cleaved at its natural cleavage site by the wild-type Ste24 but not by the catalytic mutant E298A (Figure 3.12).

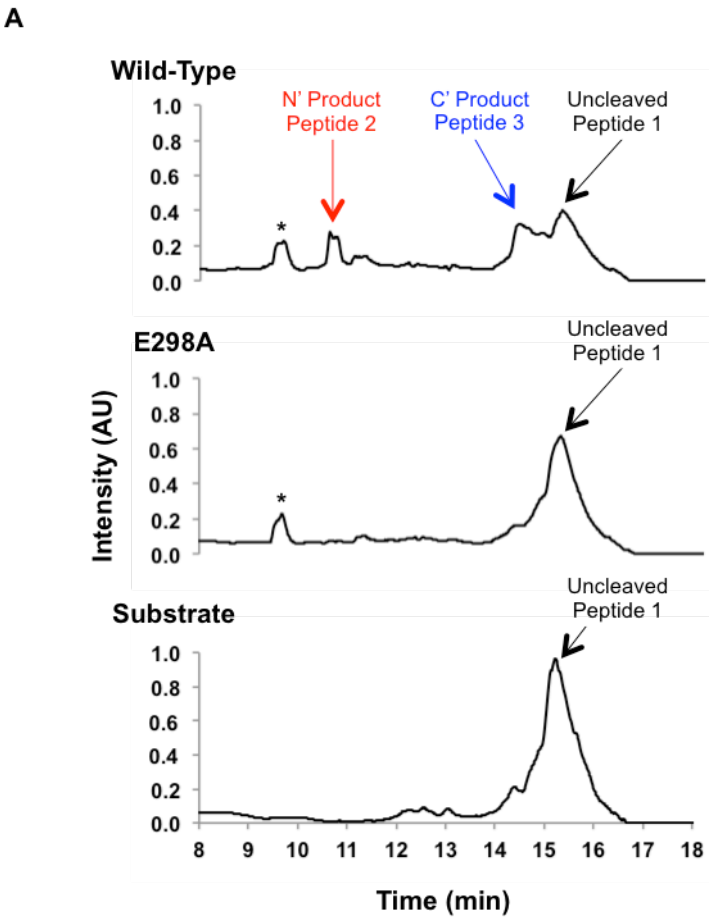

Figure 3.12. LC-MS analysis reveals that Ste24 cleaves the substrate at the expected site.

(A) LC chromatograms showing the separation of cleaved products or non-cleaved peptide produced from incubation with purified wild-type, E298A mutant Ste24 or the substrate only. Peaks corresponding to Peptide **1**, **2** and **3** are indicated. Purified Ste24 protein peaks are labeled with an asterisk. (B) An illustration of the expected proteolytic products at the native cleavage site and the theoretical molecular masses after Ste24 cleavage. Mass spectra of products derived from different LC fractions corresponding to Peptide **1**, **2**, and **3**, respectively.

Figure 3.12. continued

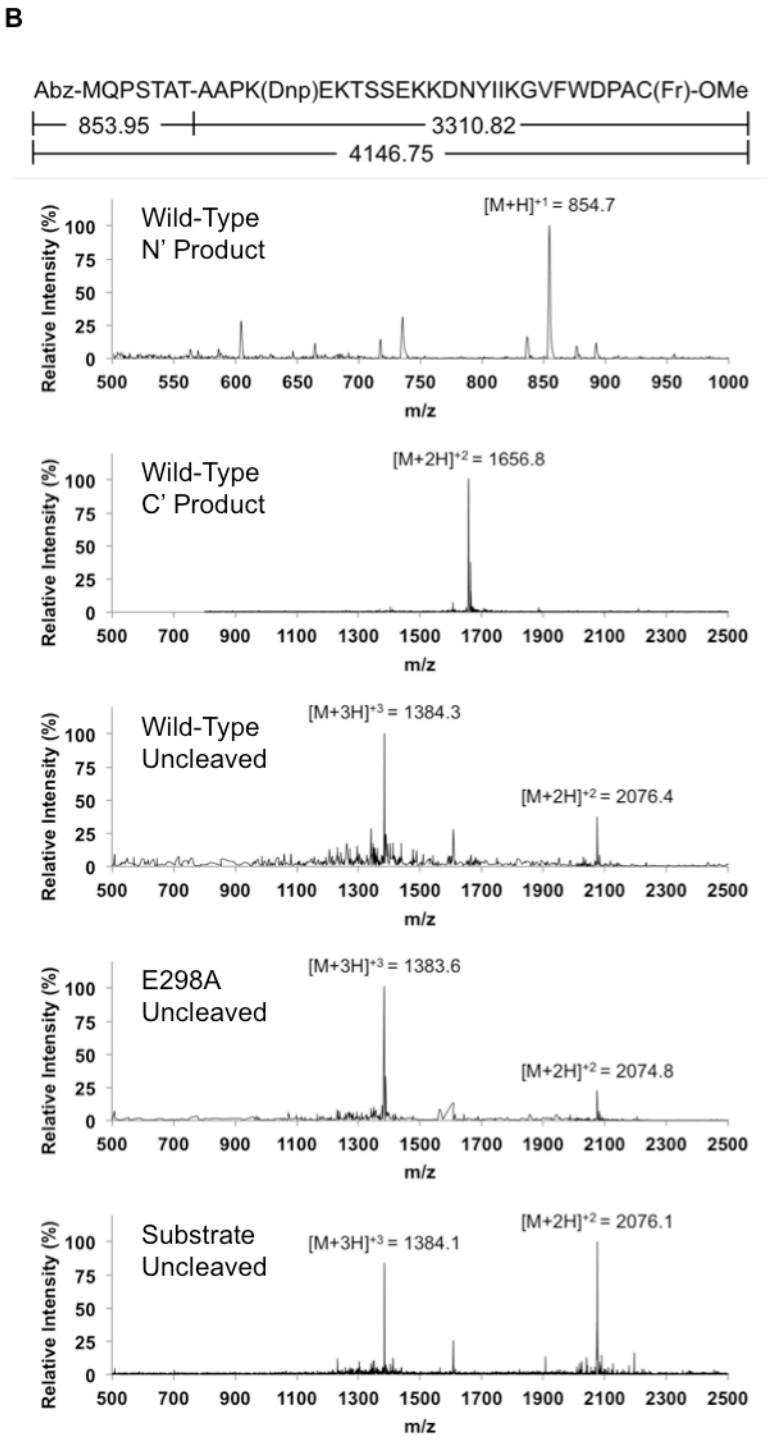

Peptide **1** without any protein was loaded as a control and showed a single major peak at 15.1 min. The molecular mass corresponded to the full-length Peptide **1** (observed: $[M+2H]^{+2}$ = 2076.1 and $[M+3H]^{+3}$ = 1384.1, calculated = 4146.8). Incubation with E298A also showed one

major peak at 15.1 min, and the molecular mass matched the uncleaved Peptide **1** (observed: $[M+2H]^{+2}$ = 2074.8 and $[M+3H]^{+3}$ = 1383.6, calculated = 4146.8). We observed three major peaks in the chromatogram of incubation with wild-type Ste24. Based on the ESI-MS spectra, the peak eluted at 10.6 min (observed: $[M+H]^{+1}$ = 854.7, calculated = 854.0) and 14.3 min (observed: $[M+2H]^{+2}$ = 1656.8, calculated = 3310.8), were the cleaved N- (Peptide **2**) and C-terminal (Peptide **3**) products, respectively. The peak at 15.1 min was the rest of the uncleaved Peptide **1** (observed: $[M+2H]^{+2}$ = 2076.4 and $[M+3H]^{+3}$ = 1384.3, calculated = 4146.8). These results demonstrate that Ste24 cleaves Peptide **1** between the expected Thr-7 and Ala-8 residues.

3.3.5 Kinetic Analysis

The reaction setup in this FRET assay allows us to quantify the Ste24 proteolytic activity directly. We first generated a calibration curve by plotting relative fluorescence unit (RFU) against concentration of the dequenched product, Peptide **2**, to convert change of fluorescence intensity to amount of product formation (Figure 3.13, *red*). However, the Abz/Dnp FRET pair is notorious for its internal quenching properties, known as the inner filter effect, which leads to decreases in fluorescence since the fluorophore is quenched by either neighboring substrate or cleaved product molecules when using a high concentration of fluorogenic substrate[135,156]. To correct for the inner filter effect, the correction curve was built from the fluorescence measurements of the dequenched product Peptide **2** incubated with equimolar amount of the other cleavage product Peptide **3** (Figure 3.13, *blue*). A correction factor for the inner filter effect was calculated based on the ratio of fluorescence readings between two curves at each concentration of peptide used in the assay.

Purified Ste24 proteins were incubated with varying substrate concentrations. The fluorescence intensities of each reaction were monitored and recorded (Figure 3.14.A). The specific activities at each concentration were determined by converting and correcting the initial rates obtained from the first linear region (Figure 3.14.B). The kinetic parameters K_m and V_{max} were calculated as 9.1 ± 1.3 μM and $37.6 \times 10^3 \pm 2.4 \times 10^3$ pmol/mg/min (or 4.7 ± 0.3 nM/sec), respectively. These are the first reported kinetic parameters for the upstream cleavage activity of Ste24. Interestingly, these kinetic parameters were comparable to the published values of the CAAX cleavage by Ste24 (Pryor *et al.*: K_m was 11 ± 2 μM and V_{max} was 6.6 ± 0.5 nM/sec)[123].

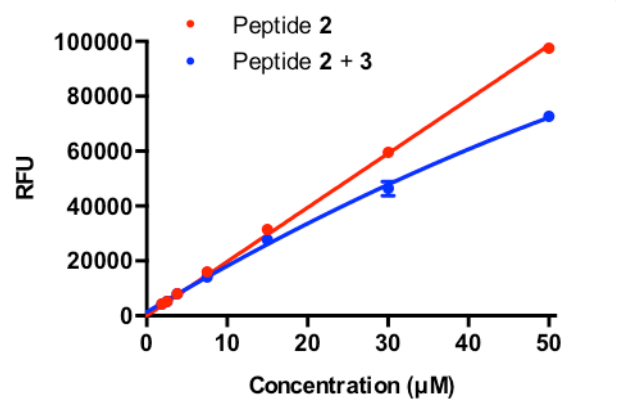

Figure 3.13. Assay calibration.

The *red* standard curve correlates the relative fluorescent unit (RFU) to a range of concentrations of Peptide **2** (dequenched). The *blue* calibration curve was measured using an equimolar mixture of Peptide **2** and Peptide **3** (internally quenched) over the same range of concentrations. The fluorescence readings were taken under standard assay conditions. Correction factors were calculated based on the ratio between dequenched and internally quenched fluorescence reading at each concentration.

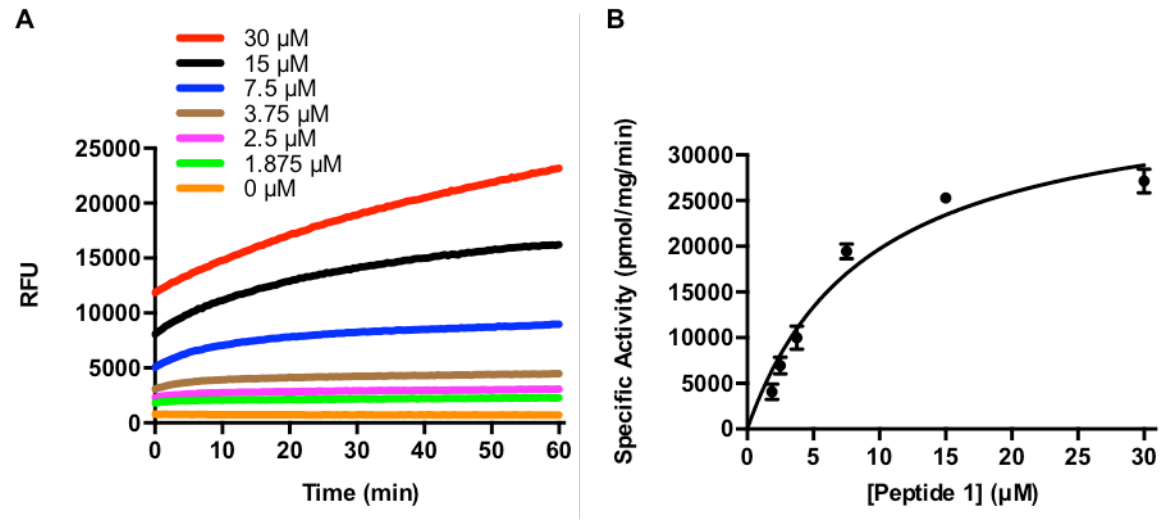

Figure 3.14. Kinetic studies of Peptide **1** substrate cleavage by purified Ste24.

(A) Fluorescence readings for purified Ste24 in liposomes with indicated concentrations of the substrate over a time course of 1 hour. Initial rates were found to be within the first 2 to 10 minutes. (B) Specific activities converted from initial rates and substrate concentrations were plotted and fitted into the Michaelis-Menten equation. From these data, the values of kinetic parameters V_{max} and K_m were determined.

The K_m and V_{max} obtained from assays with yeast crude membrane overexpressing Ste24 were 11.3 ± 1.2 μM and 895.0 ± 42.1 pmol/mg/min (or 0.27 ± 0.01 μM/min) (Figure 3.15). These kinetic data were also similar to the previously reported values obtained from both FRET-based (Hildebrandt *et al.*: V_{max} was 0.53 ± 0.01 μM/min and K_m was 16.4 ± 1.0 μM)[135,152] and radioactive-coupled assays (unpublished data from Dr. Wiley: V_{max} = 764.5 ± 27.2 μM/min, K_m = 4.1 ± 0.7 μM). Taken together, these results indicate that Ste24 has similar affinity for both CAAX and upstream substrates. Moreover, Ste24 can perform the two cleavages with similar efficiency.

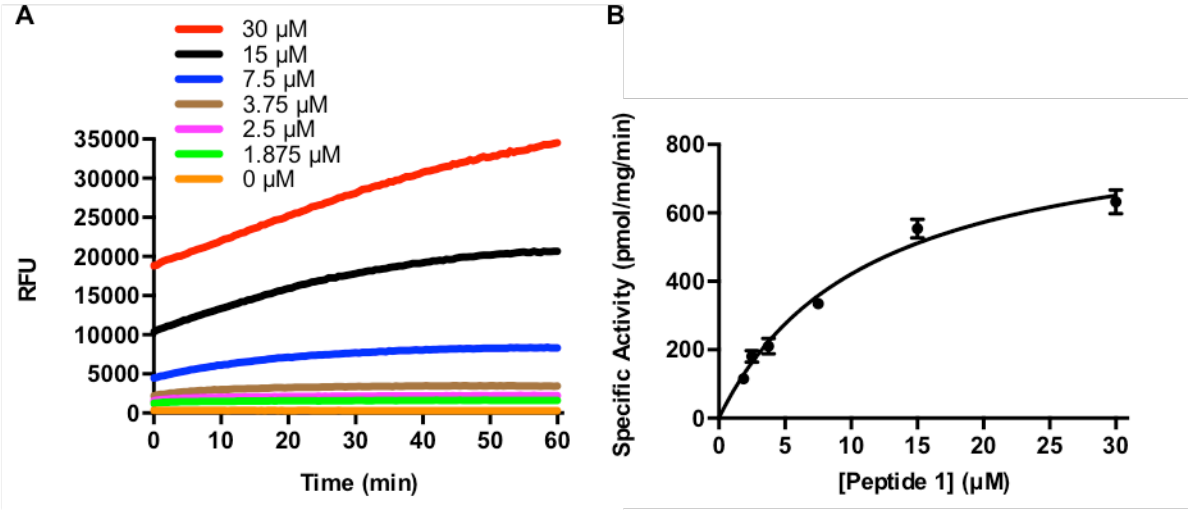

Figure 3.15. Kinetic studies of Peptide **1** substrate cleavage by crude Ste24.

(A) Fluorescence readings for crude Ste24 with indicated concentrations of the substrate over a time course of 1 hour. Initial rates were found to be within the first 2 to 10 minutes. (B) Specific activities converted from initial rates and substrate concentrations were plotted and fitted into the Michaelis-Menten equation. From these data, the values of kinetic parameters V_{max} and K_m were determined.

3.3.6 Characterization of Ste24 Disease Mutants

Mutations in the human homolog of Ste24, ZMPSTE24, have been reported from patients with metabolic syndrome (MS) and progeroid diseases, including B-type mandibuloacral dysplasia (MAD-B) and restrictive dermopathy (RD)[28,130]. The CAAX cleavage activities of the disease mutations were examined using our previously developed radioactive-coupled assay, showing little or no enzyme activity (<15%)[130]. However, both ZMPSTE24 and RCE1 could

efficiently cleave the CAAX motif from prelamin A (unpublished data from Dr. Wiley). This suggests that the upstream cleavage ability of ZMPSTE24 determines the accumulation level of prelamin A in progeroid diseases.

Here we introduced six single mutations identified in MAD-B (P248L, N265S, W340R, and L425P), MS (L438F), and RD (L426R) into the yeast *ste24* gene: P246L, N263S, W302R, L400P, L413F and L437R. These residues are highly conserved in ZMPSTE24 and Ste24 across species and all lie in the zinc metalloprotease domain (Figure 3.16.A)[20,123]. Their upstream cleavage activities were examined using the FRET assay. Disease mutant Ste24 proteins were constructed and purified as described above. Immunoblot and Coomassie stain demonstrated that the expression and purity levels of disease mutants were similar to wild-type Ste24 (Figure 3.16.B). Purified wild-type Ste24 and disease mutants were incubated with saturating concentrations (30 μM) of Peptide **1** and the specific activity was calculated (Figure 3.16.B). All the disease state mutations displayed reduced upstream activity, with L413F having the highest activity of about 17% comparing to wild-type Ste24. This may explain why metabolic syndrome (MS), characterized by an L438F mutation in ZMPSTE24, has milder symptoms than MAD-B.

3.3.7 Effects of HIV Protease Inhibitors on Ste24 Activity

As previously described, Ste24 is a known zinc metalloprotease. We also demonstrated that the conserved zinc-binding motif is important for the upstream cleavage of Ste24 in the above section. However, some interesting observations have been reported that certain types of HIV protease inhibitors (HIV-PIs), designed to target the HIV retroviral aspartyl protease, also inhibit the CAAX proteolysis of Ste24 and its human homolog ZMPSTE24. The subset of drugs which inhibit Ste24 and ZMPSTE24 includes lopinavir (LPV), ritonavir (RTV) and tipranavir (TPV), but not darunavir (DRV)[62–64,142].

Here we used the FRET assay to examine whether the HIV-PIs affect the upstream cleavage of Ste24. Purified Ste24 was incubated with varying concentrations of LPV and DRV. Specific activities were calculated and plotted to generate inhibition curves (Figure 3.17). As expected, DRV did not inhibit Ste24 appreciably up to 200 μM. Ste24 was slightly inhibited by LPV with IC_{50} of 42.2 ± 1.3 μM. However, even using a high concentration, LPV only inhibited the upstream activity of Ste24 to about 70%. One possible reason is due to the presence of excess lipid. Also, the high drug concentration may cause precipitation or non-complete solubilization

of LPV. The inhibition mechanism of HIV-PIs to the CAAX and the upstream cleavage of Ste24 will need to be further studied.

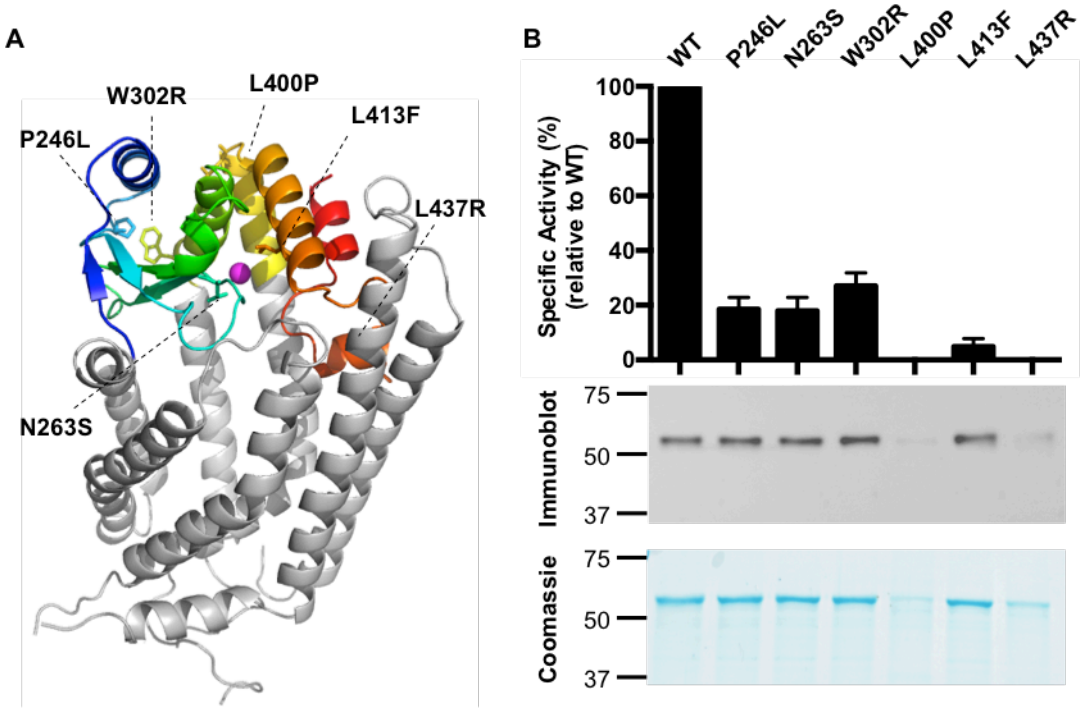

Figure 3.16. Purified Ste24 disease mutants revealed reduced upstream cleavage activity compared to wild-type (WT) Ste24.

(A) Disease variants conserved in Ste24 are labeled with black dotted lines (P246L, N263S, W302R, L400P, L413F, and L437R). All residues are located in the zinc metalloprotease domain. The zinc ion is shown in purple. PDB: 4IL3 (B) The activity of each mutant with Peptide **1** was measured using the FRET-based assay. Specific activities were reported as the percentages of relative activity to WT. Purified proteins were analyzed by western blot (0.01 μg) using the α-HA antibody and Coomassie stain (1 μg).

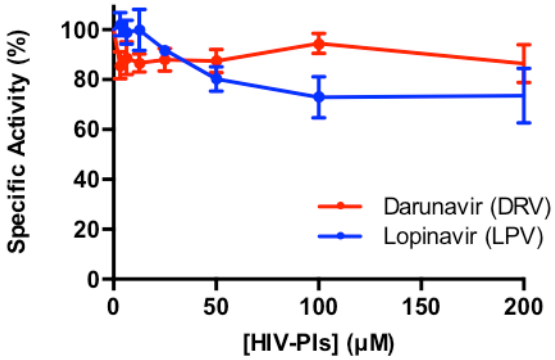

Figure 3.17. Inhibition effects of HIV-PIs on the upstream proteolytic activity of purified Ste24. Different concentrations of HIV-PIs darunavir (*red*) or lopinavir (*blue*) were incubated with purified Ste24 for 5 minutes before adding the peptide substrate to start the assay. Percentages of specific activity were plotted with HIV-PIs concentrations. Inhibition constants were determined from the fitted nonlinear regression curves.

3.4 Conclusions

Herein, we have described the first *in vitro* assay for quantification of the upstream cleavage activity of Ste24. Internally quenched fluorescent peptide with the sequence of its natural substrate, yeast **a**-factor, was synthesized and could be recognized by Ste24. Kinetic analyses suggested that Ste24 performs the upstream cleavage with similar efficiency as the AAX proteolysis and functions as a zinc metalloprotease. Disease variants were examined and revealed reduced activity as expected. Surprisingly, lopinavir, which was demonstrated to inhibit AAX cleavage of Ste24, showed slight inhibition of the upstream cleavage. Taken together, this assay will be useful for characterization of Ste24 and may be applied to its human homolog ZMPSTE24.

CHAPTER 4. EXAMINATION OF THE UPSTREAM CLEAVAGE ACTIVITY OF ZMPSTE24 DISEASE MUTANTS

Portions of the data and text in the following chapter will be published in the book chapter "A quantitative FRET assay for the upstream cleavage activity of the integral membrane proteases human ZMPSTE24 and yeast Ste24". The dissertation author designed and performed all the experiments. Nisreen Islaih helped preparing yeast crude membranes and trypsin digestion experiments. Dr. Susan Michaelis at Johns Hopkins University provided the ZMPSTE24 mutant plasmids and yeast strains. Dr. Mark Distefano at University of Minnesota synthesized the FRET peptides.

4.1 Introduction

ZMPSTE24 is a unique intramembrane zinc metalloprotease that plays important dual roles in lamin A maturation. The precursor of lamin A, prelamin A, terminates in a CAAX motif, which signals a series of post-translational modifications, including farnesylation, endoproteolysis of the AAX residues, and carboxyl methylation of the newly exposed cysteine. Prelamin A then undergoes a discrete site-specific upstream cleavage mediated only by ZMPSTE24. This step removes 15 residues from the C-terminus, including the farnesylated and carboxyl methylated cysteine, releasing mature lamin A into the nucleoplasm (Figure 4.1).

Improper prelamin A processing caused by mutations in the gene encoding ZMPSTE24 results in progeroid diseases[9,130,131]. Uncleaved, persistently prenylated prelamin A was detected in patient fibroblasts[32,36,37,48,51–53]. In previous studies, decreased mating ability has been shown in a *ste24* deletion yeast strain expressing ZMPSTE24 disease mutations[50–52,130]. Reduced AAX cleavage activity of ZMPSTE24 disease mutants was also determined using an radioactive endoprotease-coupled methylation assay[130]. However, since ZMPSTE24 and another CAAX protease, RCE1, can both efficiently cleave the CAAX motif from prelamin A (unpublished data from Dr. Wiley, shown in Chapter 2), the ability of ZMPSTE24 to perform the upstream cleavage determines the level of accumulated uncleaved prelamin A in progeroid diseases (Figure 4.1). Therefore, it is critical to develop effective tools to detect the upstream cleavage of ZMPSTE24. Currently, immunoblot analysis is commonly used to detect the upstream cleavage by ZMPSTE24 in mammalian cells, since the mature lamin A is 2 kDa smaller than its precursor and the farnesyl group is removed, causing different electrophoretic mobility[15,68,131]. A mass

spectrometry binding assay has been reported to monitor the proteolysis by ZMPSTE24[65]. However, both methods are laborious, technically demanding, and difficult to quantify.

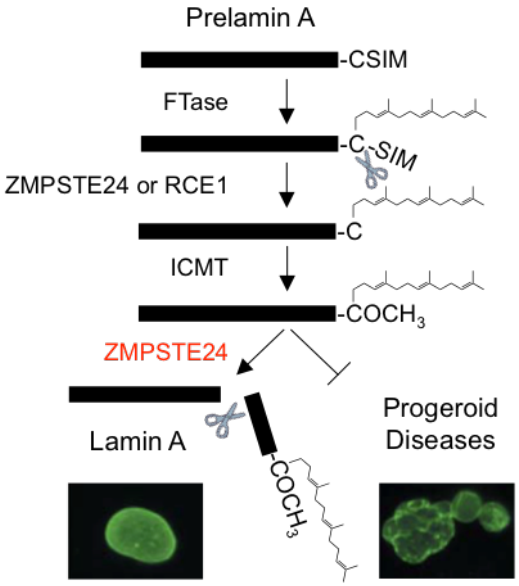

Figure 4.1. Schematic of lamin A maturation pathway.

The precursor of lamin A, prelamin A, terminates in the CSIM sequence, which triggers a series of post-translational modifications, including farnesylation by farnesyltransferase (FTase), endoproteolysis by ZMPSTE24 or RCE1, and carboxyl methylation by isoprenyl carboxyl methyltransferase (ICMT). An additional cleavage event is required by ZMPSTE24 to remove the last 15 residues, including the newly farnesylated and carboxyl methylated cysteine from the C-terminus, releasing mature lamin A into the nucleoplasm. However, if the last cleavage is blocked, uncleaved prelamin A accumulates and leads to misshapen nuclei[9,10,48]. Figure adapted with permission from "Compound heterozygous *ZMPSTE24* mutations reduce prelamin A processing and result in a severe progeroid phenotype" by Shackleton, S. *et al.*, 2005. Journal of Medical Genetics, Vol. 42, pg. e36. Copyright (2005), Journal of Medical Genetics

ZMPSTE24 has shown the ability to cleave the yeast **a**-factor peptide and complements the mating defect of *ste24* deletion yeast strain[121,125,126,130]. Herein, we adapted the FRET-based assay described in Chapter 3 to monitor the upstream cleavage of ZMPSTE24. We demonstrated that the **a**-factor sequence-based FRET peptide, which contains a 2-aminobenzoic acid (Abz) fluorophore at the N-terminus and a dinitophenol (Dnp) quencher located on the other side of the proposed cleavage site, was recognized and cleaved at the predicted position by ZMPSTE24 by LC-MS. We then examined the upstream cleavage activity of eight currently known disease-associated ZMPSTE24 missense mutants using this FRET-based assay. We also crudely

examined the protein folding of each mutant using a limited trypsin digestion method. Together with the crystal structure of ZMPSTE24, these assays can guide structure-function studies to uncover catalytic mechanisms of ZMPSTE24, by which further insights into progeroid diseases will be provided.

4.2 Methods

4.2.1 Plasmids and Yeast Strains

Plasmids used in this study are listed in Table 4.1. All plasmids contained N-terminally 10× His and 3× HA tagged human ZMPSTE24 and were constructed by the Michaelis lab (Johns Hopkins University). Each plasmid was transformed and expressed in the strain SM3614 (*MAT**a** trp1 leu2 ura3 his4 can1 ste24Δ::LEU2 rce1Δ::TRP1*)[121] and SM6186 (*MATα leu2 his3 ura3 ste24Δ::KanMX doa10Δ::KanMX*) (gift from Michaelis lab) using the Elble protocol[141]. After transformation, all yeast cells were grown at 30°C on synthetic complete medium without uracil (SC-URA).

Table 4.1. Plasmids used in this study

Plasmid	Genotype	Reference
pSM2677	*CEN URA3* P_{PGK}-His_{10}-HA_3-*ZMPSTE24*	130
pSM2678	*CEN URA3* P_{PGK}-His_{10}-HA_3-*ZMPSTE24-L94P*	130
pSM2676	*CEN URA3* P_{PGK}-His_{10}-HA_3-*ZMPSTE24-P248L*	130
pSM2671	*CEN URA3* P_{PGK}-His_{10}-HA_3-*ZMPSTE24-N265S*	130
pSM2673	*CEN URA3* P_{PGK}-His_{10}-HA_3-*ZMPSTE24-H335A*	130
pSM3162	*CEN URA3* P_{PGK}-His_{10}-HA_3-*ZMPSTE24-H339A*	131
pSM2672	*CEN URA3* P_{PGK}-His_{10}-HA_3-*ZMPSTE24-W340R*	130
pSM3186	*CEN URA3* P_{PGK}-His_{10}-HA_3-*ZMPSTE24-Y399C*	131
pSM3185	*CEN URA3* P_{PGK}-His_{10}-HA_3-*ZMPSTE24-L425P*	131
pSM2984	*CEN URA3* P_{PGK}-His_{10}-HA_3-*ZMPSTE24-L438F*	130
pSM3317	*CEN URA3* P_{PGK}-His_{10}-HA_3-*ZMPSTE24-L462R*	131

4.2.2 Cell Lysate Preparation from Yeast Cells

Cell lysates were prepared as previously described but with some modifications[131]. Yeast cells were grown in SC-URA media to log phase (3-5 OD_{600}/ml). Cells (3 OD_{600} cell equivalents) were pelleted, lysed using 0.2 M NaOH containing 1% β-mercaptoethanol on ice for

15 min, and incubated with 6% trichloracetic acid (TCA) on ice for another 15 min to precipitate the extracted proteins. After centrifugation at 13,000 × *g* for 15 min at 4˚C, pellets were then resuspended in 2× SDS loading buffer and heated at 65˚C for 20 min. Samples (0.1 OD_{600} cell equivalents) were analyzed by immunoblot.

4.2.3 Protein Purification

Yeast crude membranes overexpressing ZMPSTE24 were prepared as described in Chapter 2.2.2 for protein solubilization. Purified ZMPSTE24 proteins were prepared as Chapter 3.2.3 indicated. Protein concentration was determined using the Amido Black protein assay. Expression and purity levels were examined using immunoblot (0.5 μg of crude membrane or 0.01 μg of purified protein) and Coomassie staining (2 μg of purified protein), respectively, as Chapter 3.2.4 described.

4.2.4 LC/MS Analysis

Reactions contained 5 μg of wild-type or H335A purified ZMPSTE24 proteins, 200 μM Peptide **1** and 100 mM Tris-HCl, pH 7.5 in a total volume of 200 μl and were incubated at 30°C for 24 hours. Reactions were stopped by heating at 95°C for 2 min and then centrifuged at 13,000 × *g* to remove any precipitate. Cleavage products were analyzed by LC/MS using Waters 600 HPLC system interfaced with Waters ZQ ESI mass spectrometer. The solvent system used acetonitrile (solvent A) and water (solvent B). The reaction mixtures were injected directly onto a C8 column (2.1 mm × 25 cm) and the peptides were separated using 5% to 40% A over 10 min, 40% to 55% A over 10 min, and 55% to 95% A over 5 min at a flow rate of 33 μl/min. Eluted samples were monitored at 214 nm. Peptide intact masses were determined using ESI mass spectrometry and identified manually with software.

4.2.5 FRET-Based Assay

The assay with ZMPSTE24 was performed as described in Chapter 3.2.6. For pure proteins, 0.75 μg of purified ZMPSTE24 was rapidly reconstituted[140,142] into 6.25 μg of *E.coli* polar lipid (Avanti Polar Lipids) in 100 mM Tris-HCl, pH 7.5, incubated on ice for 5 min. For crude membranes, 30 μg of ZMPSTE24 crude membrane was added into 100 mM Tris-HCl, pH 7.5 with 10 μg/ml Chymostatin and 2 mM AEBSF. Samples were equilibrated at 30°C for 5 min then transferred to a 96-well plate. Assays were initiated by adding Peptide **1** to final

concentration of 30 μM and mixed by shaking for 30 seconds. Fluorescence readings were measured using a Synergy™ H4 microplate reader (BioTek) at excitation and emission wavelengths of 320 ± 9 nm and 420 ± 9 nm every 30 seconds over a 30 to 240 min time course at 30˚C. To record the excitation and emission spectra, excitation wavelengths ranged from 280 to 400 nm with a 5-nm increment, and the emission was measured at 420 nm. The emission wavelengths ranged from 360 to 500 nm with a 5-nm increment and excitation at 320 nm. Kinetic analysis and inhibitor studies were performed as Chapter 3.2.8 and 3.2.9 described.

4.2.6 Trypsin Digestion

To perform trypsin digestion, 10 μg of ZMPSTE24 crude membrane and 25 μg/ml trypsin (porcine pancreas, Sigma-Aldrich) or phosphate buffered saline (PBS) in 10 mM Tris-HCl, pH 7.5 were incubated at 37˚C for 30 min. Reactions were stopped by the addition of 1 mM AEBSF. The protein was then precipitated by 10% trichloroacetic acid (TCA), incubated on ice for 10 min, and then pelleted by centrifugation at 13,000 × *g* for 5 min at 4˚C. The pellets were then resuspended in 2× SDS loading buffer and heated at 65˚C for 20 min. Samples (0.5 μg of crude membranes) were analyzed by immunoblot.

4.2.7 Immunoblot Analysis

As described in Chapter 3.2.4, samples were resolved on a 10% SDS-PAGE gel and transferred to a 0.22 μm Protran® Nitrocellulose Membrane (GE Healthcare). The nitrocellulose membrane was blocked with 20% (w/v) nonfat milk in phosphate-buffered saline (137 mM NaCl, 2.7 mM KCl, 4 mM Na_2HPO_4, 1.8 mM KH_2PO_4, pH adjusted to 7.4) and 0.05% (v/v) Tween-20 (PBST), probed with α-HA antibody (1:15000) in 5% (w/v) nonfat dry milk in PBST and then detected with a horseradish peroxidase conjugated goat α-mouse antibody (1:4000). The protein bands were visualized using the SuperSignal® West Pico Chemiluminescent Substrate (Thermo Scientific).

4.3 Results and Discussion

4.3.1 Assay Validation with ZMPSTE24

To study the upstream cleavage of the ZMPSTE24 disease mutants, we first determined whether the FRET-based assay we developed in Chapter 3 could be performed with ZMPSTE24. The assay was tested with either crude or purified ZMPSTE24 successfully. Human wild-type and the proposed zinc-coordinating H335A mutant ZMPSTE24 (Figure 4.2.A) were used as positive and negative controls, respectively. Immunoblot analysis demonstrated that both crude membrane and purified protein of H335A mutant were expressed at a similar level as wild-type ZMPSTE24 (Figure 4.2.B and C). Coomassie stained SDS-PAGE showed purity was >90%, although the bands had a faster shifting rate compared to the expected molecular weight of His-HA-ZMPSTE24 at 60 kDa (Figure 4.2.D). Smearing bands below the major band may be degraded proteins or affected by the detergent. Spear *et al.* and Clark *et al.* also observed similar patterns previously[64,131].

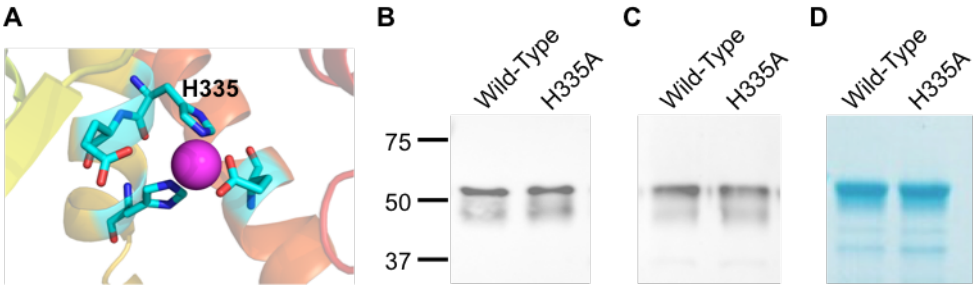

Figure 4.2. Purification of ZMPSTE24 wild-type and H335A mutant proteins.
(A) H335 is one of the proposed zinc-coordinating residues in ZMPSTE24. The zinc ion is shown in purple. Immunoblot analysis using the α-HA antibody indicated that H335A (B) crude membrane (0.5 μg) and (C) pure protein (0.01 μg) were at the similar expression level as wild-type. (D) Coomassie stain showed all proteins (2 μg) were >90% pure.

In the FRET assay with crude membranes, the maximum emission peaks occurred at 415 nm, which is close to the theoretical emission maximum of Abz fluorophore at 420 nm upon excitation at 320 nm. The fluorescence increased over time during the cleavage reaction catalyzed by wild-type ZMPSTE24 and no significant increase in fluorescence was detected with the H335A mutant (Figure 4.3.A). Purified ZMPSTE24 in liposomes also showed similar results with fluorescence intensity increasing over time with wild-type but not the catalytic mutant,

suggesting that Peptide **1** is recognized and processed by ZMPSTE24 (Figure 4.3.B). These data are consistent with the gel-based analysis results[125,131]. Together, these data suggest that ZMPSTE24 uses also a classical zinc metalloprotease mechanism for the upstream cleavage.

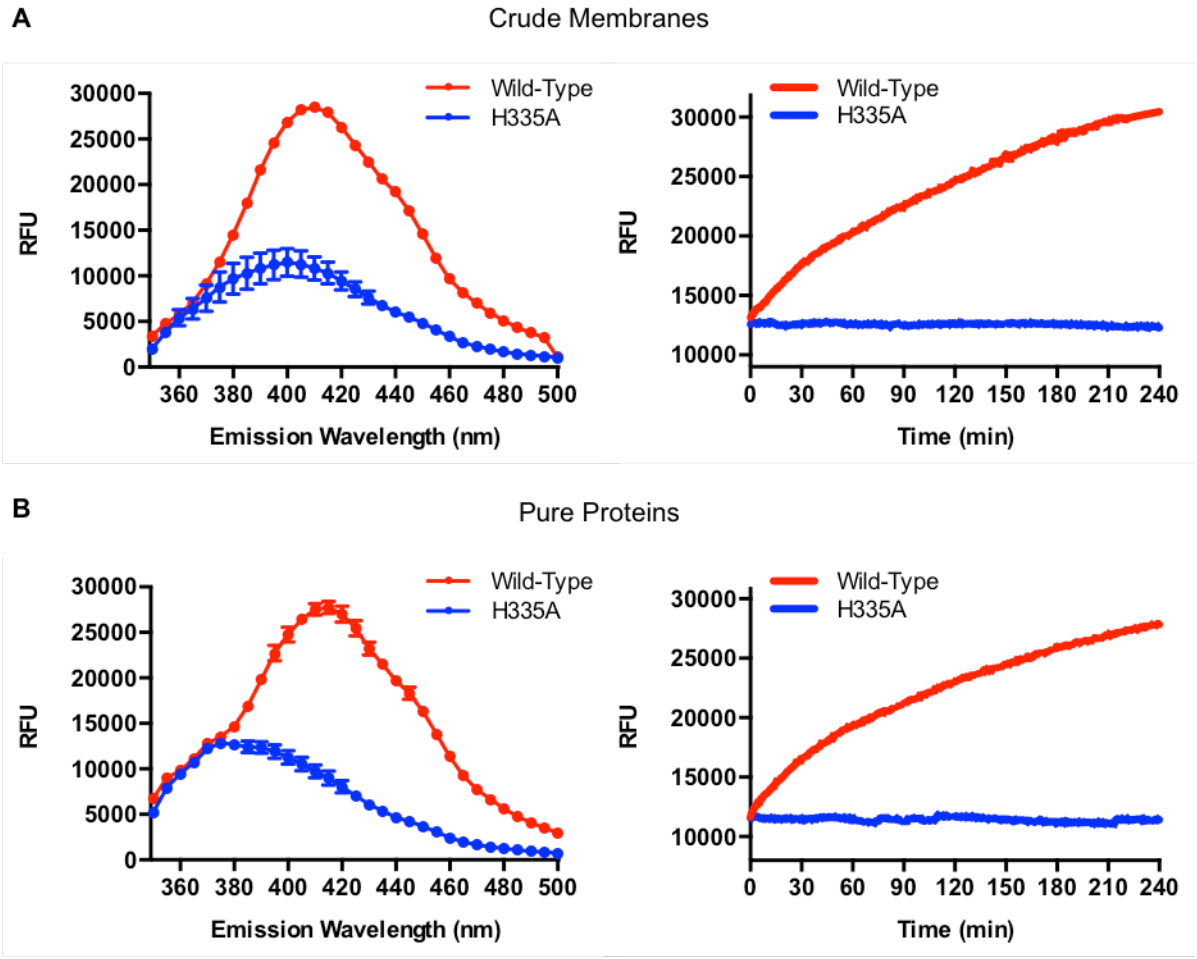

Figure 4.3. Upstream proteolytic activity of ZMPSTE24 using Peptide **1** as the substrate.

The fluorescence released from substrate cleavage by (A) crude or (B) purified wild-type or H335A mutant ZMPSTE24 were measured after incubation for 4 hours. The emission spectra were recorded and scanned from 350 to 500 nm with excitation wavelength at 320 nm. Fluorescence readings over a time course of 4 hours were detected with the excitation wavelength at 320 nm and emission wavelength at 420 nm, as described in the Methods section.

4.3.2 Verification of ZMPSTE24 Cleavage Site

The real-time monitoring data indicate that ZMPSTE24 upstream cleavage activity can be investigated by the FRET-based assay. However, since Peptide **1** is derived from yeast **a**-

factor and not prelamin A, the natural substrate of ZMPSTE24, ZMPSTE24 may cleave anywhere between the fluorophore and quencher, instead of the original cleavage site, resulting in the release of fluorescence from the substrate. To determine the precise cleavage site of the FRET substrate by ZMPSTE24, Peptide **1** was incubated with purified wild-type ZMPSTE24 or H335A mutant proteins for 24 hours. The reaction mixtures were then subjected to LC-MS for separation and identification of cleavage products. The LC-MS analysis showed that Peptide **1** was cleaved at its natural cleavage site by the wild-type ZMPSTE24 but not by the H335A mutant (Figure 4.4). Incubation with H335A showed one major peak at 18.4 min and the molecular mass matched the uncleaved Peptide **1** (observed: $[M+2H]^{+2}$ = 2075.8, calculated = 4146.8). We observed two major peaks in the chromatogram of incubation with wild-type ZMPSTE24. Based on the ESI-MS spectra, the peak eluted at 16.7 min (observed: $[M+2H]^{+2}$ = 1657.3, calculated = 3310.8) was the cleaved C-terminal (Peptide **3**) product. For the peak eluted at 10.1 min, we observed a major peak (observed: $[M+H]^{+1}$ = 854.7, calculated = 854.0), which was same the size as cleaved N- (Peptide **2**) and two minor peaks (m/z = 735.6 and 604.5), which were not consistent with any possible cleaved fragments. These results demonstrate that the major ZMPSTE24 cleavage site in the Peptide **1** is between the expected Thr-7 and Ala-8 residues.

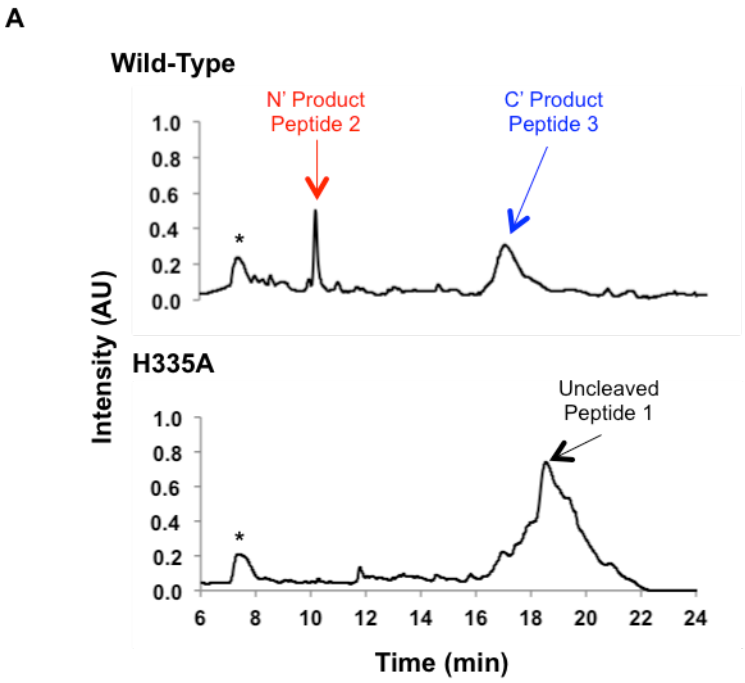

Figure 4.4. LC-MS analysis reveals that ZMPSTE24 cleaves the substrate at the expected site.

(A) LC chromatograms showing the separation of cleaved products or non-cleaved peptide produced from incubation with purified wild-type or H335A mutant ZMPSTE24. Peaks corresponding to Peptide **1**, **2**, and **3** are indicated. Purified ZMPSTE24 protein peaks are labeled with an asterisk. (B) An illustration of the expected proteolytic products at the native cleavage site and the theoretical molecular masses after ZMPSTE24 cleavage. Mass spectra of products derived from different LC fractions corresponding to Peptide **1**, **2**, and **3**, respectively.

Figure 4.4. continued

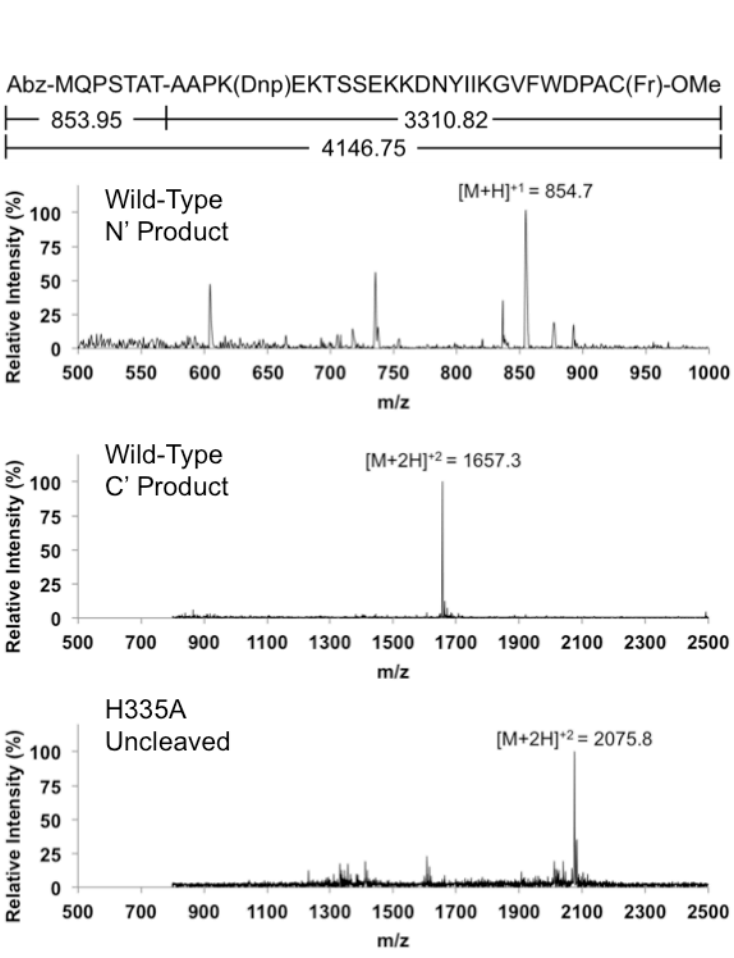

4.3.3 Kinetic Analysis

Crude or purified ZMPSTE24 proteins were incubated with varying substrate concentration. The fluorescence intensities of each reaction were monitored and recorded. As we did for the Ste24 cleavage reaction described in Chapter 3, the specific activities at each concentration were determined by converting and correcting the initial rates obtained from the first linear region. The K_m and V_{max} obtained from assays with crude ZMPSTE24 were 9.5 ± 1.0 μM and 810.4 ± 37.1 pmol/mg/min (Figure 4.5.A), showing similar affinity but slightly slower turnover compared to yeast crude membrane overexpressing Ste24. The kinetic parameters K_m and V_{max} were calculated as 6.7 ± 1.2 μM and $27.1 \times 10^3 \pm 1.9 \times 10^3$ pmol/mg/min, respectively (Figure 4.5.B). This is the first time that kinetic parameters of the ZMPSTE24 upstream cleavage

are reported. K_m value was similar to 9.1 ± 1.3 μM but the V_{max} was lower than 37.6 × 10^3 ± 2.4 × 10^3 pmol/mg/min compared to the kinetic parameters of Ste24 we have obtained in Chapter 3. Taken together, these results indicate that Peptide **1** was recognized and cleaved by ZMPSTE24 just as Ste24.

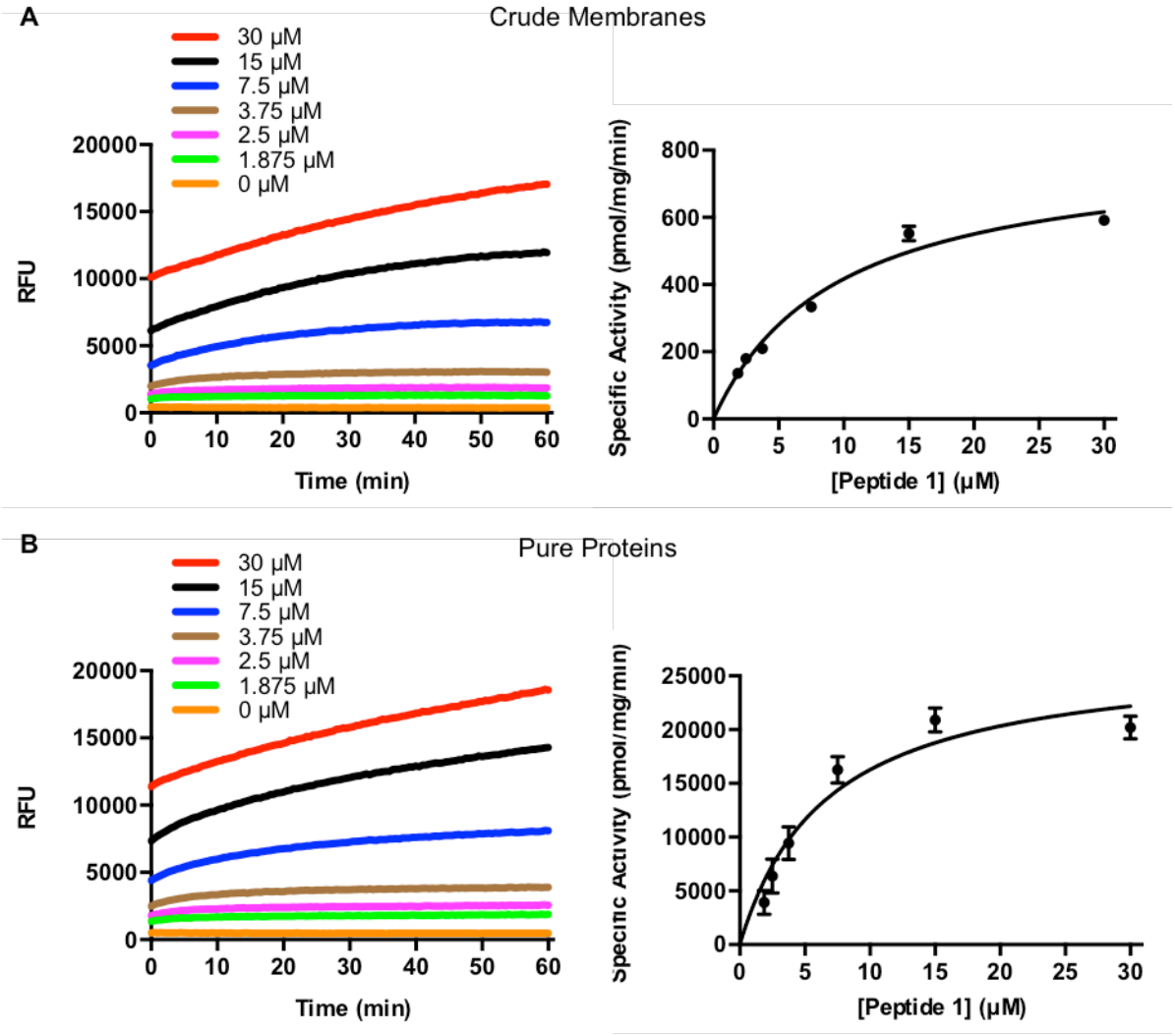

Figure 4.5. Kinetic studies of Peptide **1** substrate cleavage by ZMPSTE24.

Fluorescence readings for (A) crude or (B) purified ZMPSTE24 in liposomes with indicated concentrations of the substrate over a time course of 1 hour. Initial rates were found to be within the first 2 to 10 minutes. Specific activities converted from initial rates and substrate concentrations were plotted and fitted into the Michaelis-Menten equation. From this data, the values of kinetic parameters V_{max} and K_m were determined.

4.3.4 Inhibitor Studies

ZMPSTE24 is a known zinc metalloprotease[20,64]. Using mutants in the HEXXH zinc-binding consensus sequence, we have demonstrated that the zinc-binding HEXXH motif is important for both cleavages of ZMPSTE24. No evidence has shown that this enzyme will use other mechanisms for catalysis. Strikingly, several studies have reported that certain types of HIV protease inhibitors (HIV-PIs), designed to target the HIV retroviral aspartyl protease, lead to prelamin A accumulation in cells[57,62,63]. These HIV-PIs, including lopinavir (LPV), ritonavir (RTV) and tipranavir (TPV), but not darunavir (DRV), inhibit the CAAX proteolysis of ZMPSTE24 and have shown competitive binding to ZMPSTE24[62–65]. But the inhibition effects to ZMPSTE24 upstream cleavage have not yet been reported. Here we used the FRET assay to examine whether the HIV-PIs affect the upstream cleavage of ZMPSTE24. Purified ZMPSTE24 was incubated with varying concentrations of LPV and DRV. Specific activities were calculated and plotted to generate inhibition curves. As expected, DRV did not inhibit ZMPSTE24 appreciably up to 200 μM (Figure 4.6, *blue*). The upstream cleavage of ZMPSTE24 was inhibited by LPV with an IC_{50} of 29.5 ± 1.3 μM, which is close to the K_D value of 25 ± 1.2 μM reported from the mass spectrometry assay[65]. However, even using a high concentration, LPV only inhibited the upstream cleavage activity of ZMPSTE24 to about 40% (Figure 4.6, *red*). This effect may be due to the presence of excess lipid. However, the upstream cleavage activity of crude ZMPSTE24 was inhibited to about 30% with LPV at 200 μM (data not shown). Therefore, the high drug concentration may cause precipitation or non-complete solubilization of LPV. Compared to LPV inhibition of AAX cleavage, Hudon *et al.* reported similar results that LPV only inhibited the AAX cleavage activity of purified Ste24 in liposome, yeast homolog of ZMPSTE24, to about 50% with LPV concentration at 300 μM[142]. Moreover, Coffinier *et al.* reported that the AAX cleavage of ZMPSTE24 was inhibited by LPV with an IC_{50} of 18.4 μM[63], which is similar to the IC_{50} value for the upstream cleavage. Clark *et al.* also determined that the AAX cleavage of ZMPSTE24 was inhibited by LPV with a K_i of 5.6 ± 1.1 μM, and was fitted with the competitive model[64]. The inhibition mechanism of HIV-PIs to the upstream cleavage of ZMPSTE24 will need to be further studied.

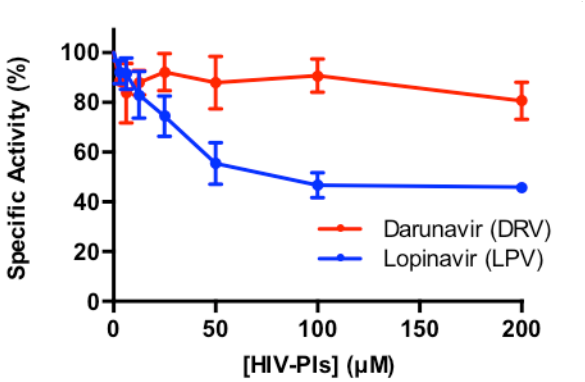

Figure 4.6. Inhibition effects of HIV-PIs on the upstream proteolytic activity of purified Ste24.

Different concentrations of HIV-PIs darunavir (*red*) or lopinavir (*blue*) were incubated with purified ZMPSTE24 for 5 minutes before adding the peptide substrate to start the assay. Percentages of specific activity were plotted with HIV-PIs concentrations. Inhibition constants were determined from the fitted nonlinear regression curves.

4.3.5 Characterization of ZMPSTE24 Disease Mutants

We have demonstrated that the FRET substrate, Peptide **1**, could be efficiently processed by wild-type ZMPSTE24, in both yeast crude membranes and purified protein systems (Figure 4.5). The upstream cleavage activity of each ZMPSTE24 disease mutant was then examined using the FRET-based assay. Mutations in ZMPSTE24 have been reported from the patients with progeroid diseases, including B-type mandibuloacral dysplasia (MAD-B) and restrictive dermopathy (RD), and metabolic syndrome (MS)[28,131]. Most of the mutations are frameshift or nonsense mutations that cause early termination, or large internal in-frame deletions that could interfere with the structural integrity of ZMPSTE24. Therefore, here we only examined eight missense mutations of ZMPSTE24. Wild-type (WT) and H335A were used as positive and negative controls, respectively. L94P, P248L, N265S, W340R, Y399C, and L425P were found in MAD patients. L438F was discovered from MS patients. L462R was reported from RD patients (Figure 4.7.A).

All mutants were purified using the detergent n-Dodecyl-β-D-maltoside (DDM). All disease mutants demonstrated 50% or more reduced activity as compared to WT (Figure 4.7.B). As predicted, the zinc-coordinating H335A and H339A mutants were completely inactive, as Chapter 4.3.1 described. Some mutants, such as L94P, L425P, and L462R, had lower expression

levels, despite loading the same total amount of protein, suggesting that they may be unstable or aggregated (Figure 4.7.B).

To confirm their low activities were not due to inherent enzymatic inactivity proteins, we also examined the upstream cleavage activity of crude membrane from SM3614 (*Δste24Δrce1*), a yeast strain without endogenous Ste24, overexpressing each ZMPSTE24 disease mutant (Figure 4.8). The H335A lost its activity as predicted. L94P, N265S, W340R, L438F, and L462R demonstrated 20% or more reduced activity as compared to WT, which were consistent with the purified protein data. However, Y399C and L425P showed about 2-fold higher and similar activity levels compared to WT, respectively, suggesting that they may lose their activities during the purification process. Surprisingly, P248L expressed in crude membranes only displayed less than 10% activity, but its purified protein showed approximate 50% activity (Figure 4.7.B). We also observed that some disease mutants, including P248L, showed lower protein expression levels in yeast membranes compared to WT (Figure 4.8).

Several studies have reported that some ZMPSTE24 mutations showed reduced expression levels in patient fibroblasts and yeast expression system[53,130,131]. Spear *et al.* suggested that these lower expression levels might be due to protein misfolding and subsequent degradation and showed that blocking the ubiquitin-dependent degradation can rescue protein levels of ZMPSTE24 disease mutants[131]. To explore whether the protein expression level affect ZMPSTE24 cleavage activity, we examined the yeast crude membrane overexpressing ZMPSTE24 from two different yeast strains, SM3614 (*Δste24Δrce1*) and SM6186 (*Δste24Δdoa10*). Therefore, we used the SM6186 yeast strain, which has a deletion of the gene encoding Doa10, a dually localized ER and INM E3 ligase known to ubiquitylate many misfolded transmembrane proteins and target them for degradation. Expression levels of ZMPSTE24 mutant proteins from yeast lysates all increased in the *Δdoa10* strain, indicating that all are substrates, either partially or fully, of this ubiquitin ligase. However, when we normalized the expression using WT as the standard, N265S, H335A, and Y399C in SM6186 showed no/slight increased percentage compared to SM3614. P248L and W340R expression were dramatically increased with by 2- and 5-fold, respectively. They also showed comparable expression levels to WT. L94P, L425P, L438F, and L462R also revealed elevated expression percentages (Figure 4.9).

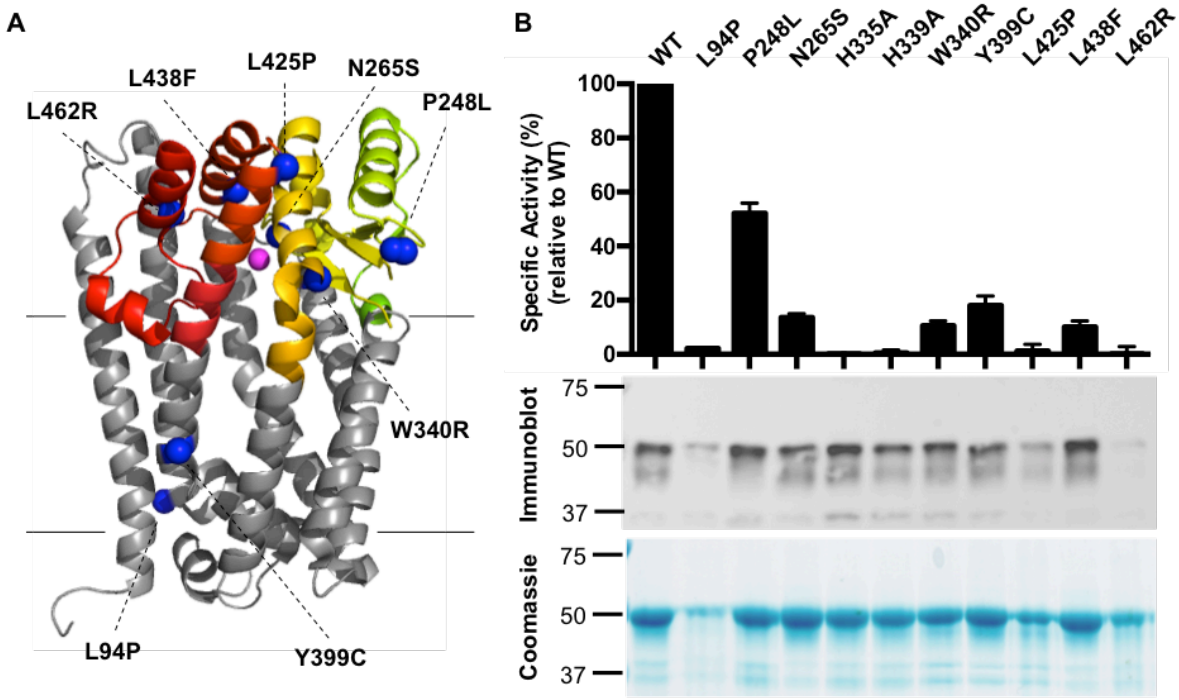

Figure 4.7. Purified ZMPSTE24 disease mutants demonstrated reduced upstream cleavage activity compared to wild-type (WT) ZMPSTE24.

(A) ZMPSTE24 disease mutations are labeled with black dotted lines. The zinc ion is shown in purple. Most of the mutations are located in the zinc metalloprotease domain, except L94P and Y399C. PDB: 4AW6 (B) The activity of each mutant with Peptide **1** was measured using the FRET-based assay and reported as the percentage of relative activity to WT. Expression and purity levels of each mutant were examined using immunoblot (0.01 μg) and Coomassie stain (2 μg), respectively.

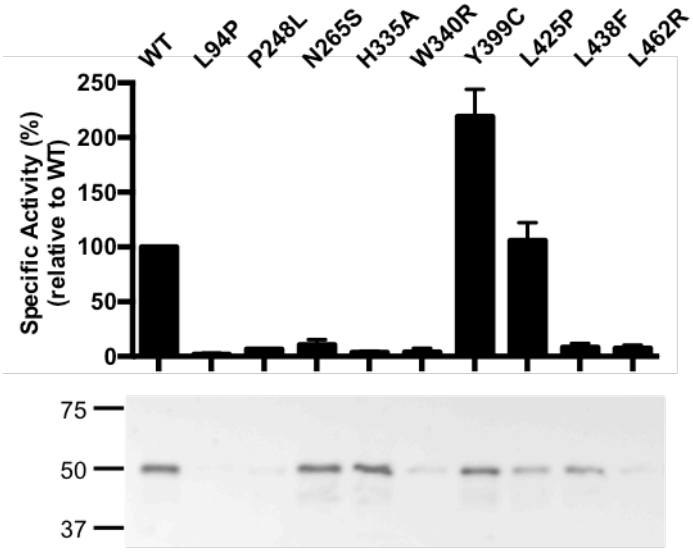

Figure 4.8. Crude ZMPSTE24 disease mutants demonstrated varied upstream cleavage activity compared to wild-type (WT) ZMPSTE24.

The activity of each mutant with Peptide **1** was measured using the FRET-based assay and reported as the percentage of relative activity to WT. The expression level of each mutant was examined using immunoblot (0.5 μg) with the α-HA antibody.

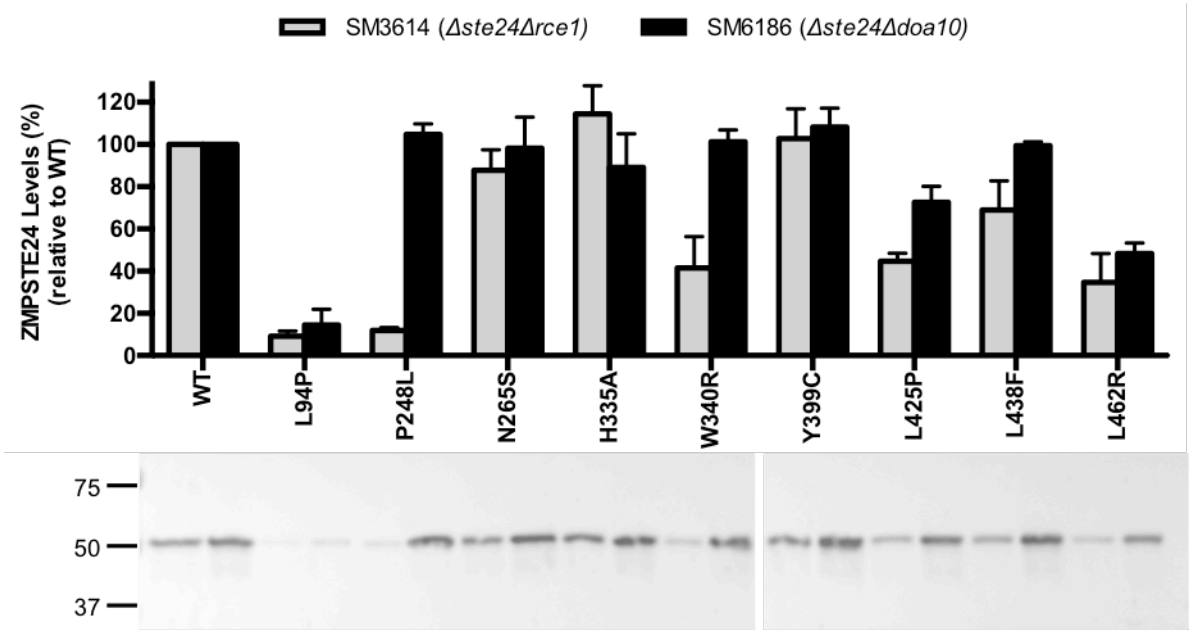

Figure 4.9. Blocking the ubiquitin-dependent degradation enhanced the expression levels of ZMPSTE24 disease mutations from yeast lysates.

To examine the effects of blocking ubiquitylation, cell lysates (0.1 OD_{600} cell equivalents) prepared from SM3614 (*Δste24Δrce1*, *grey*) and SM6186 (*Δste24Δdoa10*, *black*) yeast strains overexpressing the indicated ZMPSTE24 disease mutations were analyzed using immunoblot with the α-HA antibody. Expression levels were quantified and showed as the percentage of relative expression to wild-type (WT) ZMPSTE24.

We then compared the activity and expression level of each mutant expressed in SM3614 and SM6186 yeast strains, with normalized values using WT as 100%. As the negative control, H335A was completely inactive with a similar expression level as WT. Activity and expression levels of N265S, Y399C, and L425P did not change between the two strains, suggesting that these mutants may not be affected by ubiquitylation. Interestingly, crude Y399C and L425P were still active but purified proteins showed less than 20% activity (Figure 4.8), which is possibly affected by protein aggregation during the purification process. For P248L and W340R, their expression levels increased at least 5-fold in the *Δdoa10* strain, and they were more active, but still below 50% as compared to WT. In other disease mutants, including L94P, L438F, and L462R, both expression and activity levels increased in the *Δdoa10* strain but not as dramatically as P248L and W340R (Figure 4.10).

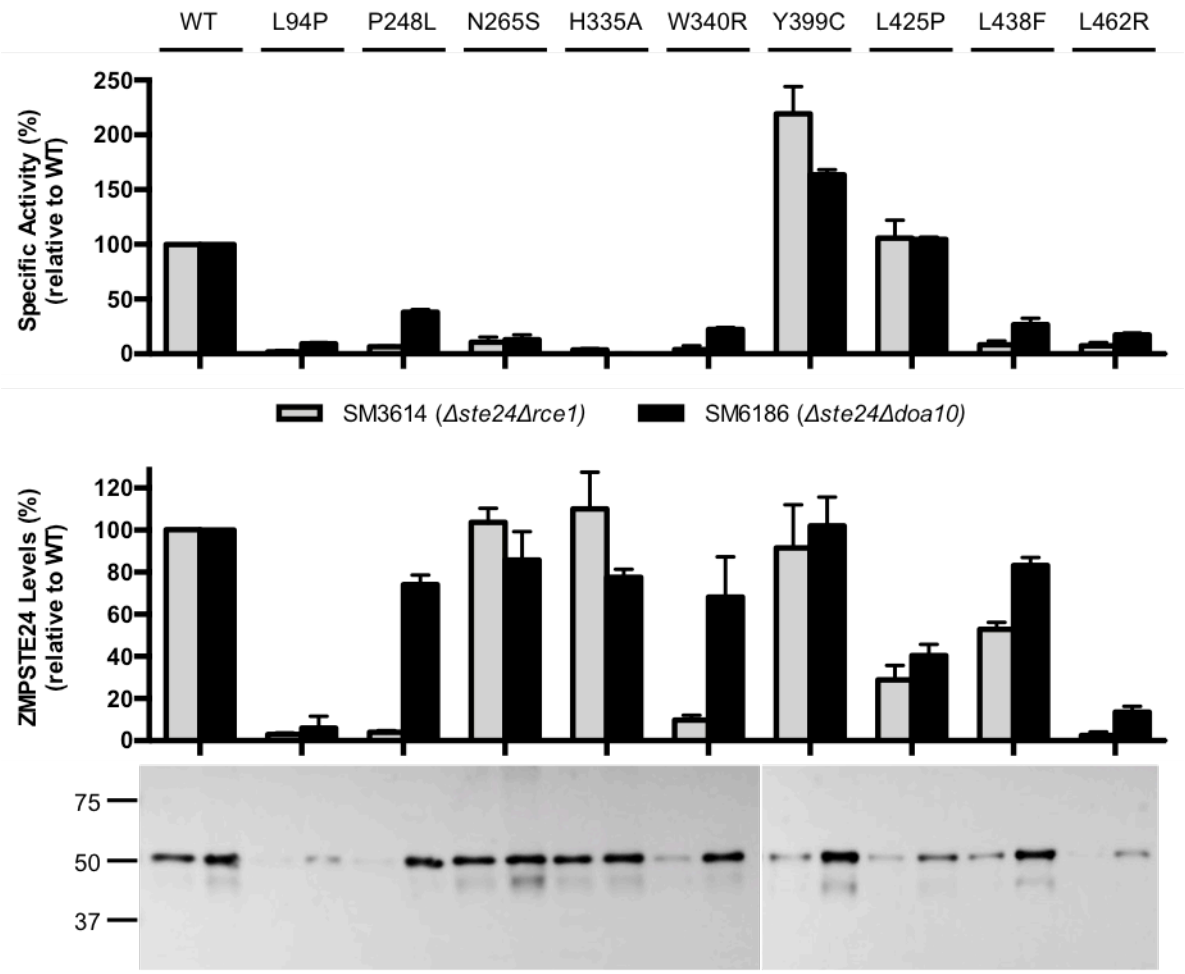

Figure 4.10. Blocking the ubiquitin-dependent degradation enhanced expression and rescued upstream cleavage activity of some ZMPSTE24 disease mutations overexpressed in yeast crude membranes.

To examine the effects of blocking ubiquitylation, yeast crude membranes prepared from SM3614 (*Δste24Δrce1*, *grey*) and SM6186 (*Δste24Δdoa10*, *black*) yeast strains overexpressing the indicated ZMPSTE24 disease mutations were analyzed using FRET-based assay and immunoblot (0.5 μg) with the α-HA antibody. The activity and expression of each mutant were reported as the percentage of relative level to wild-type (WT) ZMPSTE24.

4.3.6 Trypsin Digestion of ZMPSTE24 Disease Mutants

To determine possible structural changes within the mutant proteins, we utilized a partial trypsin digestion method to compare differences of protein folding[157]. Trypsin cleaves proteins at the C-terminus of lysine and arginine residues. Based on PeptideCutter prediction, ZMPSTE24 contains 49 possible trypsin cleavage sites, however, most of them are buried within

the membrane. We first examined if ZMPSTE24 overexpressed in yeast crude membrane could be digested by trypsin.

Yeast crude membrane overexpressing His-myc-tagged Ste14 was used as the positive control that we have previously demonstrated its cleavage. A digested band around 30 kDa was detected using α-myc antibody[157] (Figure 4.11). We also examined the yeast homolog of ZMPSTE24, Ste24, under these conditions. However, no digested band was shown, this may be because the targeted residues were not exposed to trypsin. We will optimize the conditions for Ste24. Crude ZMPSTE24 incubated with trypsin displayed two digestion bands, one slightly above 37 kDa and another slightly below 37 kDa. These results suggest that the proposed cleavage sites occurred between TMH5 and 6 (Figure 4.11).

To further confirm the digestion, ZMPSTE24 was incubated with trypsin for different time courses to 90 min. The digestion result revealed that with longer incubation, the below 37 kDa digested product increased. When the incubation time was more than 60 min, a third digested product showed up, right below the second cleavage band (Figure 4.12).

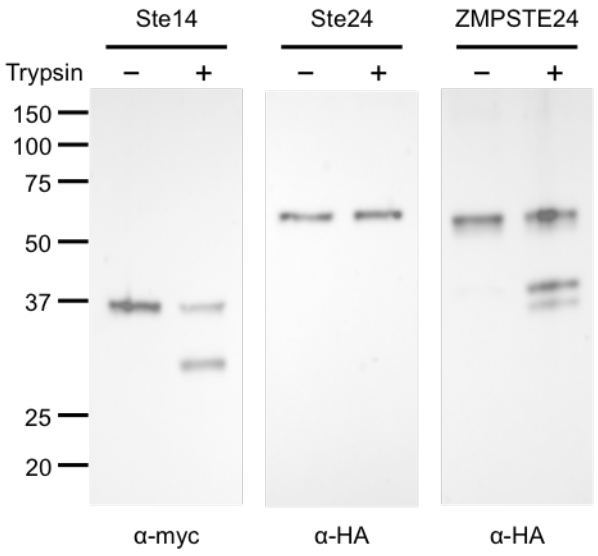

Figure 4.11. Trypsin digestion of Ste14, Ste24, and ZMPSTE24.

Ste14, Ste24, and ZMPSTE24 crude membranes were incubated with PBS or trypsin (25 μg/ml) for 30 min. Precipitated samples (0.5 μg) were then analyzed by immunoblot.

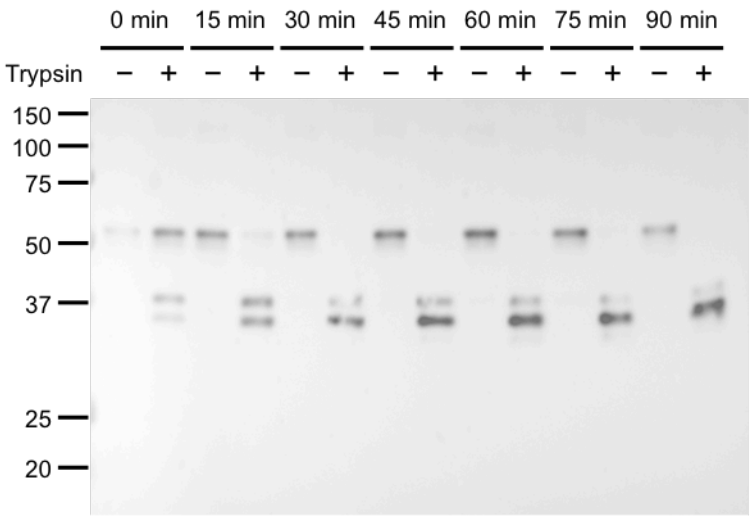

Figure 4.12. Trypsin digestion of ZMPSTE24 with different incubation period.

ZMPSTE24 crude membranes were incubated with PBS or trypsin (25 μg/ml) by a time course from 0 to 90 min. Precipitated samples (0.5 μg) were then analyzed by immunoblot using the α-HA antibody.

Yeast crude membranes overexpressing ZMPSTE24 disease mutants prepared from SM6186 (*Δste24Δdoa10*) strain were incubated with trypsin for 30 min. Due to lower expression levels, samples of L94P, L425P and L462R mutants were loaded with 5 time more protein. Wild-type (WT) showed two digestion bands as described above. Most of the mutants, except L425P and L462R, displayed the same digestion pattern as WT, with two digestion products around 37 kDa. L425P and L462R showed two extra trypsin digestion bands around 30 kDa. Moreover, these two mutants also showed degradation in samples without trypsin, suggesting they may not have proper folding as WT and other mutants (Figure 4.13).

To further confirm that formation of these extra bands was not due to increased loading, we compared trypsin digestion patterns between 1-fold, 5-fold, and 10-fold loading concentrations of WT, L94P, L425P, and L462R. From the digestion results, we did not observe extra digestion bands in WT or L94P samples when 5- or 10-fold protein was loaded. L425P and L462R still revealed extra bands around 30 kDa and degradation in non-treated samples (Figure 4.14). Together, our data suggest that the lower activity of L425P and L462R may be due to improper protein folding.

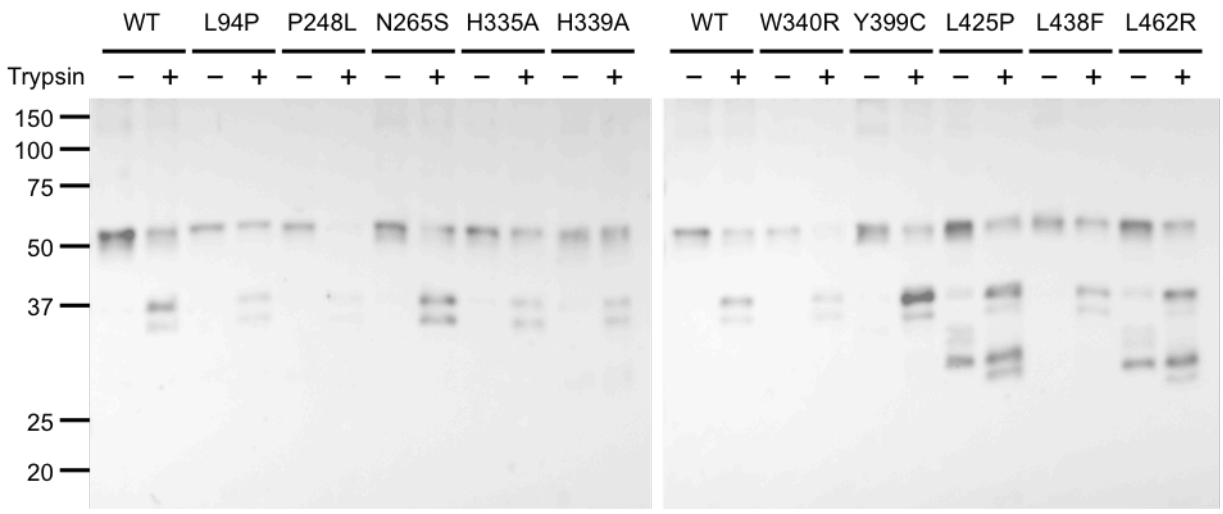

Figure 4.13. Trypsin digestion of ZMPSTE24 disease mutants.

Crude membranes overexpressing ZMPSTE24 disease mutants were incubated with PBS or trypsin (25 μg/ml) for 30 min. Precipitated samples (0.5 μg) were then analyzed by immunoblot using the α-HA antibody. L94P, L425P, and L462R were loaded with 5-fold higher concentration (2.5 μg) due to lower expression levels.

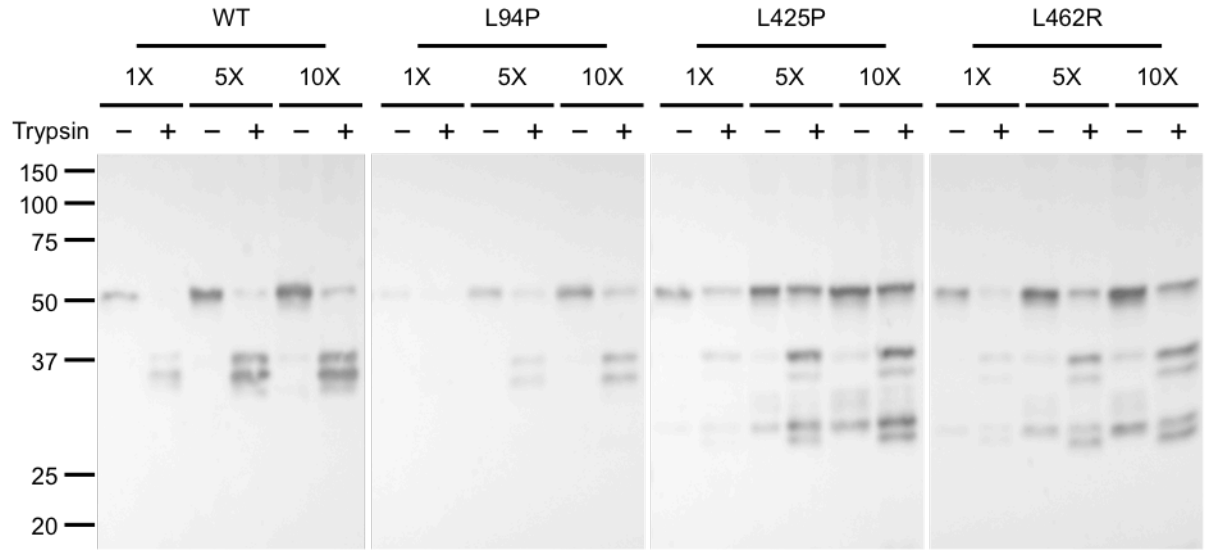

Figure 4.14. Trypsin digestion of ZMPSTE24 wild-type (WT), L94P, L425P, and L462R disease mutants.

Crude membranes overexpressing WT and ZMPSTE24 disease mutants were incubated with PBS or trypsin (25 μg/ml) for 30 min. Precipitated samples were then analyzed by immunoblot using the α-HA antibody. Each sample was loaded with 1-, 5-, and 10-fold concentration (0.5, 2.5, and 5 μg) to compare their digestion patterns.

4.4 Conclusions

In summary, we have shown that the FRET substrate, Peptide **1**, can be well recognized and cleaved by ZMPSTE24. Moreover, the proposed zinc-coordinating mutant H335A was completely inactive, suggesting that ZMPSTE24 uses a classical zinc metalloprotease mechanism for the upstream cleavage. Based on the proposed catalytic mechanism (Figure 1.12)[20], the zinc ion is coordinated by His-335, His-339, Glu-415, and a water molecule. The replacement of His-335 by alanine may affect the stability between the zinc ion and the water molecule, and thus interfere with the incoming substrate to displace the water molecule towards Glu-336. Our data is consistent with several published studies. Spear *et al.* showed that the prelamin A processing was defective in the yeast strain transformed with H335A mutant[131]. Schmidt *et al.* reported that a zinc chelator 1,10-orthophenanthroline could inhibit the upstream cleavage by ZMPSTE24[125].

Purified disease variants were examined using the FRET-based assay and showed reduced upstream cleavage activity as we predicted. However, the activity data obtained from yeast crude membranes showed different results. Two disease mutants, Y399C and L425P, demonstrated higher or similar cleavage activity compared to WT, suggesting that they become inactive during the purification process. Another disease mutant, P248L, showed highly reduced activity compared to its purified protein. Moreover, four disease mutants, L94P, P428L, W340R, and L462R showed remarkable decreases in ZMPSTE24 protein levels, which were lower than 10% compared to WT. The lower expression levels are consistent with previous observations that some disease mutants had reduced protein levels in patient fibroblasts[53] or when expressed in yeast[131]. These data suggest that these mutants may have reduced stability and thus lead to reduced activity.

Using a *doa10* deletion yeast strain, we have demonstrated that blocked ubiquitylation could restore partial activity of some disease variants, including L94P, P248L, W340R, L438F, and L462R. Moreover, our trypsin digestion data suggested that L425P and L462R may have improper protein folding. Here we classify these mutants into three different groups based on their activity and stability. The first group contains N265S, which affect activity by disrupting catalysis directly. Comparing the structure of ZMPSTE24 to thermolysin, a known zinc metalloprotease, Asn-265 is in a position similar to thermolysin Asn-112, which stabilizes the

transition state during catalysis[20,64,158,159]. Therefore, N265S mutation may not be able to form hydrogen bonds with the scissile amide and thus lose the cleavage activity (Figure 4.15).

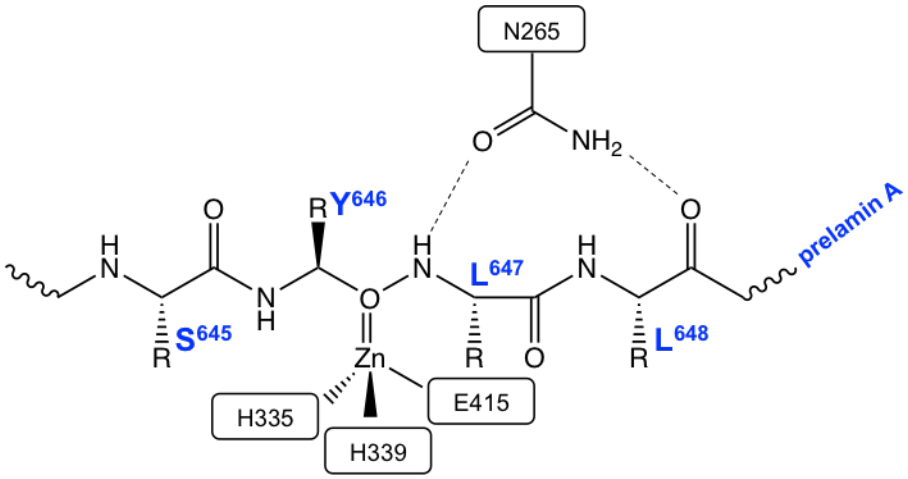

Figure 4.15. Proposed substrate binding position in the active site of ZMPSTE24.

Proposed zinc-coordinating residues, His-335, H339, and Glu-415, catalytic residue Glu-336, and predicted substrate stabilizing residue Asn-265 are shown. Asn-265 may form hydrogen bonds with Leu-647 and Leu-648 in prelamin A.

The second group includes L94P, P248L, W340R, L438F, and L462R, which affect both activity and protein stability. By comparing activity and expression levels of crude membranes between SM3614 (*Δste24Δrce1*) and SM6186 (*Δste24Δdoa10*) strains, they showed increased protein expression levels by 2- to 20-fold and elevated activity levels by 2- to 6-fold, suggesting that their activities could be partially restored with higher protein expression. However, their activities did not fully recover to 100% as compared to WT. For example, in SM6186, the expression level of P248L was about 20-fold higher compared to expression in SM3614. However, the activity level only reached to 38% compared to WT in SM6186, which was only 6-fold higher, indicating that the mutant may affect other factors, such as substrate binding or entry/exit, besides protein stability.

For the third group, crude Y399C and L425P did not show reduced cleavage activity. However, purified Y399C and L425P were only with 18% and 1% activity compared to WT, respectively. Inactive proteins may be generated due to improper purification process. However, patients with either mutation in *ZMPSTE24* gene were characterized with classical MAD-B symptoms and showed uncleaved prelamin A in fibroblasts from immunoblot analysis[54,55].

Moreover, utilizing a yeast strain expressing chromosomally integrated prelamin A, Spear *et al.* reported that transformed Y399C and L425P could only perform 26% and 42% prelamin A cleavage, respectively[131]. One possible reason of obtaining different activity levels is that we utilized the yeast **a**-factor, but not human prelamin A, sequence-based peptide as the assay substrate. ZMPSTE24 could mediate upstream cleavage of both **a**-factor (between Thr-7 and Ala-8) and prelamin A (between Tyr-646 and Leu-647)[15,121,125,126,131]; however, the cleavage site sequences are totally different, and thus, ZMPSTE24 may recognize the substrate in different ways. It will be important to develop a prelamin A sequence-based substrate to confirm the substrate specificity of ZMPSTE24. Together, this FRET-based assay will help us to understand how disease mutations affect ZMPSTE24 function, uncover ZMPSTE24 catalytic mechanism, and thus provide benefits for studying progeroid diseases.

CHAPTER 5. EVALUATION OF SUBSTRATE BINDING OF ZMPSTE24 DISEASE MUTANTS USING A PHOTOACTIVE BIOTINYLATED PROBE

The dissertation author designed and performed all the experiments. Dr. Susan Michaelis at Johns Hopkins University provided the ZMPSTE24 mutant plasmids and yeast strains. Dr. Mark Distefano at University of Minnesota synthesized the photoreactive probe.

5.1 Introduction

The nuclear scaffold protein lamin A, along with lamin B and C, comprise the laminar network underlying the inner nuclear membrane (INM) that maintains the structural integrity and proper functioning of the nucleus[1,3]. The precursor of lamin A, prelamin A, undergoes a series of post-translational modifications to form mature lamin A, including farnesylation by FTase, AAX cleavage by ZMPSTE24 or RCE1, methylation by ICMT, and upstream cleavage to remove the last 15 residues from the C-terminus by ZMPSTE24[9,10]. Improper prelamin A processing caused by mutations in the gene encoding ZMPSTE24 results in progeroid diseases[9,130,131].

ZMPSTE24 disease mutants have been shown to possess reduced cleavage levels for both AAX and upstream cleavages due to diminished cleavage activity or lowered protein stability[130,131]. Moreover, in Chapter 4, we have demonstrated that certain ZMPSTE24 disease mutants may have improper protein folding and thus lead to defective cleavage. However, how other disease mutations decrease ZMPSTE24 function is still unclear. Besides affecting protein expression and structural integrity, mutations may prevent substrate binding in the active site or occlude substrate entry based on the crystal structures of ZMPSTE24 and modeling with other zinc metalloproteases[20,64,124]. In this chapter, we have examined the substrate binding ability of ZMPSTE24 disease mutants using a photoaffinity labeling method.

Compounds containing photoactive benzophenone moieties have been used to define the protein binding sites for farnesyl and geranylgeranyl moieties. This approach was first utilized to study the interaction between the CAAX protein Rho and its regulator RhoGDI, also demonstrating that the isoprenylated probes with different photoactive groups were recognized by prenyltransferases[160]. The same strategy was used to synthesize a group of benzophenone-based farnesyl diphosphate (FPP) analogues for structural studies[161]. Moreover, a series of **a**-factor sequence-based analogs with photoactive benzophenone group were synthesized to

evaluate substrate or inhibitor binding of different enzymes related to CAAX processing, including RCE1[162,163], ICMT[164,165] and yeast pheromone receptors[166–169].

In this study, we used C10-para peptide (Figure 5.1), a photoreactive **a**-factor derived analog, to examine the substrate binding ability of ZMPSTE24 disease mutants, focusing on farnesyl group recognition since farnesylation is an important step for both cleavage reactions. C10-para is a truncated and farnesylated **a**-factor sequence-based peptide, containing a biotin tag on the N-terminus and a benzophenone photoreactive group in the farnesyl group. We have demonstrated that this C10-para peptide is a substrate of Ste24 and can be efficiently recognized and processed (unpublished data from Dr. Wiley). Since Ste24 and ZMPSTE24 have overlapping substrate specificity, the C10-para peptide may possibly be used for studying ZMPSTE24 as well. Using the radioactive endoprotease-coupled methylation assay and chemical crosslinking method, we determined the AAX cleavage activity and the ability to be photolabeled with C10-Para of eight currently known ZMPSTE24 disease-associated mutants.

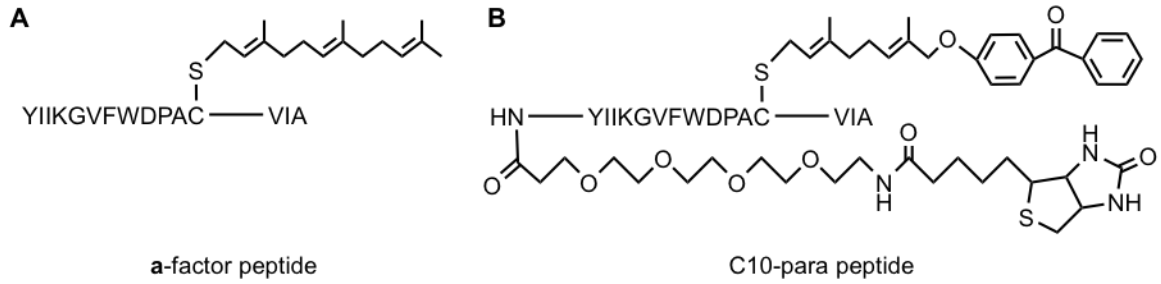

Figure 5.1. Structures of truncated **a**-factor and the photoactive analog C10-para peptide.
The C10-para peptide is farnesylated and contains a benzophenone group in place of the farnesyl group and a biotin tag. The biotin tag can be used for protein enrichment by neutravidin agarose beads. The benzophenone group allows for specific labeling of the substrate binding site.

5.2 Methods

5.2.1 Protein Purification

Yeast strains used in this study were constructed in Chapter 2.2.1 and 4.2.1. Yeast crude membranes overexpressing Ste24, Ste14, and ZMPSTE24 disease mutants were prepared as described in Chapter 2.2.2 for protein solubilization. Purified proteins were prepared as Chapter 3.2.3 indicated. Protein concentration was determined using the Amido Black protein assay.

Expression and purity levels were examined using immunoblot and Coomassie staining, respectively, as Chapter 3.2.4 described.

5.2.2 Radioactive Endoprotease-Coupled Methylation Assay

The substrate specificity was determined using the radioactive endoprotease-coupled methylation assay as previously described but with minor modifications[130,142]. For crude membranes, reactions containing 5 μg of Ste24 or ZMPSTE24 membranes, 10 μg of the Ste14 membranes[130], 15 μM or varying concentrations of **a**-factor (YIIKGVFWDPAC(Fr)-VIA, EZBioLab) peptide or C10-para peptide (synthesized by Distefano lab), and 20 μM *S*-adenosyl-[^{14}C-methyl]-L-methionine (Perkin Elmer) were incubated in 100 mM Tris-HCl, pH 7.5. For purified proteins, reactions with 0.12 μg of Ste24 or ZMPSTE24 proteins, 0.48 μg of Ste14 protein[140,142], 30 μM or varying concentrations of **a**-factor peptide or C10-para peptide were rapidly reconstituted[140,142] into 40 μg of *E.coli* polar lipid (Avanti Polar Lipids) in 100 mM Tris-HCl, pH 7.5, incubated on ice for 5 min. After incubation, 20 μM *S*-adenosyl-[^{14}C-methyl]-L-methionine was then added into the mixture. The reaction mixtures were incubated for 30 min at 30°C (yeast Ste24) or 37°C (human ZMPSTE24), quenched by 1 M NaOH and 1% SDS mixture, spotted onto pleated filter paper and then placed in the neck of a scintillation vial containing 10 ml of Biosafe II scintillation fluid (RPI) and capped. As a result of the quench reaction, the [^{14}C]-methanol was released from the cleaved and methylated substrate and diffused into the scintillation fluid for 3 hr at room temperature. After removing the filter paper, the radioactivity was quantified using a Packard TriCarb Scintillation counter. Specific activity was determined as pmol of AAX residues removed per min per mg of protease. Each value was derived from three assays performed in duplicate. The kinetic parameters were established by fitting specific activity and substrate concentrations to the Michaelis-Menton equation using GraphPad Prism 6.

5.2.3 Photocrosslinking and Neutravidin Pull-Down Assay

The photocrosslinking assay was performed as previously described but with minor modifications[164,165]. For crude membranes, reactions containing 50 μg of ZMPSTE24 membranes and 25 μM C10-para peptide were incubated in 100 mM Tris-HCl, pH 7.5 and incubated on ice for 5 min. For pure proteins, reactions with 0.5 μg of ZMPSTE24 proteins, 50 μM C10-para peptide, and 1 mM dithiothreitol (DTT) were rapidly reconstituted[140,142] into 50 μg

of *E.coli* polar lipid (Avanti Polar Lipids) in 100 mM Tris-HCl, pH 7.5 and incubated on ice for 5 min. Reactions were irradiated with or without UV light (365 nm) in 96-well plates on ice for 30 min. After UV irradiation, 2% of samples were saved as loading controls. The samples were then solubilized in 800 µl of radioimmunoprecipitation assay (RIPA) buffer (25 mM Tris-HCl, pH 7.5, 150 mM NaCl, 1% Triton X-100, 1% sodium deoxycholate, 0.1% sodium dodecylsulfate) with 1% SDS and incubated with 50 µl of 50% pre-washed slurry neutravidin agarose (Thermo Scientific) rotating for 2 hr at 4°C. Afterwards, the samples were centrifuged at 13,000 × *g* for 1 min and washed three times with RIPA buffer with 1% SDS. Following washing, the crosslinked proteins were eluted from neutravidin agarose using 30 µl of 2× SDS loading buffer. Eluted samples were incubated for 30 min at 65°C (crude) or room temperature (protein), resolved on 10% SDS-PAGE gels, and then transferred to a 0.22 µm Protran® Nitrocellulose Membrane (GE Healthcare). The nitrocellulose membrane was blocked with 20% (w/v) nonfat milk in phosphate-buffered saline (137 mM NaCl, 2.7 mM KCl, 4 mM Na_2HPO_4, 1.8 mM KH_2PO_4, pH adjusted to 7.4) and 0.05% (v/v) Tween-20 (PBST), probed with α-HA antibody (1:15000) in 5% (w/v) nonfat dry milk in PBST, and then detected with a horseradish peroxidase conjugated goat α-mouse antibody (1:4000). The protein bands were visualized using the SuperSignal® West Pico Chemiluminescent Substrate (Thermo Scientific).

5.3 Results and Discussion

5.3.1 Kinetic Analysis of Photoactive Biotinylated Probe with ZMPSTE24

We first examined whether the C10-para peptide could be recognized and processed by ZMPSTE24. The AAX cleavage activities of ZMPSTE24 with different concentrations of C10-Para were measured using the radioactive endoprotease-coupled methylation assay. From the kinetic analysis (Table 5.1), the $K_{m(app)}$ value of C10-para peptide for crude ZMPSTE24 was 2.5 ± 0.6 µM, similar to 5.5 ± 0.5 µM for crude Ste24 that confirmed the shared substrate specificity between Ste24 and ZMPSTE24. Moreover, the $K_{m(app)}$ value was also close to 1.7 ± 0.7 µM for the truncated **a**-factor peptide, indicating that both **a**-factor and C10-para exhibited similar affinities for crude ZMPSTE24. The V_{max} value of C10-para peptide was 243.0 ± 3.5 pmol/mg/min for crude ZMPSTE24, slower than 450.8 ± 10.9 for crude Ste24, possibly because yeast **a**-factor is the natural substrate of Ste24. The turnover of C10-para was also slower than

514.9 ± 40.9 pmol/mg/min of the **a**-factor, suggesting that the biotin and benzophenone groups may affect the processing rate.

The same trend of kinetic values was observed in reactions with purified ZMPSTE24. The $K_{m(app)}$ and V_{max} values were 2.7 ± 1.0 μM and 13.8 × 10^3 ± 1.3 × 10^3 pmol/mg/min, respectively. These values showed the substrate could be well recognized by purified ZMPSTE24 just like Ste24, and the similar affinity but slower turnover compared to the **a**-factor peptide as well.

Table 5.1. Kinetic constants for crude or purified Ste24 and ZMPSTE24 with **a**-factor and C10-Para peptides as substrates

a-factor	$K_{m(app)}$[a] (μM)	V_{max} (pmol/mg/min)	C10-Para	$K_{m(app)}$ (μM)	V_{max} (pmol/mg/min)
Crude Membranes					
Ste24	4.8 ± 0.5	774.6 ± 21.4	Ste24	5.5 ± 0.5	450.8 ± 10.9
ZMPSTE24	1.7 ± 0.7	514.9 ± 40.9	ZMPSTE24	2.5 ± 0.6	243.0 ± 3.5
Purified Proteins					
Ste24	5.4 ± 0.9	57.5 ± 3.1 (×10^3)	Ste24	4.2 ± 1.2	21.0 ± 1.8 (×10^3)
ZMPSTE24	3.3 ± 1.3	42.2 ± 4.4 (×10^3)	ZMPSTE24	2.7 ± 1.0	13.8 ± 1.3 (×10^3)

[a] K_m values are reported as apparent values because the concentration available to the enzyme in the crude membrane cannot be accurately determined.

5.3.2 Optimization of Photocrosslinking and Neutravidin Pull-Down Assay

After determining substrate specificity through kinetic studies, the ability of ZMPSTE24 to be photolabeled with the C10-para peptide was evaluated. Ste24 was to be used as the positive control, however, the photolabeling efficiency was much higher than ZMPSTE24, and thus the crosslinked ZMPSTE24 was difficult to detect (data not shown). Here we will only display the crosslinking results with ZMPSTE24 (Figure 5.2). Crude or purified ZMPSTE24 were incubated with saturating concentration (25 μM for crude and 50 μM for purified) of C10-Para and irradiated with UV light for 30 min on ice. The crosslinked ZMPSTE24 was pulled down using neutravidin agarose beads, size fractionated by SDS-PAGE, and detected using the α-HA antibody. As expected, crude ZMPSTE24 showed no binding with C10-para in the absence of UV exposure, and stronger crosslinking was detected when loading amounts increased. However, blurry bands and backgrounds were observed and may be affected by other

endogenous proteins expressed in the crude membrane from yeast. For purified ZMPSTE24, we first detected photolabeled proteins using neutravidin-HRP as previously reported[165]. However, strong backgrounds were observed (data not shown). Therefore, we utilized the same neutravidin agarose pull-down method as above described (Figure 5.2). Photocrosslinking did not occur without UV exposure and no signal was detected as predicted. Increased photolabel signals were observed with higher loading amounts. No obvious background was observed.

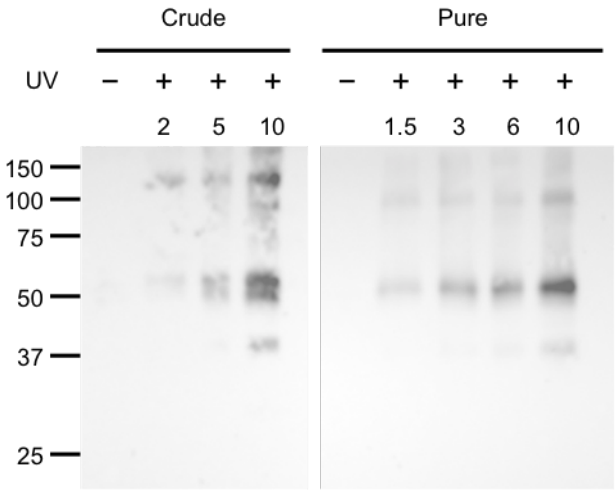

Figure 5.2. Immunoblot analysis of ZMPSTE24 photocrosslinked with C10-para peptide.

The photocrosslinking abilities of crude (*left*) or purified (*right*) ZMPSTE24 were examined using the benzophenone-containing C10-para peptide as described in the Methods section. The non-UV treated sample was the negative control. Sample was loaded with different volumes (μl) as indicated and then analyzed by immunoblot using the α-HA antibody.

5.3.3 Characterization of ZMPSTE24 Disease Mutants

The AAX cleavage activity of ZMPSTE24 with the **a**-factor and C10-para peptides was determined using the radioactive endoprotease-coupled methylation assay (Figure 5.3). Similar activity percentage levels of each disease mutant compared to the wild-type (WT) were detected between **a**-factor and C10-para peptides. Most of the disease mutants overexpressed in crude membranes showed reduced activity for both peptides, except Y399C. For purified proteins, the proposed zinc-coordinating mutant H335A lost the cleavage ability completely. L94P, N265S, L425P, and L462R showed less than 25% activity compared to the WT. Crude Y399C was highly active but purified Y399C had significantly reduced activity, which was less than 25% as

well. Interestingly, P248L retained similar cleavage ability to the WT, which is consistent to Chapter 4.3.5 data where the P248L activity was restored when its expression level was rescued. W340R also showed increased activity to about 35%.

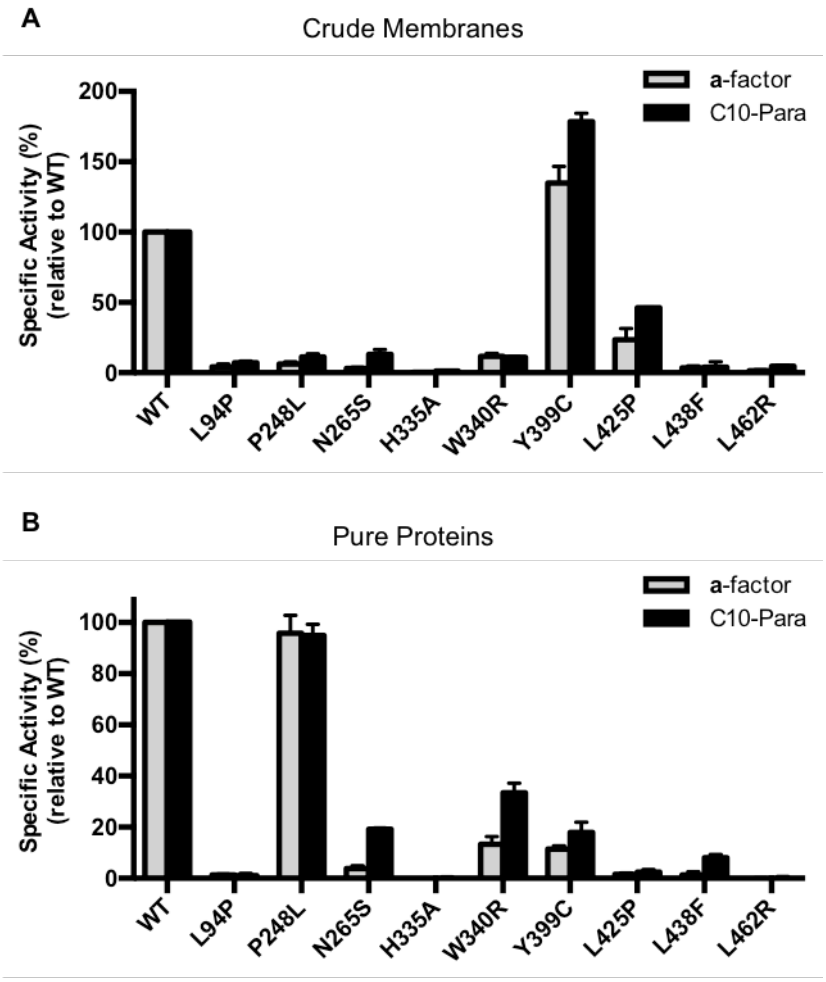

Figure 5.3. The AAX proteolytic activity of ZMPSTE24 wild-type (WT) and disease mutants with **a**-factor and C10-para peptides.

The ability of (A) crude and (B) purified ZMPSTE24 to cleave the AAX tail of **a**-factor and C10-para peptides were determined using the radioactive endoprotease-coupled methylation assay. Specific activity was reported as the percentage of relative activity to WT.

The farnesyl binding ability of purified ZMPSTE24 disease mutants was then examined by photocrosslinking with the C10-para peptide (Figure 5.4). Samples incubated in absence of UV exposure were used as negative controls. Input samples were also detected as loading controls. As expected, WT protein showed interaction with the probe. Both H335A and H339A

were able to be photolabeled, indicating that these mutants may still be able to bind the substrate but were inactive due to losing zinc-coordinating ability. P248L was photolabeled as predicted since this mutant displayed similar activity level as WT protein. Other mutants, such as N265S, W340R, Y399C, and L438F, retained binding ability, suggesting that their reduced activities may be affected by other factors. The weaker interactions of L425P and L462R may be due to the structural instability as shown in Chapter 4. Surprisingly, we did not observe photolabeled L94P protein, indicating that the reduced activity may be affected by diminished farnesyl interaction with the enzyme.

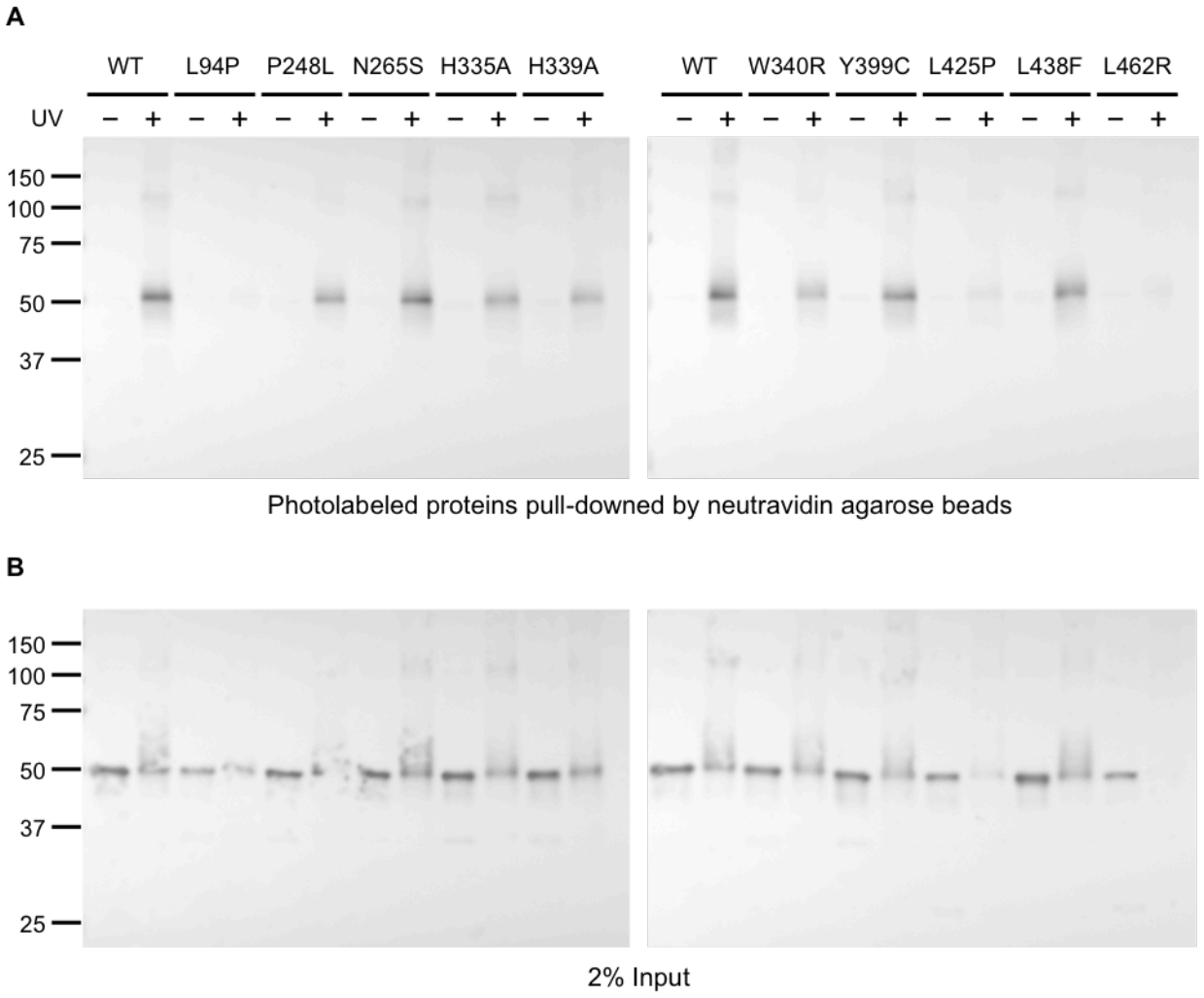

Figure 5.4. Analysis of purified ZMPSTE24 wild-type (WT) and disease mutants photocrosslinking with C10-para peptide.

(A) Purified ZMPSTE24 was incubated with C10-para peptide and irradiated with UV exposure (365 nm). Photocrosslinked proteins were then pulled-down with neutravidin beads. Pulled-down samples were eluted from neutravidin beads using 30 µl of SDS loading buffer. Eluted samples (5 µl) were then resolved on 10% SDS-PAGE gels. (B) Input samples (2%, before pulled-down by neutravidin agarose beads) were resolved as loading controls. All samples were analyzed by immunoblot using the α-HA antibody.

5.4 Conclusions

In this chapter, we examined the AAX cleavage activity of ZMPSTE24 disease mutants with the truncated **a**-factor peptide and C10-Para, an **a**-factor analog containing a photoreactive group. Most of the crude ZMPSTE24 disease mutants showed reduced cleavage activity with both peptides, which is consistent to our previously published results[130]. L425P, one of the newly reported disease mutation, also demonstrated lower cleavage activity. However, Y399C showed higher cleavage activity compared to WT, which is similar to its upstream cleavage activity as Chapter 4 described. This is the first time that the AAX cleavage activity of Y399C and L425P have been determined.

We also examined the AAX cleavage activity of purified ZMPSTE24 disease mutants. Similar to our Chapter 4 data, activity Y399C and L425P decreased greatly. Moreover, we have shown that L425P may be misfolded, and thus this mutant may form aggregates during purification process. Other purified disease mutants showed similar activity levels as their crude membranes, except P248L. In Chapter 4, we suggested that P248L may affect mostly protein stability. Here, P248L was as active as WT to perform the AAX cleavage, which further confirmed our hypothesis. However, since the *doa10* deletion strain we used in Chapter 4 expressed endogeneous yeast Rce1 as well, we were not able to examine whether the AAX cleavage activity will increase with restored protein levels by blocking ubiquitin-dependent degradation.

Based on the co-crystalized structure with the unfarnesylated peptide CSIM (Figure 5.5.A), mutants with lower AAX cleavage activity may affect catalysis, substrate binding, or interfere with substrate access pathway. N265S may affect activity by disrupting catalysis directly. The co-crystalized structure of ZMPSTE24 with the CSIM peptide showed that Asn-265 lies in the proposed substrate binding and active site (Figure 5.5.B). This residue is in a position similar to Asn-112 in thermolysin, a known zinc metalloprotease, and is likely to serve the same function to stabilize the substrate during catalysis[20,64,158,159] (Figure 5.5.C). Therefore, N265S mutation may not be able to form hydrogen bonds with the substrate and thus lose the cleavage activity.

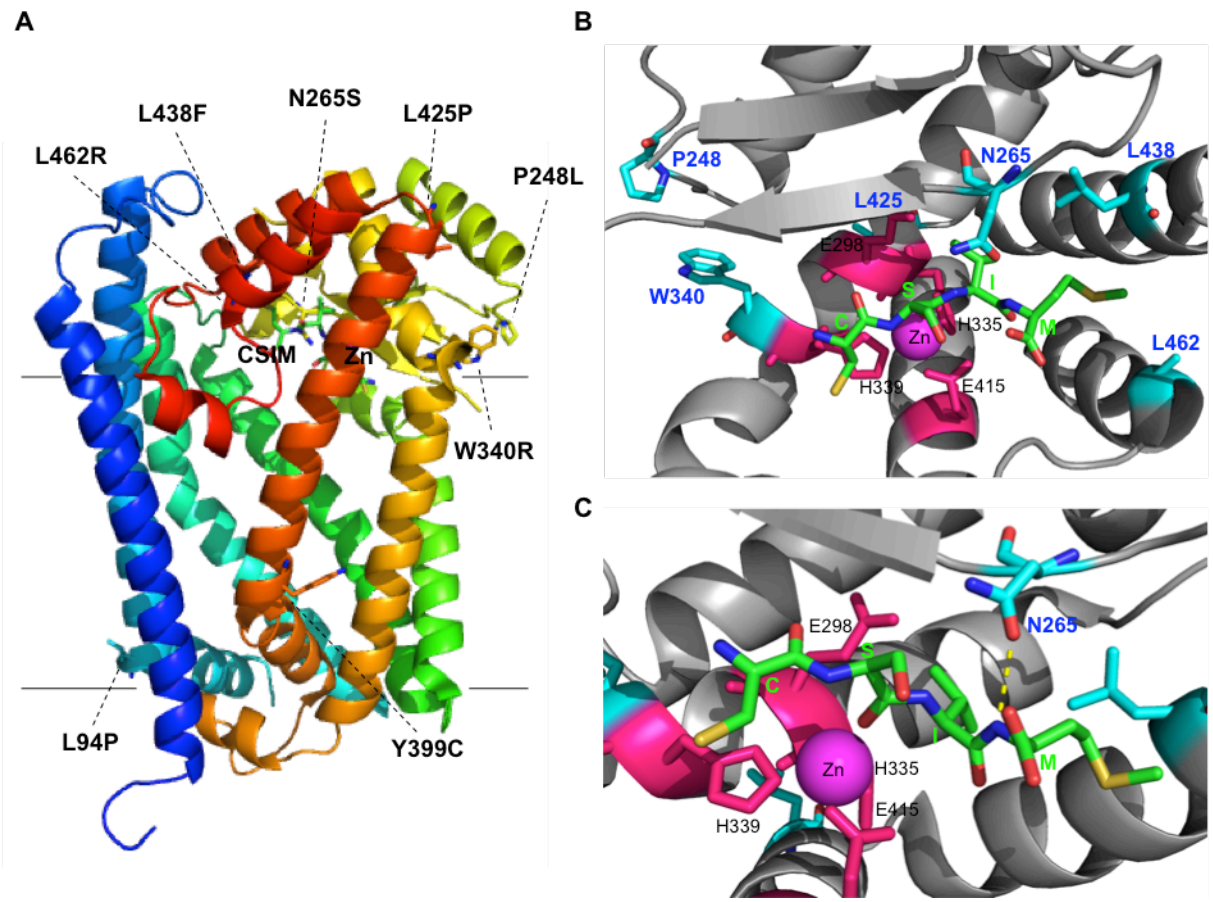

Figure 5.5. Disease mutations in the zinc metalloprotease domain of ZMPSTE24.

(A) ZMPSTE24 co-crystalized with the CSIM tetrapeptide. The structure is colored from blue to red from N- to C-terminus. The zinc ion is shown in purple. The CSIM peptide is labeled. Disease mutations are labeled with black dotted lines. PDB: 2ypt (B) Proposed zinc-coordinating residues, His-335, H339, and Glu-415, catalytic residue Glu-336, and residues associated with disease mutations (Pro-248, Asn-265, Trp-340, Leu-425, Leu-438, and Leu-462) are shown. (C) Asn-265 may form hydrogen bonds with Met-664 in prelamin A.

In this chapter, we have demonstrated that the photoactive C10-para peptide can be recognized and processed by ZMPSTE24. Moreover, ZMPSTE24 can be photolabeled by the probe, which provides a powerful tool to study the farnesyl binding ability of ZMPSTE24. Our crosslinking results revealed that three disease mutants, L94P, L425P, and L462R, showed no or faint photolabeling signals on the immunoblots. From the limited trypsin digestion experiments we described in Chapter 4, L425P and L462R showed different digestion patterns compared to WT and may not have proper folding for substrate binding. Also, these mutants showed fainter signals from input controls, suggesting that they may have faster degradation rate or less stable

compared to other mutants. It will be important to determine thermostability for each disease mutant. L94P, different to L425P and L462R, showed normal trypsin cleavage patterns, may lose the interaction with the farnesyl group. However, Leu-94 in ZMSPTE24 is located near the endoplasmic reticulum (ER) lumenal surface and is far away from the CSIM tetrapeptide and the proposed substrate binding site of AAX cleavage (Figure 5.5.A).

It should be noted that photolabeling efficiency cannot be quantified since there are many factors that could affect binding. Also, it is possible that the farnesyl group could still bind to the mutant, but with different position, and the enzyme may not be able to mediate the cleavage. For example, Leu-438 lies adjacent to the CSIM peptide binding site (Figure 5.5.B). When this residue is replaced by a bulkier amino acid phenylalanine to L438F, the mutation may interfere with the substrate binding, and thus this mutation was almost inactive. We will identify the residues that interact with the farnesyl group in the crosslinked samples using mass spectrometry. Moreover, saturation concentration will need to be further investigated by obtaining kinetic parameters for each disease mutant with C10-Para.

Another interesting finding is that a mutant could have totally different AAX and upstream cleavage activities (Figure 4.7, 4.8, and 5.3). For example, purified P248L showed almost 100% activity for the AAX cleavage, but only had about 50% activity for the upstream cleavage. Crude L425P showed about 25% activity for the AAX cleavage and above 100% activity for the upstream cleavage. It is still unclear how ZMPSTE24 recognize two different sites, with totally different sequences, lengths, and chemical compositions, in one substrate. Therefore, it is necessary to design and synthesize the probes based on the full-length **a**-factor sequence to detect the substrate binding of the upstream cleavage. Overall, we will utilize this research to describe in detail the residues involved in the substrate binding site of ZMPSTE24.

CHAPTER 6. DEFINING THE SUBSTRATE ACCESS PATHWAYS OF STE24, YEAST HOMOLOG OF ZMPSTE24

The dissertation author designed and performed all the experiments. Dr. Sarah Hudon cloned the Ste24-TA plasmid. Nisreen Islaih helped generating the Ste24-QA mutant plasmids and prepared yeast crude membranes.

6.1 Introduction

Ste24 from *Saccharomyces cerevisiae* is a bi-functional zinc metalloprotease[116,121]. The enzyme catalyzes two distinct cleavages in the yeast mating pheromone **a**-factor maturation, including the endoproteolytic removal of the C-terminal AAX residues adjacent to an isoprenylated cysteine residue, and a second discrete site-specific upstream N-terminal cleavage[116,121]. However, the precise catalytic mechanism is still unclear.

Ste24 is a unique integral membrane protein localized to the endoplasmic reticulum (ER), and is also present in the inner nuclear membrane (INM)[13]. From the published crystal structure, the seven transmembrane spans of Ste24 comprise a helical barrel that surrounds a voluminous intramembrane "hollow" chamber, large enough to accommodate around 450 water molecules. The majority of the C-terminal soluble portion, including the HEXXH zinc metalloprotease consensus motif, is on the cytoplasmic side of the ER membrane and faces the interior of the chamber to cap the cytoplasmic side of the chamber inside which proteolysis is proposed to occur. There are four large side portals apparent in the structure, and all portals are greater than 10 Å in diameter, which is large enough to allow passage of an unfolded peptide. Moreover, the farnesyl group on the **a**-factor may help attachment to the active site cavity. Therefore, at least some of the portals are likely to provide the necessary sites for **a**-factor entry, exit, and product release (Figure 6.1)[123].

To identify which portal(s) facilitate entry and exit of the substrate and the product, we have mutated selected residues surrounding each portal to the bulkier amino acid tryptophan to block the opening. The C- and N-terminal proteolytic activities were examined using the radioactive endoprotease-coupled methylation assay (Chapter 2.2.4) and FRET-based assay (Chapter 3.2.6), respectively. However, no portal occlusion mutations showed significantly reduced activity (see Appendix D). This may be due to a particular mutation affecting another

part of the enzyme. Also, the crystal structure is static and only represents one conformation. Therefore, mutating just one residue to tryptophan may not be sufficient to block the portal opening.

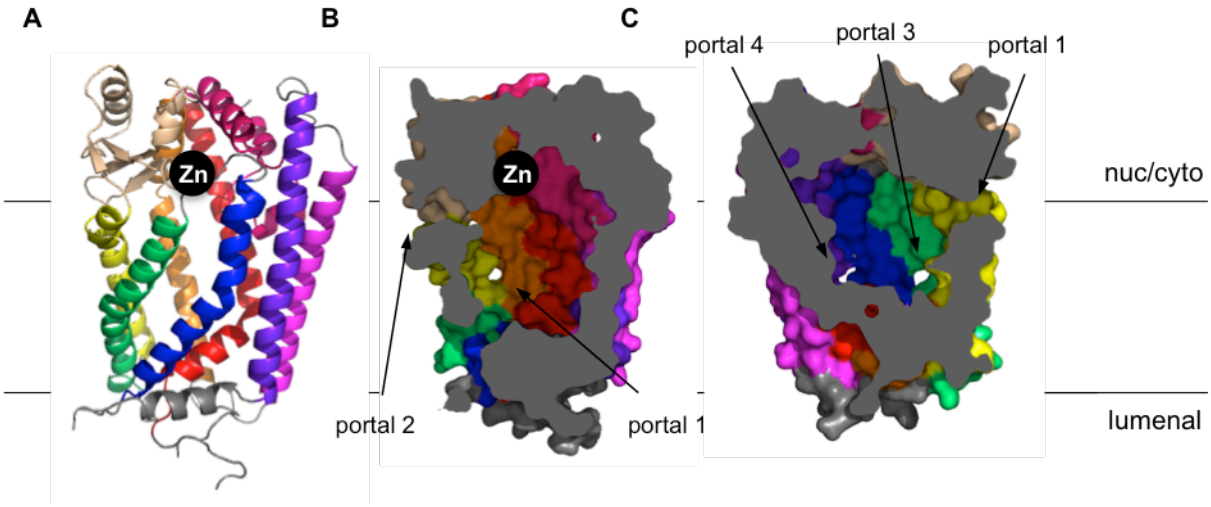

Figure 6.1. Crystal structure of Ste24.

(A) Ribbon diagram. The zinc ion is shown at the top of the chamber facing the cytosol. (B and C) Cutaway surface diagrams with zinc indicated showing the four large (>10 Å) portals leading to the interior of the chamber. PDB: 4IL3

Therefore, we developed another strategy, utilizing Ste24 cysteine mutations and membrane permeable bismaleimide sulfhydryl-to-sulfhydryl crosslinkers to occlude the portal opening. There are three native cysteine residues (C123, C376, and C407) in Ste24. We have demonstrated that mutating these three cysteine residues to alanine did not affect Ste24 activity or expression levels (unpublished data from Dr. Hudon)[170]. Based on the activity, expression, and position, we have generated three cys-less-based double cysteine mutants for portal 1. These cysteine mutants were chemically crosslinked using bis(maleimido)hexane (BMH, 13.0 Å) and bis(maleimido)ethane (BMOE, 8.0 Å) (Figure 6.2).

The AAX cleavage activity levels were examined using the radioactive endoprotease-coupled methylation assay. Some of the crosslinked double mutants showed reduced activity, especially QA-M210C-I307C with BMH showing only 13% activity compared to the DMSO control. The crosslinked single cysteine mutants we have examined all had reduced activity below 30% compared to the DMSO control. These results suggest portal 1 may be important for the C-terminal cleavage, which is consistent with our hypothesis that portal 1 serves the entry

route for the C-terminus of **a**-factor. Portal 1 is located between transmembrane helices (TMH) 5 and 6 in the chamber wall and is closest to the membrane interface (Figure 6.1.C). We will further examine the N-terminal cleavage and clarify the roles of remaining portals.

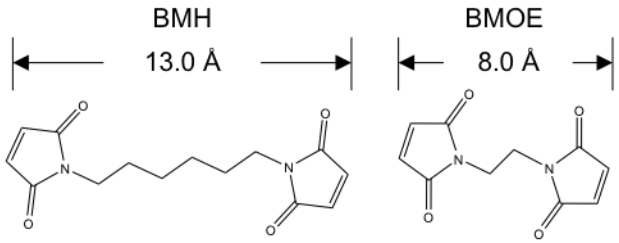

Figure 6.2. Structures of biamaleimide crosslinkers.

Bis(maleinido)hexane (BMH) and bis(maleimido)ethane (BMOE) are bismaleinide crosslinkers, with the same reactivity but differ in length, for conjugation between sulfhydrylgroups.

6.2 Methods

6.2.1 Plasmids and Yeast Strains

The plasmids and primers used in this study are listed in Table 6.1. Ste24 mutants, except the C(-3)A, were first generated on pCH1284 by overlap extension Polymerase Chain Reaction (PCR) site-directed mutagenesis as Chapter 3.2.2 described. The C(-3)A and all pCH1366-based mutants were generated using the Q5® Site-Directed Mutagenesis Kit (New England BioLabs) following the manual description. Each plasmid was sequenced, transformed, and expressed in the strain SM3614 (*MAT**a** trp1 leu2 ura3 his4 can1 ste24Δ::LEU2 rce1Δ::TRP1*)[121] using the Elble protocol[141]. After transformation, all yeast cells were grown at 30°C on synthetic complete medium without uracil (SC-URA).

Table 6.1. Plasmids and primers used in this study

Plasmid	Genotype	Reference
pCH1283	*2μ URA3* P_{PGK}*-*His_{10}*-*HA_3*-STE24*	Chapter 2.2.1
pCH1365	*2μ URA3* P_{PGK}*-*His_{10}*-*HA_3*-STE24-C(-3)A*	This study
pCH1284	*2μ URA3* P_{PGK}*-*His_{10}*-*HA_3*-STE24-TA*[a]	This study
pCH1366	*2μ URA3* P_{PGK}*-*His_{10}*-*HA_3*-STE24-QA*[b]	This study
pCH1367	*2μ URA3* P_{PGK}*-*His_{10}*-*HA_3*-STE24-QA-Q206C*	This study
pCH1368	*2μ URA3* P_{PGK}*-*His_{10}*-*HA_3*-STE24-QA-M210C*	This study

Table 6.1. continued

pCH1369	*2μ URA3* P_{PGK}*-His*$_{10}$*-HA*$_3$*-STE24-QA-P214C*	This study
pCH1370	*2μ URA3* P_{PGK}*-His*$_{10}$*-HA*$_3$*-STE24-QA-F266C*	This study
pCH1371	*2μ URA3* P_{PGK}*-His*$_{10}$*-HA*$_3$*-STE24-QA-T267C*	This study
pCH1372	*2μ URA3* P_{PGK}*-His*$_{10}$*-HA*$_3$*-STE24-QA-G268C*	This study
pCH1373	*2μ URA3* P_{PGK}*-His*$_{10}$*-HA*$_3$*-STE24-QA-I307C*	This study
pCH1374	*2μ URA3* P_{PGK}*-His*$_{10}$*-HA*$_3$*-STE24-QA-V311C*	This study
pCH1375	*2μ URA3* P_{PGK}*-His*$_{10}$*-HA*$_3$*-STE24-QA-S314C*	This study
pCH1376	*2μ URA3* P_{PGK}*-His*$_{10}$*-HA*$_3$*-STE24-QA-T318C*	This study
pCH1377	*2μ URA3* P_{PGK}*-His*$_{10}$*-HA*$_3$*-STE24-QA-M210C-I307C*	This study
pCH1378	*2μ URA3* P_{PGK}*-His*$_{10}$*-HA*$_3$*-STE24-QA-T267C-I307C*	This study
pCH1379	*2μ URA3* P_{PGK}*-His*$_{10}$*-HA*$_3$*-STE24-QA-T267C-V311C*	This study

Primer	Sequence (5’ to 3’)
Ste24-C(-3)A (+)	CGCTGCTGAGGCCGGCCGCTTTG
Ste24-C(-3)A (−)	TAATCTGGAACGTCATATGGATAGG
Ste24-C123A (+)	CAGAGTTTAGCCTTCTTGGGTCTC
Ste24-C123A (−)	GAGACCCAAGAAGGCTAAACTCTG
Ste24-Q206C (+)	GTTCGTTGTCTGTATCTTAGCCATG
Ste24-Q206C (−)	CATGGCTAAGATACAGACAACGAAC
Ste24-M210C (+)	CAAATCTTAGCCTGTACAATCATTCC
Ste24-M210C (−)	GGAATGATTGTACAGGCTAAGATTTG
Ste24-P214C (+)	CATGACAATCATTTGTGTCTTCATCATG
Ste24-P214C (−)	CATGATGAAGACACAAATGATTGTCATG
Ste24-F266C (+)	CAAACGCATATTGCACAGGTTTGCC
Ste24-F266C (−)	CAAACCTGTGCAATATGCGTTTG
Ste24-T267C (+)	GCATATTTCTGTGGTTTGCCATTC
Ste24-T267C (−)	GAATGGCAAACCACAGAAATATGC
Ste24-G268C (+)	GCATATTTCACATGTTTGCCATTCACC
Ste24-G268C (−)	GGTGAATGGCAAACATGTGAAATATGC
Ste24-I307C (+)	CAAAAAAACCACTGCGTTAATATGGTC
Ste24-I307C (−)	GACCATATTAACGCAGTGGTTTTTTTG
Ste24-V311C (+)	CACATCGTTAATATGTGCATCTTTAGTCAA
Ste24-V311C (−)	TTGACTAAAGATGCACATATTAACGATGTG
Ste24-S314C (+)	GGTCATCTTTTGTCAATTGCACACC
Ste24-S314C (−)	GGTGTGCAATTGACAAAAGATGACC
Ste24-T318C (+)	GTCAATTGCACTGCTTCCTCATTTTC
Ste24-T318C (−)	GAAAATGAGGAAGCAGTGCAATTGAC
Ste24-C376A (+)	CCACTCGAACGTGCCATGCAATTC
Ste24-C376A (−)	GAATTGCATGGCAGCTTCGAGTGG
Ste24-C407A (+)	CAAAATCTAGCTAGGGCCCTAATTG
Ste24-C407A (−)	CAATTAGGGCCCTAGCTAGATTTTG

[a] TA means “triple alanine” and obtains C123A-C376A-C407A mutations.
[b] QA means “quadruple alanine” and obtains C(-3)A-C123A-C376A-C407A mutations.

6.2.2 Crude Membrane Preparation from Yeast Cells

Yeast crude membranes overexpressing Ste24 mutants were prepared as described in Chapter 2.2.2. The AAX proteolytic activity of each mutant was determined using the radioactive endoprotease-coupled methylation assay. Reactions contained 5 μg of Ste24 membranes, 10 μg of the Ste14 membranes[130], 15 μM farnesylated 15-mer **a**-factor (YIIKGVFWDPAC(Fr)-VIA, EZBioLab) peptide, and 20 μM *S*-adenosyl-[^{14}C-methyl]-L-methionine (Perkin Elmer) were incubated in 100 mM Tris-HCl, pH 7.5. The detailed assay protocol was described in Chapter 2.2.4. Specific activity was determined as pmol of AAX residues removed per min per mg of protease. Protein expression level of each mutant from yeast crude membrane was examined using immunoblot analysis as described in Chapter 3.2.4. Samples (0.5 μg of crude membrane) were loaded on a 10% SDS-PAGE gel, transferred to a nitrocellulose membrane, probed with α-HA antibody (1:15000), and detected with a horseradish peroxidase conjugated goat α-mouse antibody (1:4000). The protein bands were visualized using the SuperSignal® West Pico Chemiluminescent Substrate (Thermo Scientific).

6.2.3 Crosslinking Analysis with Bismaleimide Crosslinkers

Both AAX cleavage activity and expression of crosslinked Ste24 mutants were examined by the radioactive endoprotease-coupled methylation assay and immunoblot, respectively. Reactions with 5 μg of Ste24 crude membrane and 7 μM DMSO, BMH, or BMOE (Thermo Scientific) in 100 μM Tris-HCl, pH 7.5 were incubated at room temperature for 30 min. The concentration of bismaleimide crosslinkers was decided based on the manual suggestion. After incubation, for activity samples, 10 μg of Ste14 crude membrane, 15 μM farnesylated 15-mer **a**-factor (YIIKGVFWDPAC(Fr)-VIA, EZBioLab) peptide, and 20 μM *S*-adenosyl-[^{14}C-methyl]-L-methionine (Perkin Elmer) were added to the mixture and incubated as the previous section described. Specific activity was determined as pmol of AAX residues removed per min per mg of protease. For expression samples, 5× SDS loading buffer without β-mercaptoethanol and 40 mM L-cysteine (Sigma-Aldrich) were added to mixtures to stop the reaction and incubated at room temperature for at least 30 min. Samples (0.5 μg of crude membrnae) were loaded to a 10% SDS-PAGE gel, transferred to a nitrocellulose membrane, probed and visualized as the previous section described.

6.3 Results and Discussion

In order to generate cysteine mutations for crosslinking, we first mutated native cysteine residues in Ste24 to alanine. There are three native cysteine residues (C123, C376, and C407) in Ste24. A previous study (unpublished data from Dr. Hudon[170]) demonstrated that the triple alanine (TA) mutant is biologically active. However, there is one extra cysteine residue (C(-3)) in the linker region. Therefore, C(-3)A and quadruple alanine (QA) mutants have been generated and retained similar AAX cleavage activity and expression level to the wild-type Ste24 (Figure 6.3).

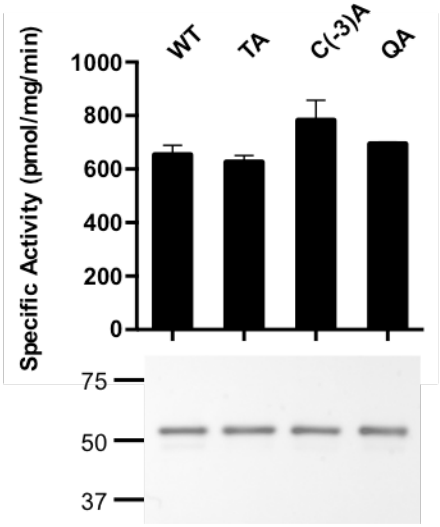

Figure 6.3. QA mutant displays similar activity and expression levels as wild-type (WT) Ste24. The AAX cleavage activity and expression levels of WT, triple alanine (TA), C(-3)A, and quadruple alanine (QA) were examined using radioactive endoprotease-coupled methylation assay and immunoblot (0.5 μg), respectively. All mutants showed comparable activity and expression levels as WT.

The ability of the QA mutant to be crosslinked was examined. As expected, we did not observe any crosslinked QA from the immunoblot analysis (Figrue 6.4), indicating that the QA construct is suitable for the cysteine mutagenesis of the residues surrounding each portal. Portal 1 is located between transmembrane helices (TMH) 5 and 6 in the chamber wall and is closest to the membrane interface. It is predicted, based on the co-crystalized structure with tetrapeptide in ZMPSTE24[20], the human homolog of Ste24, to be the entry route for the C-terminus of **a**-factor. Therefore, we first mutated residues surrounding portal 1 to cysteine (Figure 6.5). Using the

radioactive endoprotease-coupled methylation assay, QA-based cysteine mutants, except Q206C, P214C, F266C, and G268C, showed similar or slightly lower AAX cleavage activity (all above 70%) compared to the QA mutant. These active mutants, except T267C, also expressed similarly to the QA mutant (Figure 6.6). Among these active mutants, using Pymol prediction, we selected four of them based on their position to generate three different double cysteine mutants, QA-M210C-I307C (7.8 Å), QA-T267C-I307C (11.6 Å), and QA-T267C-V311C (14.5 Å) (Figure 6.7). The distances between two cysteine residues are in a range of 7 to 15 Å, which is expected to be able to crosslink using BMOE (8 Å) or BMH (13 Å). All double mutants, except QA-M210C-I307 which lost about 35% activity, showed similar C-terminal cleavage activity and expression as the QA mutant (Figure 6.8).

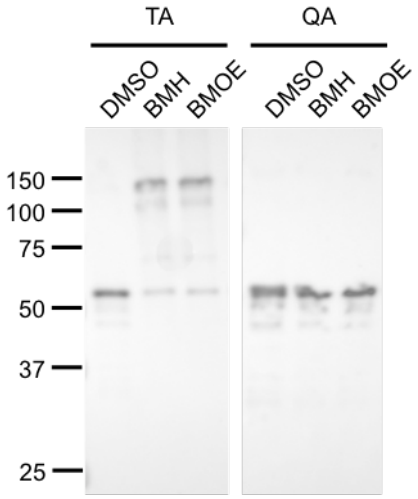

Figure 6.4. Immunoblot of crosslinked TA and QA mutants.

Ste24 mutants, TA (*left*) and QA (*right*), were chemically crosslinked with DMSO (control), BMH, or BMOE. All samples (0.5 μg) were analyzed by immunoblot using the α-HA antibody. Dimer and trimer formation were observed in BMH- and BMOE-treated TA but not in the QA mutant.

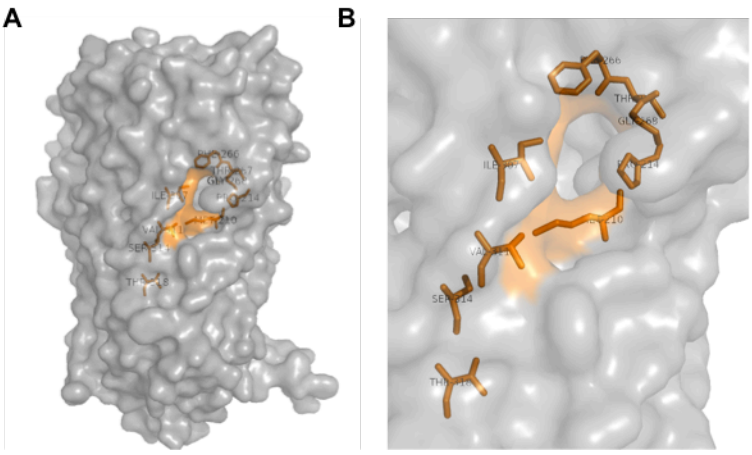

Figure 6.5. Crystal structure of Ste24 highlighting the residues surrounding the portal 1.

Portal 1 is located between TMH 5 and 6. (A) Portal 1 surrounding residues selected for mutation are labeled in orange. (B) Enlarged structure. PDB: 4IL3

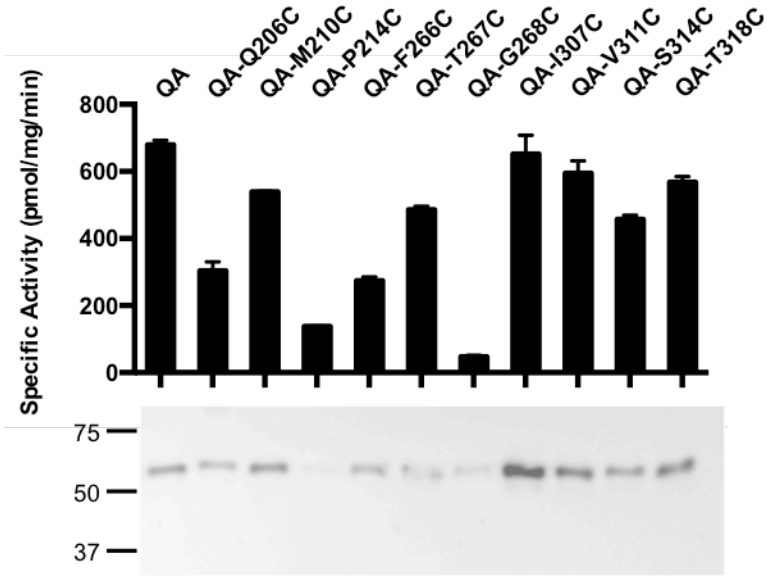

Figure 6.6. QA-based single cysteine mutants of Ste24 display varied AAX cleavage activity and expression levels compared to the QA mutant.

The AAX cleavage activity and expression levels of QA-based single cysteine mutants were examined using radioactive endoprotease-coupled methylation assay and immunoblot (0.5 μg), respectively. Most of the mutants, except Q206C, P214C, F266C, and G268C, were active and expressed as the QA mutant.

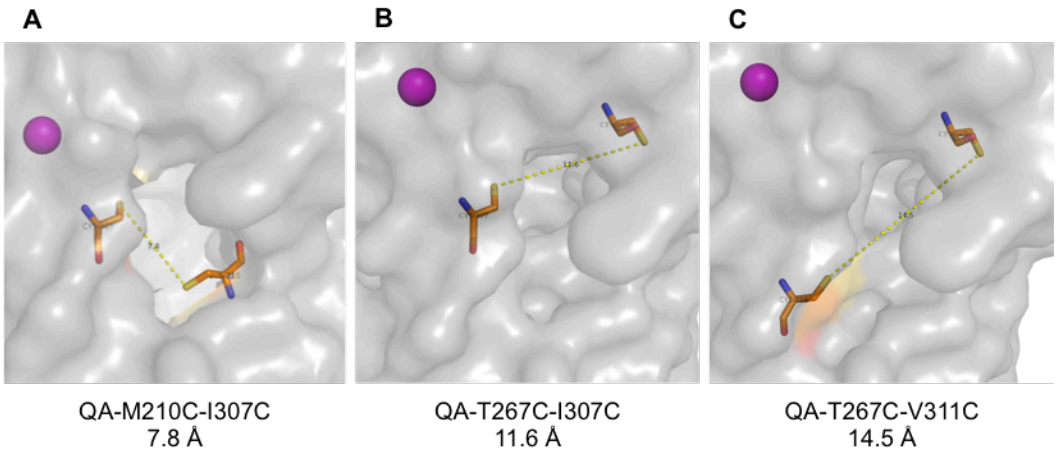

Figure 6.7. Pymol prediction of QA-based double cysteine mutants of Ste24.

Based on activity, expression, and position of the single cysteine mutants, we have designed three different double cysteine mutants, (A) QA-M210C-I307C, (B) QA-T267C-I307C, and (C) QA-T267C-V311C, with different distances for chemical crosslinking to occlude the portal 1, which is closest to the active site. The zinc ion is shown as a purple ball. PDB: 4IL3

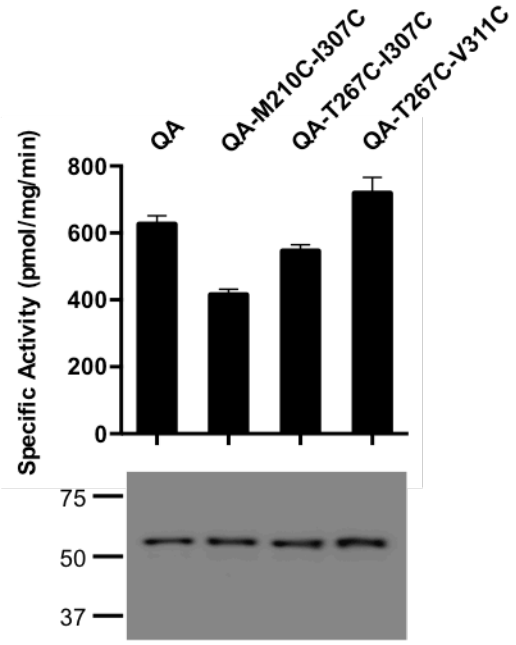

Figure 6.8. QA-based double cysteine mutants display similar AAX cleavage activity and expression levels as the QA mutant.

The AAX cleavage activity and expression levels of the QA-based double cysteine mutants were examined using radioactive endoprotease-coupled methylation assay and immunoblot (0.5 μg), respectively. All mutants showed comparable activity and expression levels to the QA mutant.

To determine the importance of the portal 1 in the entry of the C-terminus of the substrate, we examined the AAX cleavage activity of DMSO-, BMH-, and BMOE-treated double cysteine mutants by the radioactive endoprotease-coupled methylation assay (Figure 6.9.A). As expected, the activity of crosslinker-treated QA did not change compared to the DMSO-treated sample, since there are no cysteine residues in the QA mutant. For double cysteine mutants, we expected to see reduced activities after crosslinking with BMH or BMOE. Indeed, they showed lower, but different activity levels with BMH or BMOE. For example, the crosslinked QA-M210C-I307C with BMH was 13% active compared to the DMSO control. However, the activity with BMOE was much higher, retaining about 76% activity to the control. QA-T267C-V311C also showed lower activity with BMH but similar activity with BMOE compared to the control. Different to other mutants, QA-T267C-I307C treated with BMH or BMOE revealed about 65% and 35% activities compared to the control, respectively. These differences may be due to the different length of the crosslinkers resulting in varied crosslinking efficiency. For the single cysteine mutants, which were not predicted to lose their activities, reduced activities were observed in both BMH- and BMOE-treated samples. It is possible that one side of the crosslinker attached to the single cysteine and thus blocked the portal opening or interfered with substrate entry. To confirm the crosslinking efficiency, all the samples were loaded and analyzed by the immunoblot. However, no mobility shift difference was detected from the crosslinker-treated samples (Figure 6.9.B). We will utilize commercial a colorimetric maleimide assay to quantify the amount of free sulfhydryl group. Our crosslinking results suggest that portal 1 is critical for the C-terminal AAX cleavage, but its detailed role will still need to be further clarified.

6.4 Conclusions

We have shown that portal 1 may be the substrate entry route for the C-terminal AAX cleavage. To further confirm this hypothesis, we will utilize an **a**-factor sequence-based photoaffinity probe (Chapter 5.2.3) to detect the substrate binding ability of cysteine mutants, which are expected to show the loss of photolabeling signals due to the occlusion of the portal opening. Moreover, we will also examine the role of portal 1 in the N-terminal cleavage. Since the zinc-binding motif is also important for the N-terminal cleavage (Chapter 3.3.2), the crosslinked cysteine mutants are expected to show reduced N-terminal cleavage activity as well.

Mass spectrometry and a sensitive yeast mating assay will be used to explore how the cleaved substrate is released from the enzyme. The remaining portals will also be examined using similar approaches to clarify their roles.

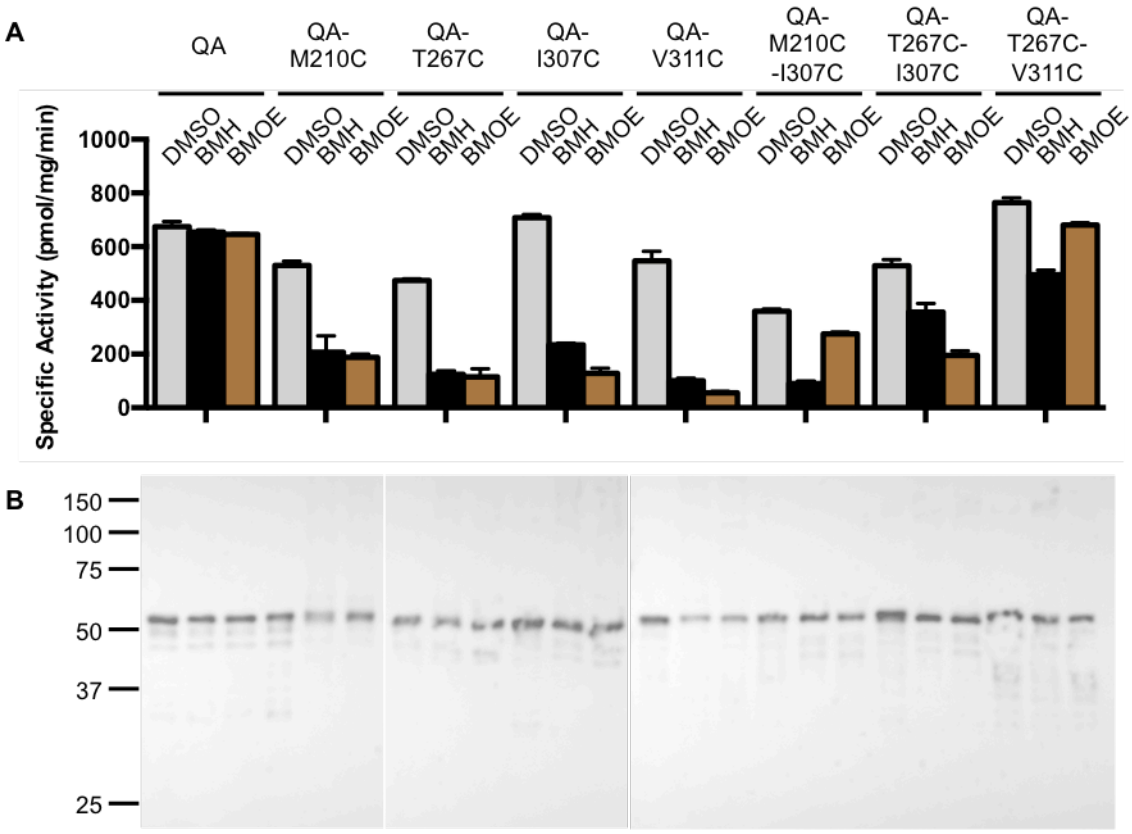

Figure 6.9. Crosslinked cysteine mutants were less active compared to the DMSO control.

(A) The AAX cleavage activity and (B) expression levels of control (*grey*), BMH- (*black*), or BMOE- (*brown*) crosslinked QA-based cysteine mutants were examined using radioactive endoprotease-coupled methylation assay and immunoblot (0.5 μg), respectively. All single cysteine mutants and some of the double cysteine mutants showed reduced activities after crosslinking compared to the control.

APPENDIX A

Portions of the data and text in the following chapter have been published in the journal article "*ZMPSTE24* missense mutations that cause progeroid diseases decrease prelamin A cleavage activity and/or protein stability"[131]. The dissertation author designed and performed all the experiments.

A.1 Introduction

As described in Chapter 1, ZMPSTE24 has a crucial role in human health and longevity through its role in the maturation of the nuclear scaffold protein lamin A from its precursor, prelamin A. The enzyme catalyzes two distinct cleavage steps in the maturation pathway, including the endoproteolytic removal of the C-terminal AAX residues adjacent to an isoprenylated cysteine residue, and a second discrete site-specific upstream cleavage. In progeroid disorders, this second cleavage of prelamin A by ZMPSTE24 is compromised, leading to the accumulation of a permanently farnesylated and carboxyl methylated form of prelamin A, which is the toxic 'culprit' in these diseases. However, there was no effective tool to detect this ZMPSTE24-mediated upstream cleavage. Here, we report how we collaborated with Michaelis lab to develop a yeast system to specifically assay this upstream cleavage step in prelamin A maturation. We demonstrated that ZMPSTE24 could perform the upstream cleavage of prelamin A in yeast. However, the expression levels were not consistent. Therefore, we created a yeast strain with chromosomally integrated gene for stable substrate expression[131].

A.2 Methods

The plasmids and yeast strains used in this study are listed in Table A.1. pCH1100, pCH1101, and pCH1102 were digested using *Xho*I and *Sac*II and inserted into pRS425-Ste14 backbone to generate pCH1103, pCH1104, and pCH1105, respectively. All constructs were sequenced bidirectionally to confirm the DNA sequence. SM2331 and SM6015 were gifts from Michaelis lab. Each plasmid was transformed into indicated yeast strains using using the Elble protocol[141]. After transformation, all yeast cells were grown at 30°C on synthetic complete medium without uracil (SC-URA), leucine (SC-URA), or both (SC-URA-LEU). Cell lysates were prepared as previously described but with some modifications[131]. Yeast cells were grown in

selected media to log phase (3-5 OD_{600}/ml). Cells (3 OD_{600} cell equivalents) were pelleted, lysed using 0.2 M NaOH containing 1% β-mercaptoethanol on ice for 15 min, and incubated with 6% trichloracetic acid (TCA) on ice for another 15 min to precipitate the extracted proteins. After centrifugation at 13,000 × *g* for 15 min at 4˚C, pellets were then resuspended in 2× SDS loading buffer and heated at 65˚C for 30 min. Samples (0.2 OD_{600} cell equivalents) were loaded on 10% SDS-PAGE gels, transferred to nitrocellulose membranes, probed with α-HA antibody (1:15000) or α-myc antibody (1:10000), and detected with a horseradish peroxidase conjugated goat α-mouse antibody (1:4000). The protein bands were visualized using the SuperSignal® West Pico Chemiluminescent Substrate (Thermo Scientific).

Table A.1. Plasmids and yeast strains used in this study

Plasmid	Genotype	Reference
pCH1100	*2μ URA3* P_{PGK}*-*His_{10}*-*myc_3*-LMNA*$_{(431-664)}$	129
pCH1101	*2μ URA3* P_{PGK}*-*His_{10}*-*myc_3*-LMNA*$_{(431-664,\ L647R)}$	129
pCH1102	*2μ URA3* P_{PGK}*-*His_{10}*-*myc_3*-LMNA*$_{(431-646)}$	129
pCH1103	*2μ LEU2* P_{PGK}*-*His_{10}*-*myc_3*-LMNA*$_{(431-664)}$	This study
pCH1104	*2μ LEU2* P_{PGK}*-*His_{10}*-*myc_3*-LMNA*$_{(431-664,\ L647R)}$	This study
pCH1105	*2μ LEU2* P_{PGK}*-*His_{10}*-*myc_3*-LMNA*$_{(431-646)}$	This study
pRS425-Ste14	*2μ LEU2* P_{PGK}*-STE14*	171
pSM2677	*CEN URA3* P_{PGK}*-*His_{10}*-*HA_3*-ZMPSTE24*	130

Yeast Strain	Genotype	Reference
SM2331	*MAT**a** trp1 leu2 ura3 his4 can1 mfa1Δ mfa2Δ*	This study
SM6015[a]	*ste24Δ::Kan rce1Δ::TRP1*	This study

[a] Strain is isogenic to SM2331.

A.3 Results and Discussion

Since prelamin A and ZMPSTE24 are not expressed in yeast, we aimed to develop a system to co-transform plasmids with *LMNA* and *ZMPSTE24* gene into yeast for overexpression, then detect prelamin A cleavage using immunoblot. We first generated plasmids encoding C-terminal segment from human prelamin A protein (amino acids 431 to 664), which contains all the necessary signals from CAAX processing and the upstream cleavage. To serve as size markers for comparison, we also constructed a mutant prelamin A, L647R, which is known to be uncleavable by ZMPSTE24 in mammalian cells[15], as well as a version expressing the correctly

processed mature form of lamin A (amino acid 431 to 646). All versions were with *LEU2* gene for selection and tagged at the N-terminus with His_{10}-myc_3 to allow detection by immunoblot. These plasmids were transformed into SM6015, a double protease deletion yeast strain with no **a**-factor expression. The following immunoblot analysis with cell lysates showed that each plasmid was expressing correct product as we expected. Moreover, the mature lamin A revealed faster migration rate since it is 2 kDa smaller then uncleaved prelamin A (Figure A.1).

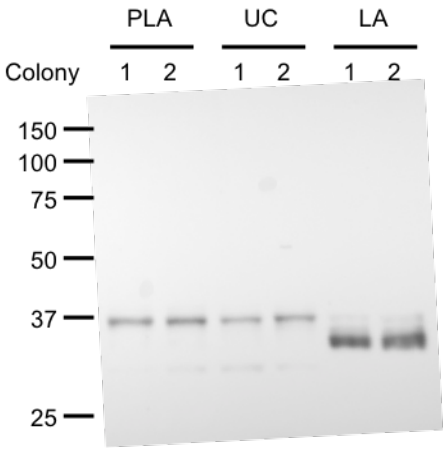

Figure A.1. Prelamin A and mature lamin A can be expressed in yeast.
Lysates from SM6015 strain expressing prelamin A (PLA, pCH1103), L647R mutant uncleavable prelamin A (UC, pCH1104), or mature lamin A (LA, pCH1105) were analyzed by immunoblot and detected with α-myc antibody.

Next, we then co-transformed the aforementioned plasmids with wild-type ZMPSTE24 to determine whether ZMPSTE24 can cleave prelamin A in yeast or not. We prepared cell lysates from two colonies of each strain. From immunoblot probed with α-myc antibody (Figure A.2, *top*), we did observe "cleaved" prelamin A band in lane 1 with the same migration rate as mature lamin A in lane 5. Uncleaved prelamin A in lane 4 showed slower migration as expected. However, not all colonies showed same results. For example, colony of lane 2 was from the same plate as lane 1, but it did not show cleaved prelamin A and no ZMPSTE24 was detected from immunoblot probed with α-HA antibody (Figure A.2, *bottom*). We also observed different expression levels of mature lamin A between lane 5 and 6.

The different expressions might due to overexpression from two plasmids. Therefore, we decided to integrate the *LMNA* gene into yeast chromosome to express stable prelamin A or

lamin A. Also, our strain background also deleted Rce1, so all proteolytic activity could be attributed to ZMPSTE24. Thus mutant ZMPSTE24 protein might also affect the cleavage efficiency of the first step. The results were published in Spear *et al.*, Disease Models & Mechanisms in 2018[131].

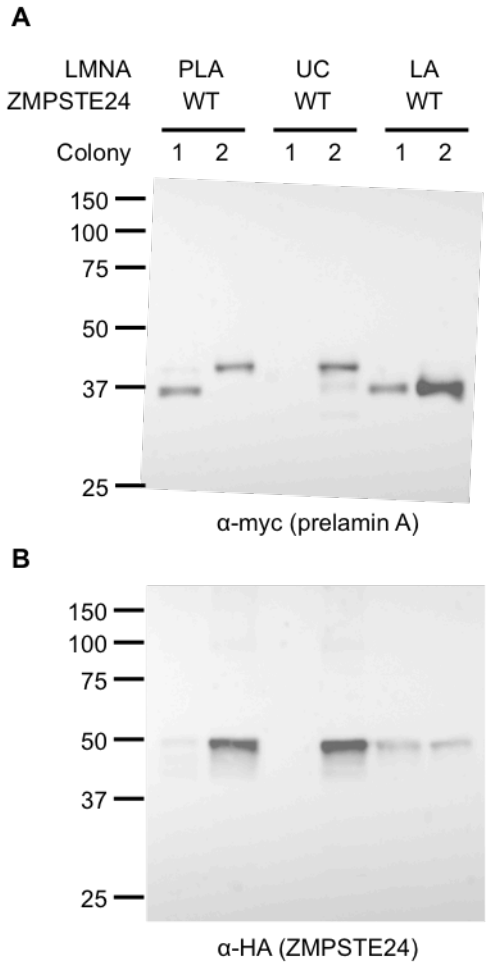

Figure A.2. Prelamin A is processed to mature lamin A by ZMPSTE24 in yeast.

Lysates from SM6015 strain co-expressing prelamin A (PLA, pCH1103), L647R mutant uncleavable prelamin A (UC, pCH1104), or mature lamin A (LA, pCH1105) with wild-type ZMPSTE24 (WT, pSM2677) were analyzed by immunoblot and detected with α-myc (*top*) or α-HA antibodies (*bottom*).

APPENDIX B

Portions of the data and text in the following chapter have been published in the journal article "**a**-factor Analogues Containing Alkyne- and Azide-Functionalized Isoprenoids Are Efficiently Enzymatically Processed and Retain Wild-Type Bioactivity"[172]. The dissertation author examined the activity of Ste24, Rce1, and Ste14 membranes with each peptide using radioactive endoprotease-coupled methylation assays. Dr. Mark Distefano at University of Minnesota synthesized the **a**-factor analogue peptides.

B.1 Introduction

Protein prenylation is a post-translational modification that involves the addition of one or two isoprenoid groups to the C-terminus of selected proteins using either farnesyl diphosphate or geranylgeranyl diphosphate. The yeast **a**-factor peptide is particularly useful for studies of protein prenylation because it is post-translationally processed similarly to other CAAX proteins to generate the same C-terminal farnesylated cysteine methyl ester substructure present in larger farnesylated proteins. Recently, several groups have developed isoprenoid analogs bearing azide and alkyne groups that can be used in metabolic labeling experiments. Those compounds have proven useful for profiling prenylated proteins and also show great promise as tools to study how the levels of prenylated proteins vary in different disease models.

Herein, we describe the use of prenylated **a**-factor analogs, and precursor peptides, to evaluate whether **a**-factor-derived precursor peptides can be efficiently processed by the yeast proteases Rce1 and Ste24 as well as the yeast methyltransferase Ste14 to yield mature **a**-factor analogues. The results reported here indicate that metabolic labeling experiments with azide- and alkyne-functionalized isoprenoids can yield prenylated products that are fully processed. Overall, these observations suggest that the isoprenoids studied here that incorporate bio-orthogonal functionality can be used in metabolic labeling experiments without concern that they will induce undesired physiological changes that may complicate data interpretation.

B.2 Methods

The pCH1283 (*2μ URA3* P_{PGK}*-His*$_{10}$*-HA*$_3$*-STE24*) and pCHH$_{10}$m$_3$C-Rce1 (*2μ URA3* P_{PGK}*-RCE1-His*$_{10}$*-myc*$_3$) were transformed into SM3614[121], a double protease deletion yeast strain (*MAT**a** trp1 leu2 ura3 his4 can1 ste24Δ::LEU2 rce1Δ::TRP1*). The pCHH$_{10}$m$_3$N-Ste14

(*2μ URA3* P_{PGK}*-His*$_{10}$*-myc*$_3$*-STE14*) was transformed into SM1188 yeast strain (*MAT**a** trp1 leu2 ura3 his4 can1 ste14Δ::TRP1*)[146]. Plasmid construction and transformation were described in Chapter 2.2.1. After transformation, all yeast cells were grown at 30°C on synthetic complete medium without uracil (SC-URA). Yeast crude membranes overexpressing Ste24, Rce1, and Ste14 were then prepared as described in Chapter 2.2.2. The substrate specificity was determined using the radioactive assays as previously described with minor modifications[140,142]. For endoprotease-coupled methylation assay, reactions with 5 μg of Ste24 or Rce1 membranes, 10 μg of the Ste14 membranes[130], 5 or 15 μM substrate, and 20 μM *S*-adenosyl-[^{14}C-methyl]-L-methionine (Perkin Elmer) were incubated in 100 mM Tris-HCl, pH 7.5. For methylation assay, reactions with 5 μg of the Ste14 membranes, 25 μM substrate, and 20 μM *S*-adenosyl-[^{14}C-methyl]-L-methionine (Perkin Elmer) were incubated in 100 mM Tris-HCl, pH 7.5. The reaction mixtures were incubated for 30 min at 30°C, quenched by 1 M NaOH and 1% SDS mixture, spotted onto pleated filter paper and then placed in the neck of a scintillation vial containing 10 ml of Biosafe II scintillation fluid (RPI) and capped. As a result of the quench reaction, the [^{14}C]-methanol was released from the cleaved and methylated substrate and diffused into the scintillation fluid for 3 hr at room temperature. After removing the filter paper, the radioactivity was quantified using a Packard TriCarb Scintillation counter. Background counts from the DMSO control were subtracted from each sample. Each value was derived from three assays performed in duplicate.

B.3 Results and Discussion

The peptide analogs (Figure B.1) were evaluated as substrates for the different processing enzymes. The analog **3b** to **3f** that contain a free C-terminal cysteine were first tested for their ability to be methylated by Ste14. In this assay, a radiolabeled methyl group from ^{14}C-labeled SAM is transferred to the peptide substrate. Upon saponification, ^{14}C-labeled methanol is liberated and the resulting radioactivity is quantified via liquid scintillation counting. Analysis of reactions containing peptides **3b** to **3f** revealed that all of the peptides were substrates for Ste14 to varying degrees (Figure B.2). Some modest differences in specific activities as compared to the farnesylated a-factor substrate were observed. The values obtained with the alkyne-containing peptides (**3c** and **3d**) were approximately 20% higher, and those for the azide-

containing peptides (**3e** and **3f**) were approximately 50% higher compared to the parent farnesylated peptide (**3b**). Overall, it is clear that the peptides incorporating the non-natural isoprenoids studied here are efficiently methylated comparably to the peptide containing a natural farnesyl group (**3b**). Moreover, these results suggest that the presence of these modified isoprenoid substructures will not interfere with the methylation of larger protein substrates.

Next, endoproteolytic processing of the **a**-factor precursor peptides containing azide- and alkyne-modified isoprenoids was studied. The efficient methylation of **3b** to **3f** by Ste14 described above made it possible to employ an indirect endoprotease-coupled methylation assay to measure Rce1 or Ste24 activity. In this assay, if peptides **4b** to **4f** are substrates for the protease, they would be converted to the corresponding products, **3b** to **3f**. Following this cleavage, in the presence of excess Ste14 and [^{14}C]-SAM, **3b** to **3f** would be rapidly converted to **2b** to **2f** whose production could be determined via the radiolabeling methylation assay described above. Using this assay, the cleavage of peptides **4b** to **4f** by Ste24 was investigated first (Figure B.3.A). Analysis of reactions containing a final peptide concentration of 15 μM showed that all peptides were effectively processed by Ste24, although some relatively small differences in the specific activities were observed. Reactions performed using 5 μM peptide gave similar results, although the specific activities were approximately 2-fold lower overall. In sum, the reaction rates for Ste24 cleavage of peptides **4b** to **4f** varied less than 2-fold.

The same assay was used to explore the cleavage of peptides **4b** to **4f** by Rce1 (Figure B.3.B). In this case, a slightly different pattern of reactivity was observed. Using 15 μM peptide, a similar specific activity was observed for the C10Alk-modified peptide (**4c**) compared to the farnesylated analogue (**4b**) whereas the activity of the C15Alk-modified molecule (**4d**) was 2-fold higher. The specific activities obtained using both azide-containing peptides (**4e** and **4f**) were approximately 1.5-fold higher than the farnesylated peptide **4b**. A similar pattern was observed in reactions performed using 5 μM peptide. Overall, these results with Rce1 show that peptides prenylated with alkyne- and azide-functionalized isoprenoids are processed comparably or modestly better than the peptide bearing a naturally occurring farnesyl group.

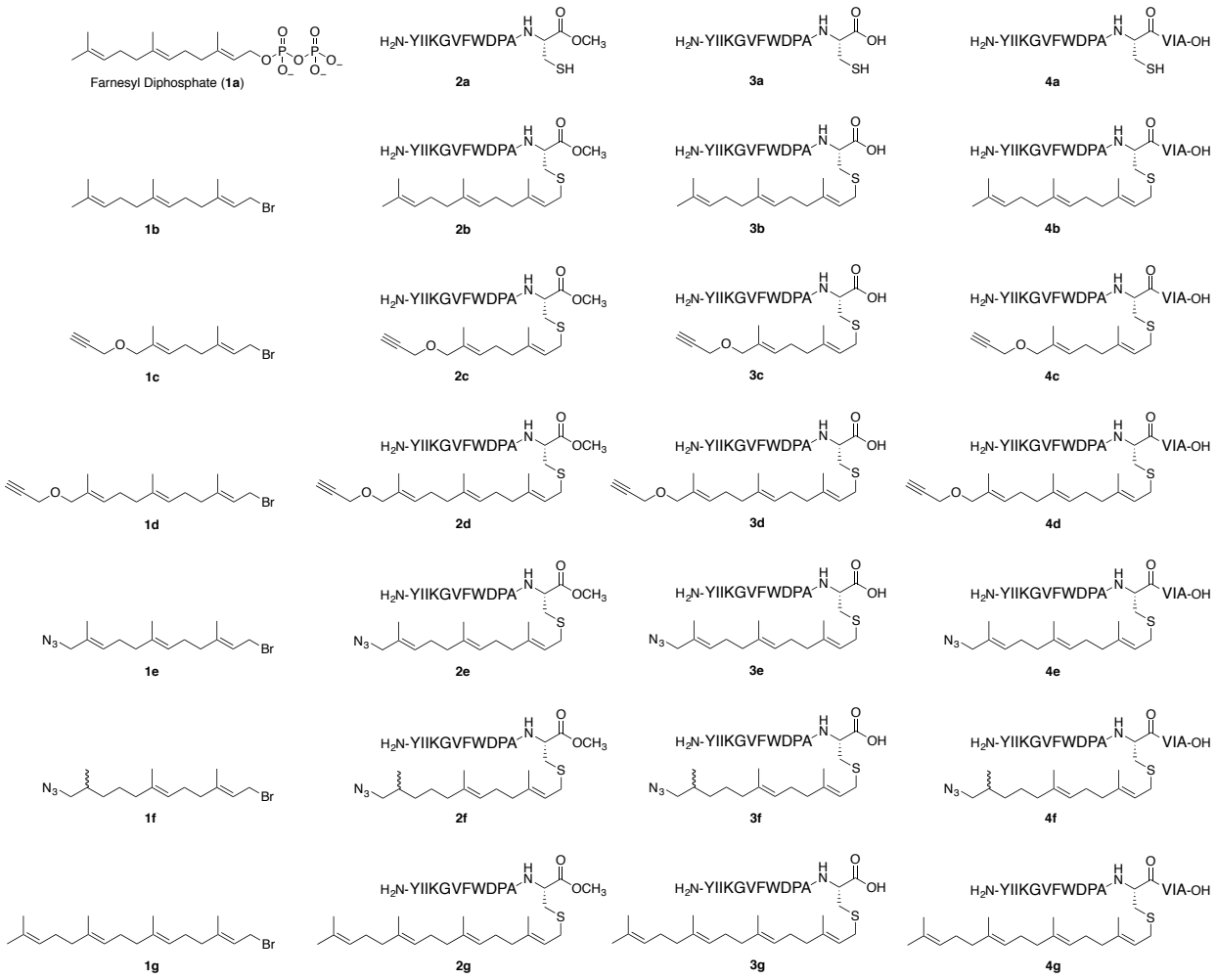

Figure B.1. **a**-factor analogues and precursor peptides incorporating alkyne- and azide-containing isoprenoids.

a-Factor analogues **2b** to **2f** were prepared by alkylation of **2a** using 1b to **1f**. **a**-Factor precursors **3b** to **3f** that can serve as substrates for the methyltransferase Ste14 were prepared by alkylation of **3a** with **1b** to **1f**. **a**-Factor precursors **4b** to **4f** that can serve as substrates for the proteases Ste24 and Rce1 to yield **3b** to **3f** were prepared by alkylation of **4a** with **1b** to **1f**. Geranylgeranylated forms of **a**-factor precursors **3g** and **4g** were prepared in an analogous fashion. To facilitate discussion in the text, the isoprenoids derived from 1c to 1f are designated as C10Alk, C15Alk, C15Az, and C15dhAz, respectively. Reprinted with permission from "**a**-factor Analogues Containing Alkyne- and Azide-Functionalized Isoprenoids Are Efficiently Enzymatically Processed and Retain Wild-Type Bioactivity" by Diaz-Rodriguez, V. *et al.*, 2018. Bioconjugate Chemistry, Vol. 29, pg. 316–323. Copyright (2018), American Chemical Society

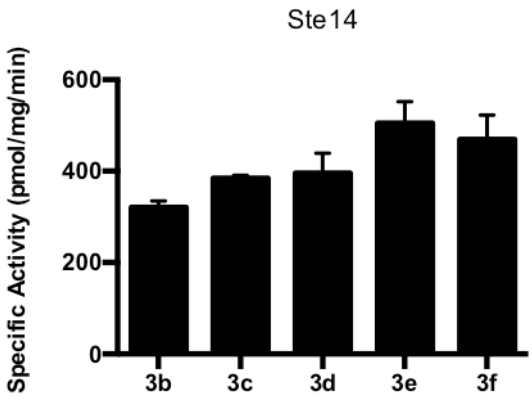

Figure B.2. Assessment of **a**-factor precursor peptides **3b** to **3f** as substrates for Ste14.

Reprinted with permission from "**a**-factor Analogues Containing Alkyne- and Azide-Functionalized Isoprenoids Are Efficiently Enzymatically Processed and Retain Wild-Type Bioactivity" by Diaz-Rodriguez, V. *et al.*, 2018. Bioconjugate Chemistry, Vol. 29, pg. 316–323. Copyright (2018), American Chemical Society

While **a**-factor is normally farnesylated, many proteins are geranylgeranylated. Some of those latter proteins undergo proteolysis and methylation to yield polypeptides containing a C-terminal geranylgeranyl cysteine methyl ester, similar to the C-terminal farnesyl cysteine methyl ester present in **a**-factor. Since the methylation of geranylgeranylated substrates by Ste14 is well established[140], the same coupled assay described above could be employed to study the proteolyic reactions. Accordingly, geranylgeranylated **a**-factor precursor peptide (**4g**) was prepared using the same methods outlined above for **4b** to **4f**. Using the coupled assay, we first studied the cleavage of **4g** by Ste24 to yield **3g**. Interestingly, in reactions containing 15 μM peptide, **4g** demonstrated a specific activity that was only 35% of that of the farnesylated peptide **4b** (Figure B.3.A); similar results were obtained using 5 μM peptide. Different results were observed with Rce1 (Figure B.3.B). Using 15 μM peptide, **4g** was recognized and cleaved similarly to **4b**; the same relative activity was observed using 5 μM peptide. Since the processing of the farnesylated peptide (**4b**) and those incorporating modified isoprenoids (**4c** to **4f**) was always equal to or higher than that of the geranylgeranylated peptide (**4g**), it is likely that the presence of modified isoprenoid groups in proteins that are typically geranylgeranylated would not impede their proteolysis and methylation.

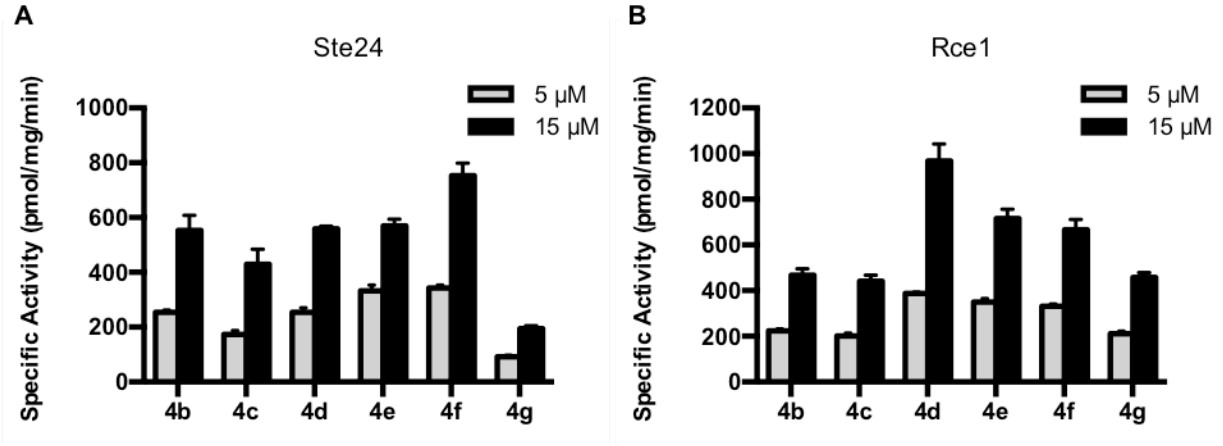

Figure B.3. Assesment of **a**-factor precursor peptides **4b** to **4g** as substrates for the proteases (A) Ste24 and (B) Rce1.

Reprinted with permission from "**a**-factor Analogues Containing Alkyne- and Azide-Functionalized Isoprenoids Are Efficiently Enzymatically Processed and Retain Wild-Type Bioactivity" by Diaz-Rodriguez, V. *et al.*, 2018. Bioconjugate Chemistry, Vol. 29, pg. 316–323. Copyright (2018), American Chemical Society

APPENDIX C

Portions of the data and text in the following chapter have been published in the journal article "AIM2 inflammasome is activated by pharmacological disruption of nuclear envelope integrity"[173]. The dissertation author examined the inhibition effect of HIV-protease inhibitors with crude ZMPSTE24 membrane using radioactive endoprotease-coupled methylation assays.

C.1 Introduction

The HIV protease inhibitors (HIV-PIs), in particular nelfinavir, have been proposed to induce cellular stress both *in vivo* and *in vitro*. Beyond their broad use as anti-HIV drugs, these molecules display beneficial functions unrelated to HIV, such as anti-malaria, anti-tuberculosis, and anti-tumor properties. At the cellular level, the HIV-PIs trigger an atypical ER stress-like transcriptional response that relies mostly on the activation of the integrated stress response. However, the exact nature of the stress response engaged by these drugs is poorly understood, and its possible contribution to inflammation has not been investigated. Our collaborators found that nelfinavir impaired the maturation of lamin A, a structural component of the nuclear envelope, thereby triggering a specific perturbation of cellular homeostasis defined as "nuclear envelope stress". These alterations of nuclear envelope integrity promoted the release of DNA in the cytosol and consequent AIM2 activation. Here, we examined the ability of several HIV-PIs, including nelfinavir, to inhibit ZMPSTE24, and demonstrated that nelfinavir inhibited the enzyme AAX cleavage activity of ZMPSTE24 as a measure of overall activity in a dose-dependent manner with IC_{50} of 27.0 μM.

C.2 Methods

The AAX proteolytic activity of ZMPSTE24 in crude membranes was measured using a radioactive endoprotease-coupled methylation assay as previously described with minor modifications[130]. Reactions contained 5 μg of ZMPSTE24 membranes[130], 10 μg of the Ste14 membranes[130], 15 μM **a**-factor (YIIKGVFWDPAC(Fr)-VIA, EZBioLab) peptide, and 20 μM *S*-adenosyl-[^{14}C-methyl]-L-methionine (Perkin Elmer) were incubated in 100 mM Tris-HCl, pH 7.5. The reactions also contained HIV-PIs at the indicated concentration. After incubating for 30 min at 37°C, the reactions were quenched by 1 M NaOH and 1% SDS mixture, spotted onto

pleated filter paper and then placed in the neck of a scintillation vial containing 10 ml of Biosafe II scintillation fluid (RPI) and capped. As a result of the quench reaction, the [^{14}C]-methanol was released from the cleaved and methylated substrate and diffused into the scintillation fluid for 3 hr at room temperature. After removing the filter paper, the radioactivity was quantified using a Packard TriCarb Scintillation counter. Specific activity was determined as pmol of AAX residues removed per min per mg of protease. Each value was derived from three assays performed in duplicate. The inhibition parameters were calculated using GraphPad Prism 6.

C.3 Results and Discussion

ZMPSTE24 enzymatic activity was measured with a radioactive endoprotease-coupled methylation assay using a synthetic farnesylated **a**-factor peptide substrate. In this assay, ZMPSTE24 cleaves the substrate, rendering it available for methylation by Ste14. We found that nelfinavir (IC_{50}: 27.0 μM) inhibited ZMPSTE24 in a dose-dependent manner similarly to geranylgeranyltransferase inhibitor (IC_{50}: 20.2 μM), ritonavir (IC_{50}: 27.8 μM), and lopinavir (IC_{50}: 8.4 μM). In contrast, amprenavir did not inhibit ZMPSTE24 activity (Figure C.1). These data support that nelfinavir inhibits ZMPSTE24 and thus affects lamin A maturation to promote accumulation of prelamin A in cells.

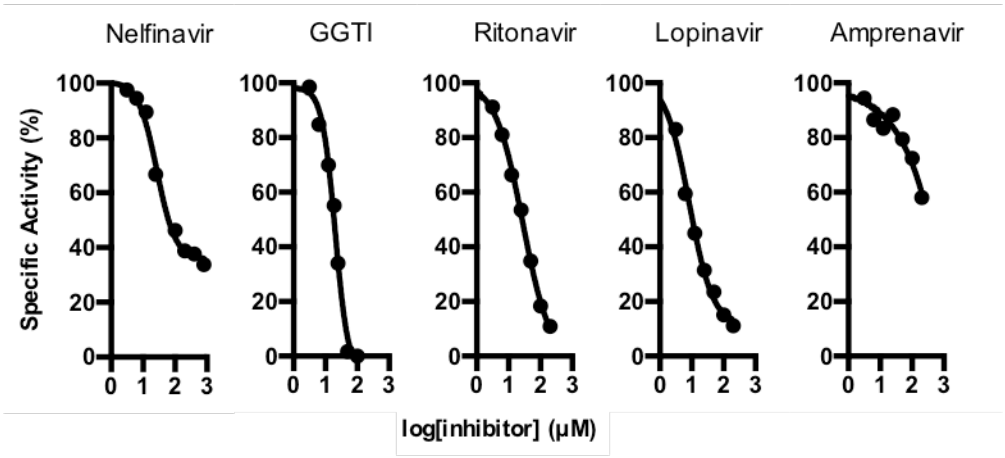

Figure C.1. ZMPSTE24 inhibition curves of HIV-PIs measured by the radioactive endoprotease-coupled methylation assay.

Inhibition effects of nelfinavir, geranylgeranyltransferase inhibitor (GGTI), ritonavir, lopinavir, and amprenavir to ZMPSTE24 were examined. The assay was performed on ZMPSTE24 crude membrane using the truncated **a**-factor as the substrate. The results are presented as the percentage of the specific activity measured in the presence of vehicle. Data are representative of three independent experiments. Reprinted with permission from "AIM2 inflammasome is activated by pharmacological disruption of nuclear envelope integrity" by Di Micco, A. *et al.*, 2016. PNAS, Vol. 113, pg. E4671–E4680. Copyright (2016), National Academy of Sciences, U.S.A.

APPENDIX D

The dissertation author designed and performed all the experiments. Rebecca Sterner helped generating the Ste24 mutant plasmids and prepared yeast crude membranes.

D.1 Introduction

A unique aspect of ZMPSTE24 and Ste24 is that substrates and products must enter and leave an enclosed intramembrane chamber for proteolysis. There are four large side portals apparent in the structure, and all portals are greater than 10 Å in diameter, which is large enough to allow passage of an unfolded peptide. To investigate the roles of these portals, using pymol, we first modeled possible mutations in Ste24 for each of the four portals utilizing the bulkier amino acid tryptophan for portal occlusion. The C- and N-terminal proteolytic activities were examined using the radioactive endoprotease-coupled methylation assay and FRET-based assay, respectively. However, we did not observe consistent result from mutations blocking the same portal. This may due to a particular mutation affecting another part of the enzyme, or mutating just one residue to tryptophan is not enough to block the portal opening. Also, artifacts of the crystallization may interfere the predicted structure as well.

D.2 Methods

The plasmids and primers used in this study are listed in Table D.1. Ste24 mutants were generated on pCH1284 by overlap extension Polymerase Chain Reaction (PCR) site-directed mutagenesis as Chapter 3.2.2 described. Yeast crude membranes overexpressing Ste24 mutants were prepared as described in Chapter 2.2.2. The C-terminal AAX cleavage activity of each mutant was determined using the radioactive endoprotease-coupled methylation assay. Reactions contained 5 μg of Ste24 membranes, 10 μg of the Ste14 membranes, 15 μM **a**-factor (YIIKGVFWDPAC(Fr)-VIA, EZBioLab) peptide, and 20 μM *S*-adenosyl-[^{14}C-methyl]-L-methionine (Perkin Elmer) in 100 mM Tris-HCl, pH 7.5. The N-terminal upstream cleavage activity of each mutant was examined using the FRET-based assay. Reactions contained 30 μg of Ste24 crude membrane in 100 mM Tris-HCl, pH 7.5 with 10 μg/ml Chymostatin and 2 mM AEBSF. The detailed assay protocol was described in Chapter 6.2.2 and 3.2.6.

Table D.1. Plasmids and primers used in this study

Plasmid	Genotype	Reference
pCH1283	*2μ URA3* P_{PGK}*-His*$_{10}$*-HA*$_3$*-STE24*	Chapter 2.2.1
pCH1333	*2μ URA3* P_{PGK}*-His*$_{10}$*-HA*$_3$*-STE24-S132W*	This study
pCH1350	*2μ URA3* P_{PGK}*-His*$_{10}$*-HA*$_3$*-STE24-Y173W*	This study
pCH1337	*2μ URA3* P_{PGK}*-His*$_{10}$*-HA*$_3$*-STE24-I175W*	This study
pCH1331	*2μ URA3* P_{PGK}*-His*$_{10}$*-HA*$_3$*-STE24-G176W*	This study
pCH1332	*2μ URA3* P_{PGK}*-His*$_{10}$*-HA*$_3$*-STE24-G177W*	This study
pCH1348	*2μ URA3* P_{PGK}*-His*$_{10}$*-HA*$_3$*-STE24-I179W*	This study
pCH1349	*2μ URA3* P_{PGK}*-His*$_{10}$*-HA*$_3$*-STE24-A209W*	This study
pCH1330	*2μ URA3* P_{PGK}*-His*$_{10}$*-HA*$_3$*-STE24-I213W*	This study
pCH1336	*2μ URA3* P_{PGK}*-His*$_{10}$*-HA*$_3$*-STE24-T267W*	This study
pCH1334	*2μ URA3* P_{PGK}*-His*$_{10}$*-HA*$_3$*-STE24-P270W*	This study
pCH1323	*2μ URA3* P_{PGK}*-His*$_{10}$*-HA*$_3$*-STE24-V311W*	This study
pCH1324	*2μ URA3* P_{PGK}*-His*$_{10}$*-HA*$_3$*-STE24-Q315W*	This study

Primer	Sequence (5’ to 3’)
Ste24-S132W (+)	CTCTTATCCAGTTTGTGGACCTTGGTTG
Ste24-S132W (−)	CAACCAAGGTCCACAAACTGGATAAGAG
Ste24-Y173W (+)	CTGACTTTGGCGTGGGCTATTGG
Ste24-Y173W (−)	CCAATAGCCCACGCCAAAGTCAG
Ste24-I175W (+)	CTTTGGCGTATGCTTGGGGTGG
Ste24-I175W (−)	CCACCCCAAGCATACGCCAAAG
Ste24-G176W (+)	GTATGCTATTTGGGGCCCAATCCTTTAC
Ste24-G176W (−)	GTAAAGGATTGGGCCCCAAATAGCATAC
Ste24-G177W (+)	CTATTGGTTGGCCAATCCTTTACCTGTTC
Ste24-G177W (−)	GAACAGGTAAAGGATTGGCCAACCG
Ste24-I179W (+)	GGCCCATGGCTTTACCTGTTCC
Ste24-I179W (−)	GGAACAGGTAAAGCCATGGGCC
Ste24-A209W (+)	CTTGTTCGTTGTCCAAATCTTATGGATGACAATC
Ste24-A209W (−)	GATTGTCATCCATAAGATTTGGACAACGAACAAG
Ste24-I213W (+)	GACAATCTGGCCAGTCTTCATCATGCC
Ste24-I213W (−)	GGCATGATGAAGACTGGCCAGATTGTC
Ste24-T267W (+)	CTTCTCATTCAAACGCATATTTCTGGGGTTTG
Ste24-T267W (−)	CAAACCCCAGAAATATGCGTTTGAATGAGAAG
Ste24-P270W (+)	GGTTTGTGGTTCACCTCCAAGAGAATTG
Ste24-P270W (−)	CAATTCTCTTGGAGGTGAACCACAAACC
Ste24-V311W (+)	CACATCGTTAATATGTGGATCTTTAGTC
Ste24-V311W (−)	GACTAAAGATCCACATATTAACGATGTG
Ste24-Q315W (+)	CTTTAGTTGGTTGCACACCTTCCTCATTTTC
Ste24-Q315W (−)	GAAAATGAGGAAGGTGTGCAACCAACTAAAG

D.3 Results and Discussion

Using Pymol modeling, we have selected 12 residues surrounding four portals. These residues were mutated to tryptophan for blocking portal opening (Figure D.1). The C- and N-terminal cleavage activities of each mutant overexpressed in crude membrane were examined using the radioactive endoprotease-coupled methylation assay and the FRET-based assay, respectively (Figure D.2). Specific activities of WT from both assays were defined as 100%. The proposed catalytic E298A mutant showed no C- or N-cleavage activity as predicted. A conserved residue mutant, I175W had no activity from both assays either. The portal 1 mutant T267W and P270W showed between 30% to 50% C-terminal cleavage and less than 20% N-terminal cleavage activities. Interestingly, Q315W from portal 1 and I213W from portal 2 both revealed increased N-terminal cleavage activities. Moreover, I213W also displayed reduced C-terminal cleavage activity of about 40% comparing to WT, suggesting that this residue, or the mutation, may affect substrate entry of both cleavages. However, since other mutants from portal 2 did not show significant changes, we would not able to draw any conclusion from the data obtained from tryptophan portal blocking mutants.

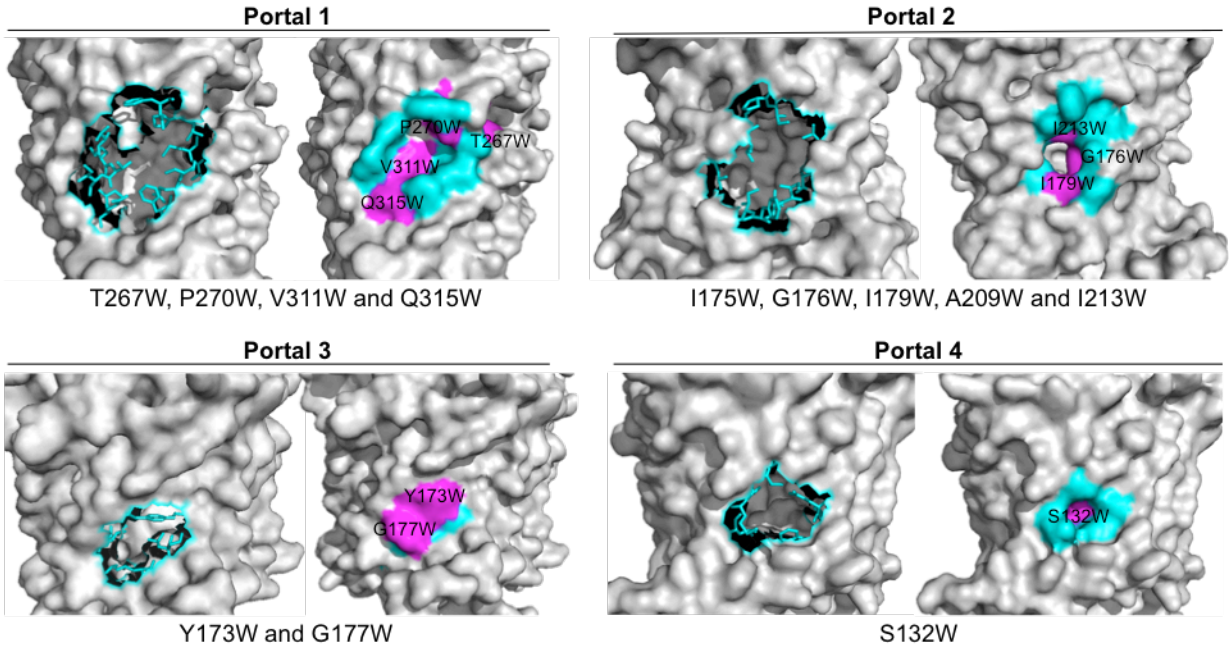

Figure D.1. Crystal structure of Ste24 highlighting the residues surrounding four portals. Residues that form the opening of each portal are labeled in cyan. Mutations occluding each portal are labeled in magenta. PDB: 4IL3

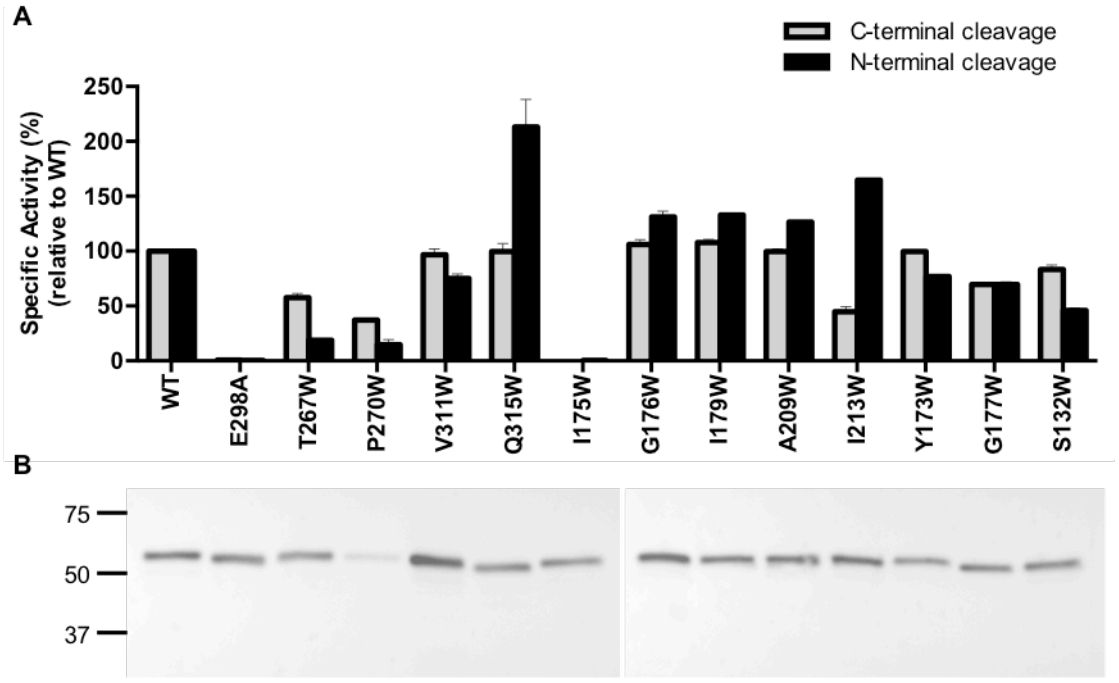

Figure D.2. Enzymatic activities of Ste24 wild-type (WT) and tryptophan mutants.

(A) Specific activities of the C- (*grey*) and N-terminal (*black)* cleavages were calculated from the radioactive endoprotease-coupled methylation assay and the FRET-based assay, respectively. The activity of each mutant was reported as the percentage of relative activity of WT. (B) Expression level of each mutant was examined using immunoblot (1 μg) with the α-HA antibody.

REFERENCES

1. Mounkes, L. & Stewart, C. L. Structural Organization and Functions of the Nucleus in Development, Aging, and Disease. *Curr. Top. Dev. Biol.* **61,** 191–228 (2004).

2. Gruenbaum, Y., Margalit, A., Goldman, R. D., Shumaker, D. K. & Wilson, K. L. The nuclear lamina comes of age. *Nat. Rev. Mol .Cell. Biol.* **6,** 21–31 (2005).

3. Dittmer, T. & Misteli, T. The lamin protein family. *Genome Biol.* **12,** 222 (2011).

4. Hutchison, C. J. Lamins: Building blocks or regulators of gene expression? *Nat. Rev. Mol. Cell Biol.* **3,** 848–858 (2002).

5. de Leeuw, R., Gruenbaum, Y. & Medalia, O. Nuclear Lamins: Thin Filaments with Major Functions. *Trends Cell Biol.* **28,** 34–45 (2018).

6. Simon, D. N. & Wilson, K. L. Partners and post-translational modifications of nuclear lamins. *Chromosoma* **122,** 13–31 (2013).

7. Clarke, S. Protein isoprenylation and methylation at carboxyl-terminal cysteine residues. *Annu. Rev. Biochem.* **61,** 355–386 (1992).

8. Zhang, F. L. & Casey, P. J. Protein prenylation: molecular mechanisms and functional consequences. *Annu. Rev. Biochem.* **65,** 241–269 (1996).

9. Davies, B. S. J., Fong, L. G., Yang, S. H., Coffinier, C. & Young, S. G. The posttranslational processing of prelamin A and disease. *Annu. Rev. Genomics Hum. Genet.* **10,** 153–74 (2009).

10. Barrowman, J. & Michaelis, S. ZMPSTE24, an integral membrane zinc metalloprotease with a connection to progeroid disorders. *Biol. Chem.* **390,** 761–73 (2009).

11. Lehner, C. F., Furstenberger, G., Eppenberger, H. M. & Nigg, E. A. Biogenesis of the nuclear lamina: in vivo synthesis and processing of nuclear protein precursors. *Proc. Natl. Acad. Sci.* **83,** 2096–2099 (1986).

12. Goldman, A. E., Moir, R. D., Montag-Lowy, M., Stewart, M. & Goldman, R. D. Pathway of incorporation of microinjected lamin A into the nuclear envelope. *J. Cell Biol.* **119,** 725–735 (1992).

13. Barrowman, J., Hamblet, C., George, C. M. & Michaelis, S. Analysis of prelamin A biogenesis reveals the nucleus to be a CaaX processing compartment. *Mol. Biol. Cell* **19,** 5398–5408 (2008).

14. Beck, L. A., Hosick, T. J. & Sinensky, M. Isoprenylation is required for the processing of the lamin A precursor. *J. Cell Biol.* **110,** 1489–1499 (1990).

15. Barrowman, J., Hamblet, C., Kane, M. S. & Michaelis, S. Requirements for efficient proteolytic cleavage of prelamin A by ZMPSTE24. *PLoS One* **7,** e32120 (2012).

16. Varela, I. *et al.* Combined treatment with statins and aminobisphosphonates extends longevity in a mouse model of human premature aging. *Nat. Med.* **14,** 767–772 (2008).

17. Capell, B. C. *et al.* Inhibiting farnesylation of progerin prevents the characteristic nuclear blebbing of Hutchinson-Gilford progeria syndrome. *Proc. Natl. Acad. Sci.* **102,** 12879–12884 (2005).

18. Lee, R. *et al.* Genetic studies on the functional relevance of the protein prenyltransferases in skin keratinocytes. *Hum. Mol. Genet.* **19,** 1603–1617 (2010).

19. Yang, S. H. *et al.* Severe hepatocellular disease in mice lacking one or both *CaaX* prenyltransferases. *J. Lipid Res.* **53,** 77–86 (2012).

20. Quigley, A. *et al.* The structural basis of ZMPSTE24-dependent laminopathies. *Science* **339,** 1604–7 (2013).

21. Corrigan, D. P. *et al.* Prelamin A endoproteolytic processing in vitro by recombinant Zmpste24. *Biochem. J.* **387,** 129–138 (2005).

22. Carrero, D., Soria-Valles, C. & López-Otín, C. Hallmarks of progeroid syndromes: lessons from mice and reprogrammed cells. *Dis. Model. Mech.* **9,** 719–735 (2016).

23. Gordon, L. B., Rothman, F. G., López-Otín, C. & Misteli, T. Progeria: A paradigm for translational medicine. *Cell* **156,** 400–407 (2014).

24. Gordon, L. B. *et al.* Association of Lonafarnib Treatment vs No Treatment With Mortality Rate in Patients With Hutchinson-Gilford Progeria Syndrome. *Jama* **319,** 1687 (2018).

25. Jung, H.-J. *et al.* Regulation of prelamin A but not lamin C by miR-9, a brain-specific microRNA. *Proc. Natl. Acad. Sci.* **109,** E423–E431 (2012).

26. Eriksson, M. *et al.* Recurrent de novo point mutations in lamin A cause Hutchinson-Gilford progeria syndrome. *Nature* **423,** 293–298 (2003).

27. Hennekam, R. C. M. Hutchinson–Gilford Progeria Syndrome: Review of the Phenotype. *Am. J. Med. Genet. Part A* **140A,** 2603–2624 (2006).

28. Navarro, C. L. *et al.* New ZMPSTE24 (FACE1) mutations in patients affected with restrictive dermopathy or related progeroid syndromes and mutation update. *Eur. J. Hum. Genet.* **22,** 1002–1011 (2014).

29. Cunningham, V. J., D'Apice, M. R., Licata, N., Novelli, G. & Cundy, T. Skeletal phenotype of mandibuloacral dysplasia associated with mutations in ZMPSTE24. *Bone* **47,** 591–597 (2010).

30. Sander, C. S. *et al.* A newly identified splice site mutation in ZMPSTE24 causes restrictive dermopathy in the Middle East. *Br. J. Dermatol.* **159,** 961–967 (2008).

31. Decaudain, A. *et al.* New metabolic phenotypes in laminopathies: LMNA mutations in patients with severe metabolic syndrome. *J. Clin. Endocrinol. Metab.* **92,** 4835–4844 (2007).

32. Dutour, A. *et al.* High prevalence of laminopathies among patients with metabolic syndrome. *Hum. Mol. Genet.* **20,** 3779–3786 (2011).

33. Galant, D. *et al.* A Heterozygous ZMPSTE24 Mutation Associated with Severe Metabolic Syndrome, Ectopic Fat Accumulation, and Dilated Cardiomyopathy. *Cells* **5,** 21 (2016).

34. Brady, G. F. *et al.* Nuclear lamina genetic variants, including a truncated LAP2, in twins and siblings with nonalcoholic fatty liver disease. *Hepatology* **67,** 1710–1725 (2018).

35. Smigiel, R. *et al.* Novel frameshifting mutations of the ZMPSTE24 gene in two siblings affected with restrictive dermopathy and review of the mutations described in the literature. *Am. J. Med. Genet. Part A* **152,** 447–452 (2010).

36. Moulson, C. L. *et al.* Homozygous and Compound Heterozygous Mutations in ZMPSTE24 Cause the Laminopathy Restrictive Dermopathy. *J. Invest. Dermatol.* 913–919 (2005).

37. Navarro, C. L. *et al.* Loss of ZMPSTE24 (FACE-1) causes autosomal recessive restrictive dermopathy and accumulation of Lamin A precursors. *Hum. Mol. Genet.* **14,** 1503–13 (2005).

38. Li, C. Homozygosity for the common mutation c.1085dupT in the ZMPSTE24 Gene in a mennonite baby with restrictive dermopathy and placenta abruption. *Am. J. Med. Genet. Part A* **152,** 262–263 (2010).

39. Ahmad, Z., Zackai, E., Medne, L. & Garg, A. Early onset mandibuloacral dysplasia due to compound heterozygous mutations in ZMPSTE24. *Am. J. Med. Genet. A* **152A,** 2703–10 (2010).

40. Ahmad, Z. *et al.* Homozygous null mutations in ZMPSTE24 in restrictive dermopathy: evidence of genetic heterogeneity. *Clin. Genet.* **81,** 158–64 (2012).

41. Yesil, G. *et al.* Restrictive dermopathy in a Turkish newborn. *Pediatr. Dermatol.* **28,** 408–411 (2011).

42. Kariminejad, A., Goodarzi, P., Thanh Huong, L. T. & Wehnert, M. S. Restrictive dermopathy. Molecular diagnosis of restrictive dermopathy in a stillborn fetus from a consanguineous Iranian family. *Saudi Med. J.* **30,** 150–3 (2009).

43. Morais, P. *et al.* Restrictive dermopathy-a lethal congenital laminopathy. Case report and review of the literature. *Eur. J. Pediatr.* **168,** 1007–1012 (2009).

44. Thill, M. *et al.* Restrictive dermopathy: A rare laminopathy. *Arch. Gynecol. Obstet.* **278,** 201–208 (2008).

45. Chen, M. *et al.* A case of restrictive dermopathy with complete chorioamniotic membrane separation caused by a novel homozygous nonsense mutation in the ZMPSTE24 gene. *Am. J. Med. Genet. Part A* **149,** 1550–1554 (2009).

46. Lu, C. S. *et al.* Restrictive dermopathy: Report of two siblings. *Pediatr. Neonatol.* **54,** 198–201 (2013).

47. Jagadeesh, S., Bhat, L., Suresh, I. & Muralidhar, S. L. Prenatal diagnosis of restrictive dermopathy. *Indian Pediatr.* **46,** 349–51 (2009).

48. Shackleton, S. *et al.* Compound heterozygous ZMPSTE24 mutations reduce prelamin A processing and result in a severe progeroid phenotype. *J. Med. Genet.* **42,** e36 (2005).

49. Agarwal, A. K. *et al.* Focal segmental glomerulosclerosis in patients with mandibuloacral dysplasia owing to ZMPSTE24 deficiency. *J. Investig. Med.* **54,** 208–13 (2006).

50. Agarwal, A. K., Fryns, J. P., Auchus, R. J. & Garg, A. Zinc metalloproteinase ZMPSTE24, is mutated in mandibuloacral dysplasia. *Hum. Mol. Genet.* **12,** 1995–2001 (2003).

51. Denecke, J. *et al.* A Homozygous in Combination With a Heterozygous Mutation LMNA ZMPSTE 24 Null MutationGene Causes Hutchinson-Gilford Progeria Syndrome (HGPS): Insights into the Pathophysiology of HGPS. *Hum. Mutat.* **27,** 796–802 (2006).

52. Miyoshi, Y. *et al.* Severe mandibuloacral dysplasia caused by novel compound heterozygous ZMPSTE24 mutations in two Japanese siblings. *Clin. Genet.* **73,** 535–44 (2008).

53. Ben Yaou, R. *et al.* Type B mandibuloacral dysplasia with congenital myopathy due to homozygous ZMPSTE24 missense mutation. *Eur. J. Hum. Genet.* **19,** 647–54 (2011).

54. Haye, D. *et al.* Failure of ossification of the occipital bone in mandibuloacral dysplasia type B. *Am. J. Med. Genet. Part A* **170,** 2750–2755 (2016).

55. Harhouri, K. *et al.* Antisense-Based Progerin Downregulation in HGPS-Like Patients' Cells. *Cells* **5,** 31 (2016).

56. Carr, A. & Cooper, D. A. Adverse effects of antiretroviral therapy. *Lancet (London, England)* **356,** 1423–30 (2000).

57. Caron, M., Auclair, M., Sterlingot, H., Kornprobst, M. & Capeau, J. Some HIV protease inhibitors alter lamin A/C maturation and stability, SREBP-1 nuclear localization and adipocyte differentiation. *AIDS* **17,** 2437–44 (2003).

58. Lloyd, D. J., Trembath, R. C. & Shackleton, S. A novel interaction between lamin A and SREBP1: implications for partial lipodystrophy and other laminopathies. *Hum. Mol. Genet.* **11,** 769–777 (2002).

59. Capanni, C. *et al.* Altered pre-lamin A processing is a common mechanism leading to lipodystrophy. *Hum. Mol. Genet.* **14,** 1489–1502 (2005).

60. Duband-Goulet, I. *et al.* Subcellular localization of SREBP1 depends on its interaction with the C-terminal region of wild-type and disease related A-type lamins. *Exp. Cell Res.* **317,** 2800–2813 (2011).

61. Vadrot, N. *et al.* The p.R482W substitution in a-type lamins deregulates SREBP1 activity in dunnigan-type familial partial lipodystrophy. *Hum. Mol. Genet.* **24,** 2096–2109 (2014).

62. Coffinier, C. *et al.* HIV protease inhibitors block the zinc metalloproteinase ZMPSTE24 and lead to an accumulation of prelamin A in cells. *Proc. Natl. Acad. Sci. U. S. A.* **104,** 13432–7 (2007).

63. Coffinier, C. *et al.* A potent HIV protease inhibitor, darunavir, does not inhibit ZMPSTE24 or lead to an accumulation of farnesyl-prelamin A in cells. *J. Biol. Chem.* **283,** 9797–804 (2008).

64. Clark, K. M., Jenkins, J. L., Fedoriw, N. & Dumont, M. E. Human CaaX protease ZMPSTE24 expressed in yeast: structure and inhibition by HIV protease inhibitors. *Protein Sci.* **26,** 242–257 (2016).

65. Mehmood, S. *et al.* Mass spectrometry captures off-target drug binding and provides mechanistic insights into the human metalloprotease ZMPSTE24. *Nat. Chem.* 1–18 (2016).

66. Leung, G. K. *et al.* Biochemical Studies of Zmpste24-deficient Mice. *J. Biol. Chem.* **276,** 29051–29058 (2001).

67. Pendas, A. M. *et al.* Defective prelamin A processing and muscular and adipocyte alterations in Zmpste24 metalloproteinase-deficient mice. *Nat Genet* **31,** 94–99 (2002).

68. Bergo, M. O. *et al.* Zmpste24 deficiency in mice causes spontaneous bone fractures, muscle weakness, and a prelamin A processing defect. *Proc. Natl. Acad. Sci. U. S. A.* **99,** 13049–54 (2002).

69. Yang, S. H. *et al.* Blocking protein farnesyltransferase improves nuclear blebbing in mouse fibroblasts with a targeted Hutchinson-Gilford progeria syndrome mutation. *Proc. Natl. Acad. Sci.* **102,** 10291–10296 (2005).

70. Yang, S. H., Qiao, X., Fong, L. G. & Young, S. G. A farnesyltransferase inhibitor improves disease phenotypes in mice with a Hutchinson-Gilford progeria syndrome mutation. *Biochim. Biophys. Acta - Mol. Cell Biol. Lipids* **116,** 3 (2006).

71. Osorio, F. G. *et al.* Splicing-directed therapy in a new mouse model of human accelerated aging. *Sci Transl Med* **3,** 106ra107 (2011).

72. Villa-Bellosta, R. *et al.* Defective extracellular pyrophosphate metabolism promotes vascular calcification in a mouse model of Hutchinson-Gilford progeria syndrome that is ameliorated on pyrophosphate treatment. *Circulation* **127,** 2442–2451 (2013).

73. Vidak, S. & Foisner, R. Molecular insights into the premature aging disease progeria. *Histochem. Cell Biol.* **145,** 401–417 (2016).

74. Gonzalo, S., Kreienkamp, R. & Askjaer, P. Hutchinson-Gilford Progeria Syndrome: A premature aging disease caused by LMNA gene mutations. *Ageing Res. Rev.* **33,** 18–29 (2017).

75. Espada, J. *et al.* Nuclear envelope defects cause stem cell dysfunction in premature-aging mice. *J. Cell Biol.* **181,** 27–35 (2008).

76. Hernandez, L. *et al.* Functional coupling between the extracellular matrix and nuclear lamina by wnt signaling in progeria. *Dev. Cell* **19,** 413–425 (2010).

77. Scaffidi, P. & Misteli, T. Lamin A-dependent misregulation of adult stem cells associated with accelerated ageing. *Nat. Cell Biol.* **10,** 452–459 (2008).

78. Osorio, F. G., López-Otín, C. & Freije, J. M. P. NF-kB in premature aging. *Aging (Albany. NY).* **4,** 726–7 (2012).

79. Dechat, T. *et al.* Lamina-associated polypeptide 2alpha binds intranuclear A-type lamins. *J. Cell Sci.* **113 Pt 19,** 3473–84 (2000).

80. Vidak, S., Kubben, N., Dechat, T. & Foisner, R. Proliferation of progeria cells is enhanced by lamina-associated polypeptide 2alpha (LAP2alpha) through expression of extracellular matrix proteins. *Genes Dev* **29,** 2022–2036 (2015).

81. Chojnowski, A. *et al.* Progerin reduces LAP2α-telomere association in hutchinson-gilford progeria. *Elife* **4,** 1–21 (2015).

82. Liu, B. *et al.* Genomic instability in laminopathy-based premature aging. *Nat. Med.* **11,** 780–785 (2005).

83. Kubben, N. *et al.* Repression of the antioxidant NRF2 pathway in premature aging. *Cell* **165,** 1361–1374 (2016).

84. Scaffidi, P. & Misteli, T. Lamin A – Dependent Nuclear Defects in Human Aging. *Science (80-.).* **312,** 1059–1063 (2006).

85. Rodriguez, S., Coppedè, F., Sagelius, H. & Eriksson, M. Increased expression of the Hutchinson-Gilford progeria syndrome truncated lamin A transcript during cell aging. *Eur. J. Hum. Genet.* **17,** 928–937 (2009).

86. McClintock, D. *et al.* The mutant form of Lamin A that causes Hutchinson-Gilford progeria is a biomarker of cellular aging in human skin. *PLoS One* **2,** (2007).

87. Ragnauth, C. D. *et al.* Prelamin a acts to accelerate smooth muscle cell senescence and is a novel biomarker of human vascular aging. *Circulation* **121,** 2200–2210 (2010).

88. Strandgren, C., Revêchon, G., Carvajal, A. S. & Eriksson, M. Emerging candidate treatment strategies for Hutchinson-Gilford progeria syndrome. *Biochem. Soc. Trans.* **45,** 1279–1293 (2017).

89. Glynn, M. W. & Glover, T. W. Incomplete processing of mutant lamin A in Hutchinson-Gilford progeria leads to nuclear abnormalities, which are reversed by farnesyltransferase inhibition. *Hum. Mol. Genet.* **14,** 2959–2969 (2005).

90. Toth, J. I. *et al.* Blocking protein farnesyltransferase improves nuclear shape in fibroblasts from humans with progeroid syndromes. *Proc. Natl. Acad. Sci. USA* **102,** 12873–8 (2005).

91. Fong, L. G. *et al.* A protein farnesyltransferase inhibitor ameliorates disease in a mouse model of progeria. *Science* **311,** 1621–3 (2006).

92. Yang, S. H., Qiao, X., Fong, L. G. & Young, S. G. Treatment with a farnesyltransferase inhibitor improves survival in mice with a Hutchinson-Gilford progeria syndrome mutation. *Biochim. Biophys. Acta - Mol. Cell Biol. Lipids* **1781,** 36–39 (2008).

93. Capell, B. C. *et al.* A farnesyltransferase inhibitor prevents both the onset and late progression of cardiovascular disease in a progeria mouse model. *Proc. Natl. Acad. Sci.* **106,** 13143–13143 (2009).

94. Gordon, L. B. *et al.* Clinical trial of a farnesyltransferase inhibitor in children with Hutchinson-Gilford progeria syndrome. *Proc. Natl. Acad. Sci.* **109,** 16666–16671 (2012).

95. Ullrich, N. J. *et al.* Neurologic features of Hutchinson-Gilford progeris syndrome after lonafarnib treatment. *Neurology* **81,** 427–430 (2013).

96. Gordon, L. B. *et al.* Impact of farnesylation inhibitors on survival in Hutchinson-Gilford progeria syndrome. *Circulation* **130,** 27–34 (2014).

97. Gordon, L. B. *et al.* Survey of plasma proteins in children with progeria pre-Therapy and on-Therapy with lonafarnib. *Pediatr. Res.* **83,** 982–992 (2018).

98. Gordon, L. B. *et al.* Clinical Trial of the Protein Farnesylation Inhibitors Lonafarnib, Pravastatin, and Zoledronic Acid in Children With Hutchinson-Gilford Progeria SyndromeClinical Perspective. *Circulation* **134,** 114–125 (2016).

99. Johnson, S. C., Rabinovitch, P. S. & Kaeberlein, M. mTOR is a key modulator of ageing and age-related disease. *Nature* **493,** 338–345 (2013).

100. Cao, K. *et al.* Rapamycin Reverses Cellular Phenotypes and Enhances Mutant Protein Clearance in Hutchinson-Gilford Progeria Syndrome Cells. *Sci. Transl. Med.* **3,** 89ra58-89ra58 (2011).

101. Cenni, V. *et al.* Autophagic degradation of farnesylated prelamin A as a therapeutic approach to lamin-linked progeria. *Eur. J. Histochem.* **55,** 200–205 (2011).

102. Gabriel, D., Roedl, D., Gordon, L. B. & Djabali, K. Sulforaphane enhances progerin clearance in Hutchinson-Gilford progeria fibroblasts. *Aging Cell* **14,** 78–91 (2015).

103. Pellegrini, C. *et al.* All-trans retinoic acid and rapamycin normalize Hutchinson Gilford progeria fibroblast phenotype. *Oncotarget* **6,** (2015).

104. Gabriel, D., Gordon, L. B. & Djabali, K. Temsirolimus partially rescues the Hutchinson-Gilford progeria cellular phenotype. *PLoS One* **11,** 1–25 (2016).

105. Ramos, F. J. *et al.* Rapamycin Reverses Elevated mTORC1 Signaling in Lamin A/C-Deficient Mice, Rescues Cardiac and Skeletal Muscle Function, and Extends Survival. *Sci. Transl. Med.* **4,** 144ra103-144ra103 (2012).

106. Choi, J. C. *et al.* Temsirolimus activates autophagy and ameliorates cardiomyopathy caused by lamin A/C gene mutation. *Sci. Transl. Med.* **4,** (2012).

107. Liao, C. Y. *et al.* Rapamycin Reverses Metabolic Deficits in Lamin A/C-Deficient Mice. *Cell Rep.* **17,** 2542–2552 (2016).

108. Ibrahim, M. X. *et al.* Targeting isoprenylcysteine methylation ameliorates disease in a mouse model of progeria. *Science* **340,** 1330–3 (2013).

109. Scaffidi, P. & Misteli, T. Reversal of the cellular phenotype in the premature aging disease Hutchinson-Gilford progeria syndrome. *Nat. Med.* **11,** 440–445 (2005).

110. Lee, J. M. *et al.* Modulation of LMNA splicing as a strategy to treat prelamin A diseases. *J. Clin. Invest.* **126,** 1592–1602 (2016).

111. Liu, B. *et al.* Resveratrol rescues SIRT1-dependent adult stem cell decline and alleviates progeroid features in laminopathy-based progeria. *Cell Metab.* **16,** 738–750 (2012).

112. Xiong, Z. M. *et al.* Methylene blue alleviates nuclear and mitochondrial abnormalities in progeria. *Aging Cell* **15,** 279–290 (2016).

113. Kreienkamp, R. *et al.* Vitamin D receptor signaling improves Hutchinson-Gilford progeria syndrome cellular phenotypes. *Oncotarget* **7,** (2016).

114. Bárcena, C. *et al.* Methionine Restriction Extends Lifespan in Progeroid Mice and Alters Lipid and Bile Acid Metabolism. *Cell Rep.* 2392–2403 (2018). doi:10.1016/j.celrep.2018.07.089

115. Herskowitz, I. Life cycle of the budding yeast Saccharomyces cerevisiae. *Microbiol. Rev.* **52,** 536–553 (1988).

116. Michaelis, S. & Barrowman, J. Biogenesis of the Saccharomyces cerevisiae pheromone a-factor, from yeast mating to human disease. *Microbiol. Mol. Biol. Rev.* **76,** 626–51 (2012).

117. Chen, P. & Sapperstein, S. Biogenesis of the Saccharomyces cerevisiae Mating Pheromone a-Factor. *J. Cell Biol.* **136,** 251–269 (1997).

118. Huyer, G. *et al.* Saccharomyces cerevisiae a-factor mutants reveal residues critical for processing, activity, and export. *Eukaryot. Cell* **5,** 1560–70 (2006).

119. Caldwell, G. a, Wang, S. H., Naider, F. & Becker, J. M. Consequences of altered isoprenylation targets on a-factor export and bioactivity. *Proc. Natl. Acad. Sci. U. S. A.* **91,** 1275–1279 (1994).

120. Boyartchuk, V. L., Ashby, M. N. & Rine, J. Modulation of Ras and a-Factor Function by Carboxyl-Terminal Proteolysis. *Science (80-.).* **275,** 1796–1800 (1997).

121. Tam, A. *et al.* Dual Roles for Ste24p in Yeast a-factor Maturation: NH2-terminal Proteolysis and COOH-terminal CAAX Processing. *J. Cell Biol.* **142,** 635–649 (1998).

122. Trueblood, C. E. *et al.* The CaaX proteases, Afc1p and Rce1p, have overlapping but distinct substrate specificities. *Mol. Cell. Biol.* **20,** 4381–4392 (2000).

123. Pryor, E. E. *et al.* Structure of the integral membrane protein CAAX protease Ste24p. *Science* **339,** 1600–1604 (2013).

124. Michaelis, S. & Hrycyna, C. A. A protease for the ages. *Science* **339,** 1529–30 (2013).

125. Schmidt, W. K., Tam, A. & Michaelis, S. Reconstitution of the Ste24p-dependent N-terminal Proteolytic Step in Yeast a-Factor Biogenesis. *J. Biol. Chem.* **275,** 6227–6233 (2000).

126. Tam, A., Schmidt, W. K. & Michaelis, S. The multispanning membrane protein Ste24p catalyzes CAAX proteolysis and NH2-terminal processing of the yeast a-factor precursor. *J. Biol. Chem.* **276,** 46798–806 (2001).

127. Matthews, B. Structural basis of the action of thermolysin and related zinc peptidases. *Acc. Chem. Res.* 333–340 (1988).

128. Fujimura-kamada, K., Nouvet, F. J. & Michaelis, S. A Novel Membrane-associated Metalloprotease, Ste24p, Is Required for the First Step of NH2 -terminal Processing of the Yeast a-Factor Precursor. *J. Cell Biol.* **136,** 271–285 (1997).

129. Wiley, P. A. Molecular and biochemical analysis of prelamin a proteolytic processing by the novel zinc metalloprotease, zmpste24 and mechanistic studies of its yeast homolog, Ste24p. (Purdue University, 2015).

130. Barrowman, J., Wiley, P. A., Hudon-Miller, S. E., Hrycyna, C. A. & Michaelis, S. Human ZMPSTE24 disease mutations: residual proteolytic activity correlates with disease severity. *Hum. Mol. Genet.* **21,** 4084–93 (2012).

131. Spear, E. D. *et al. ZMPSTE24* missense mutations that cause progeroid diseases decrease prelamin A cleavage activity and/or protein stability. *Dis. Model. Mech.* **11,** dmm.033670 (2018).

132. Moiseeva, O. *et al.* Mutant lamin A links prophase to a p53 independent senescence program. *Cell Cycle* **14,** 2408–2421 (2015).

133. Matralis, A. N. *et al.* Molecular tools that block maturation of the nuclear lamin A and decelerate cancer cell migration. *Bioorg. Med. Chem.* 1–8 (2018). doi:10.1016/j.bmc.2018.10.001

134. Lee, J. H., Yoo, N. J., Kim, M. S., An, C. H. & Lee, S. H. Mutational and expressional alterations of ZMPSTE24, DNA damage response-related gene, in gastric and colorectal cancers. *Pathol. Res. Pract.* **212,** 1113–1118 (2016).

135. Hildebrandt, E. R., Arachea, B. T., Wiener, M. C. & Schmidt, W. K. Ste24p Mediates Proteolysis of Both Isoprenylated and Non-prenylated Oligopeptides. *J. Biol. Chem.* **291,** 14185–98 (2016).

136. Blanden, M. J. *et al.* Efficient farnesylation of an extended C-terminal C(x)3X sequence motif expands the scope of the prenylated proteome. *J. Biol. Chem.* **293,** 2770–2785 (2018).

137. Ast, T., Michaelis, S. & Schuldiner, M. The Protease Ste24 Clears Clogged Translocons. *Cell* **164,** 103–114 (2016).

138. Kayatekin, C. *et al.* Translocon Declogger Ste24 Protects against IAPP Oligomer-Induced Proteotoxicity. *Cell* 1–12 (2018). doi:10.1016/j.cell.2018.02.026

139. Fu, B., Wang, L., Li, S. & Dorf, M. E. ZMPSTE24 defends against influenza and other pathogenic viruses. *J. Exp. Med.* 1–11 (2017). doi:10.1084/jem.20161270

140. Anderson, J. L., Frase, H., Michaelis, S. & Hrycyna, C. A. Purification, functional reconstitution, and characterization of the Saccharomyces cerevisiae isoprenylcysteine carboxylmethyltransferase Ste14p. *J. Biol. Chem.* **280,** 7336–45 (2005).

141. Elble, R. C. A simple and efficient procedure for transformation of Schizosaccharomyces pombe. *Biotechniques* **13,** 18–20 (1992).

142. Hudon, S. E. *et al.* HIV-protease inhibitors block the enzymatic activity of purified Ste24p. *Biochem. Biophys. Res. Commun.* **374,** 365–8 (2008).

143. Bergo, M. O. *et al.* Absence of the CAAX endoprotease Rce1: effects on cell growth and transformation. *Mol. Cell. Biol.* **22,** 171–181 (2002).

144. Sinensky, M. *et al.* The processing pathway of prelamin A. *J. Cell Sci.* **107,** 61–67 (1994).

145. Hrycyna, C. A. & Clarke, S. Farnesyl cysteine C-terminal methyltransferase activity is dependent upon the STE14 gene product in Saccharomyces cerevisiae. *Mol. Cell. Biol.* **10,** 5071–6 (1990).

146. Hrycyna, C. A., Sapperstein, S. K., Clarke, S. & Michaelis, S. The Saccharomyces cerevisiae STE14 gene encodes a methyltransferase that mediates C-terminal methylation of a-factor and RAS proteins. *EMBO J.* **1,** 1699–1709 (1991).

147. Dolence, J. M., Steward, L. E., Dolence, E. K., Wong, D. H. & Poulter, C. D. Studies with recombinant Saccharomyces cerevisiae CaaX prenyl protease Rce1p. *Biochemistry* **39,** 4096–4104 (2000).

148. Manolaridis, I. *et al.* Mechanism of farnesylated CAAX protein processing by the intramembrane protease Rce1. *Nature* **504,** 301–5 (2013).

149. Barrowman, J. & Michaelis, S. in *Handbook of Proteolytic Enzymes, 3rd* 668–676 (Elsevier, 2013). doi:10.1016/B978-0-12-382219-2.00141-1

150. Hollander, I., Frommer, E. & Mallon, R. Human ras-converting enzyme (hRCE1) endoproteolytic activity on K-ras-derived peptides. *Anal. Biochem.* **286,** 129–37 (2000).

151. Plummer, L. J. *et al.* Mutational analysis of the ras converting enzyme reveals a requirement for glutamate and histidine residues. *J. Biol. Chem.* **281,** 4596–605 (2006).

152. Porter, S. S. B. *et al.* Inhibition of the CaaX proteases Rce1p and Ste24p by peptidyl (acyloxy)methyl ketones. *Biochim. Biophys. Acta - Mol. Cell Res.* **1773,** 853–862 (2007).

153. Diaz-Rodriguez, V., Mullen, D. G., Ganusova, E., Becker, J. M. & Distefano, M. D. Synthesis of peptides containing C-terminal methyl esters using trityl side-chain anchoring: Application to the synthesis of a-factor and a-factor analogs. *Org. Lett.* **14,** 5648–5651 (2012).

154. Diaz-Rodriguez, V., Ganusova, E., Rappe, T. M., Becker, J. M. & Distefano, M. D. Synthesis of Peptides Containing C-Terminal Esters Using Trityl Side-Chain Anchoring: Applications to the Synthesis of C-Terminal Ester Analogs of the Saccharomyces cerevisiae Mating Pheromone a -Factor. *J. Org. Chem.* **80,** 11266–11274 (2015).

155. Atherton, E., Hardy, P. M., Harris, D. E. & Matthews, B. H. Racemisation of C-terminal cysteine during peptide assembly. *Pept. 1990 Proc. Twenty-First Eur. Pept. Symp. Giralt, E., Andreu, D., Eds.; ESCOM Sci. Publ. Leiden, Netherlands* 243–244 (1991).

156. Arachea, B. T. & Wiener, M. C. Acquisition of accurate data from intramolecular quenched fluorescence protease assays. *Anal. Biochem.* **522,** 30–36 (2017).

157. Funk, A. L. BIOCHEMICAL ELUCIDATION OF THE ISOPRENOID BINDING SITE OF THE YEAST ISOPRENYLCYSTEINE CARBOXYL METHYLTRANSFERASE, STE14P. (Purdue University, 2017).

158. Selkti, M. *et al.* Interactions of a new α-aminophosphinic derivative inside the active site of TLN (thermolysin): A model for zinc-metalloendopeptidase inhibition. *Acta Crystallogr. - Sect. D Biol. Crystallogr.* **59,** 1200–1205 (2003).

159. Arolas, J. L., Botelho, T. O., Vilcinskas, A. & Gomis-Rüth, F. X. Structural evidence for standard-mechanism inhibition in metallopeptidases from a complex poised to resynthesize a peptide bond. *Angew. Chemie - Int. Ed.* **50,** 10357–10360 (2011).

160. Kale, T. A. T., Raab, C., Yu, N., Dean, D. C. & Distefano, M. D. A photoactivatable prenylated cysteine designed to study isoprenoid recognition. *J. Am. Chem. Soc.* **123,** 23633–23641 (2001).

161. DeGraw, A. J. *et al.* A photoactive isoprenoid diphosphate analogue containing a stable phosphonate linkage: Synthesis and biochemical studies with prenyltransferases. *J. Org. Chem.* **72,** 4587–4595 (2007).

162. Kyro, K., Manandhar, S. P., Mullen, D., Schmidt, W. K. & Distefano, M. D. Photoaffinity labeling of Ras converting enzyme 1 (Rce1p) using a benzophenone-containing peptide substrate. *Bioorg. Med. Chem.* **18,** 5675–84 (2010).

163. Kyro, K., Manandhar, S. P., Mullen, D., Schmidt, W. K. & Distefano, M. D. Photoaffinity labeling of Ras converting enzyme using peptide substrates that incorporate benzoylphenylalanine (Bpa) residues: improved labeling and structural implications. *Bioorg. Med. Chem.* **19,** 7559–69 (2011).

164. Hahne, K. *et al.* Evaluation of substrate and inhibitor binding to yeast and human isoprenylcysteine carboxyl methyltransferases (Icmts) using biotinylated benzophenone-containing photoaffinity probes. *Biochem. Biophys. Res. Commun.* **423,** 98–103 (2012).

165. Vervacke, J. S. *et al.* Diazirine-containing photoactivatable isoprenoid: synthesis and application in studies with isoprenylcysteine carboxyl methyltransferase. *J. Org. Chem.* **79,** 1971–8 (2014).

166. Henry, L. K. *et al.* Identification of a contact region between the tridecapeptide alpha-factor mating pheromone of Saccharomyces cerevisiae and its G protein-coupled receptor by photoaffinity labeling. *Biochemistry* **41,** 6128–6139 (2002).

167. Son, C. D., Sargsyan, H., Naider, F. & Becker, J. M. Identification of ligand binding regions of the Saccharomyces cerevisiae α-factor pheromone receptor by photoaffinity cross-linking. *Biochemistry* **43,** 13193–13203 (2004).

168. Son, C. D., Sargsyan, H., Hurst, G. B., Naider, F. & Becker, J. M. Analysis of ligand-receptor cross-linked fragments by mass spectrometry. *J. Pept. Res.* **65,** 418–426 (2005).

169. Mullen, D. G. *et al.* Synthesis of a-factor peptide from Saccharomyces cerevisiae and photoactive analogues via Fmoc solid phase methodology. *Bioorganic Med. Chem.* **19,** 490–497 (2011).

170. Hudon-Miller, S. E. CHARACTERIZATION AND INHIBITION OF THE CAAX PROCESSING PRELAMIN A PROTEASE ZMPSTE24. (Purdue University, 2009).

171. Griggs, A. M., Hahne, K. & Hrycyna, C. A. Functional oligomerization of the Saccharomyces cerevisiae isoprenylcysteine carboxyl methyltransferase, Ste14p. *J. Biol. Chem.* **285,** 13380–7 (2010).

172. Diaz-Rodriguez, V. *et al.* a-Factor analogues containing alkyne- and azide functionalized isoprenoids are efficiently enzymatically processed and retain wild type bioactivity. *Bioconjug. Chem.* **29,** 316–323 (2018).

173. Di Micco, A. *et al.* AIM2 inflammasome is activated by pharmacological disruption of nuclear envelope integrity. *Proc. Natl. Acad. Sci.* **113,** E4671–E4680 (2016).

VITA

Erh-Ting Hsu was born and raised in Taipei, Taiwan. She is the eldest daughter in the family. She attended Taipei First Girls High School and graduated in the top 10% of her class in June 2008. Throughout high school, Erh-Ting played the marimba in a percussion band. She was also a member of Biology club, where she first learned how fun science could be. For her undergraduate studies, Erh-Ting attended National Taiwan University. She enjoyed school activities, such as hosting science camp for high school students and writing scripts for retreat performances. Erh-Ting also served as President for Biochemical Science and Technology Student Association. Additionally, after her sophomore year, Erh-Ting began research in the lab of Dr. Po-Huang Liang studying enzyme kinetics of prenyltransferases, where she began to realize her passion for working in the laboratory and performing experiments. After obtaining her Bachelor of Science in June 2012, Erh-Ting worked for a year in the lab of Dr. Chin-Su Liu as a research coordinator, studying stem cell therapy for liver diseases.

From this work and her past research experience, Erh-Ting decided to pursue her Doctorate degree at Purdue University in 2013. As a first-year graduate student in the Interdisciplinary Life Science program, she rotated in four different labs and decided to join the lab of Dr. Christine Hrycyna where her research focused on a progeroid-disease associated enzyme, ZMPSTE24. During her work, she developed new fluorescence assay to examine enzyme activity. She also presented her projects at several local and national science conferences and received three best presentation awards. Besides academic achievements, Erh-Ting was Vice President of Purdue University Taiwanese Graduate Student Association. She also volunteered in Science in Schools program to promote science education for kids. Erh-Ting graduated from Purdue University with a Ph.D. in Chemistry in December 2018. She will move to Portland, Oregon after graduation with her husband Han-Ting Tseng. In the future, she hopes to pursue a career in the pharmaceutical industry.

PUBLICATIONS

Spear, E., **Hsu, E.-T.**, Nie, L., Carpenter, E.P., Hrycyna, C.A., and Michaelis, S. "ZMPSTE24 Missense Mutations that Cause Progeroid Diseases Decrease Prelamin A Cleavage Activity and/or Protein Stability" *Disease Models & Mechanisms*, **2018**, *11*: dmm033670

Diaz-Rodriguez, V., **Hsu, E.-T.**, Ganusove, E., Werst, E.R., Becker, J.M., Hrycyna, C.A., and Distefano, D.M. "**a**-factor Analogues Containing Alkyne- and Azide-Functionalized Isoprenoids Are Efficiently Enzymatically Processed and Retain Wild-Type Bioactivity" *Bioconjugate Chem.*, **2018**, *29*(2), pp 316 - 323

Di Micco, A., Frera, G., Lugrin, J., Jamilloux, Y., **Hsu, E.-T.**, Tardivel, A., De Gassart, A., Zaffalon, L., Bujisic, B., Siegert, S., Quadroni, M., Broz, P., Henry, T., Hrycyna, C.A., and Martinon, F. "AIM2 inflammasome is activated by pharmacological disruption of nuclear envelope integrity" *Proc. Natl. Acad. Sci.*, **2016**, *113*(32) E4671-E4680